(NASA CR-54000;
A-P-FR-20516) OTS: $10.50 pl, $4.40 mf

FINAL REPORT

Title all cap

NUCLEAR ROCKET ENGINE NOZZLE STUDY

~~By~~
Sidney Elkind

Prepared for

NATIONAL AERONAUTICS AND SPACE ADMINISTRATION

3 Feb~~ruary~~ 1964 140 p

CJ

(NASA Contract NAS 3-3670)

Technical Management
NASA-Lewis Research Center
Advanced Development and Evaluation Division
Cleveland, Ohio

Rudolph A. Duscha

ARDE-PORTLAND, INC.
100 West Century Road
Paramus, New Jersey

NUCLEAR ROCKET ENGINE

NOZZLE STUDY

By

Sidney Elkind

ABSTRACT

A

19479

A study was made of selected aspects of nuclear nozzles and an uncooled design for long duration firings was evolved.

Nozzle walls that are adequate with limited cooling were investigated and two designs that could be cooled with 5% of core gas flow are described.

The effects of start-up and shutdown were treated and use of gas side coatings was investigated.

Internal heat generation due to gamma heating was considered and the methods of computing transient temperature distributions are reviewed.

Limited stress analysis and comparative weights for both cooled and uncooled nozzles are reported.

Author

TABLE OF CONTENTS

LIST OF TABLES

LIST OF ILLUSTRATIONS

LIST OF ILLUSTRATIONS (-2-)

LIST OF ILLUSTRATIONS (-3-)

LIST OF ILLUSTRATIONS (-4-)

SUMMARY

A feasibility study was made of an uncooled nozzle for long firing durations. Internal heat generation due to gamma attenuation was considered and the method of computing gamma heating is briefly discussed. The method of computing the transient temperature within the nozzle wall is reviewed and results presented for the configurations considered.

An uncooled nuclear nozzle wall is feasible for a 20-minute firing duration. The wall must be internally shielded by two three-eighths inch tungsten shells to reduce gamma heating to a tolerable level. These shields effectively reduce gamma flux by a factor of four. The uncooled wall, including internal shields, weighs 6232 lbs. from inlet to nozzle throat.

An analysis was made to establish walls that required only limited cooling. The same general component arrangement as in chemical rocket nozzles was used: a liner; insulation; and a structural wall. The transient temperatures were computed for proposed designs.

Two nozzle walls that can be adequately cooled with 5% of core flow have been evolved. They both consist of: .0625 inches of tungsten; .125 inches of pyrolytic graphite and a structural shell. In one case, the shell is Rene 41, in the other 7178-6T aluminum. The materials are the same thickness, varying from .726 inches at the inlet to .089 inches at the throat.

The aluminum wall configuration weighs 450 lbs. from the inlet to the throat. It requires 100°R coolant and also ten percent of the limited cooling flow is needed during shutdown.

The weight of the Rene 41 wall is 880 lbs. It can be adequately cooled during shutdown by radiation to space.

The thermal effects of start-up and shutdown on the nozzle walls were considered. During start-up the cooled walls reach steady state temperature distributions within one to three minutes. The uncooled wall does not reach steady state in a twenty-minute firing.

I. INTRODUCTION

Nuclear rocket systems are currently being considered for many future space missions. In general the missions are of long duration, requiring high propulsion power levels, long duration firings, and multiple start-stop capability. Reliability of all components is of paramount importance.

The nozzle is a critical component in nuclear rocket systems. Not only must it withstand the propellant gas temperature and pressure, as in chemical fueled systems, it must also tolerate gamma heating during both operating periods and shutdown.

Arde-Portland has studied various aspects of nuclear rocket nozzles under NASA Lewis Research Center Contract NAS 3-3670.

The specified design conditions include:

Power Rating	15,000 MW
Flow Rate (Hydrogen)	830 pps
Inlet Diameter	6 feet
Chamber Pressure	1,000 psia
Chamber Temperature	4,500 °R
Exit Area Ratio	40:1
Number of Firings	3
Each Firing Duration	20 minutes
Shut-Down Period	10 days
Core Data	Classified

This study has emphasized the following areas, as required by the contract work statement and coordinated with cognizant Lewis Research Center personnel:

A. Feasibility of an uncooled nozzle.
B. "Limited" cooling studies of a thin composite wall.
C. The use of gas side coatings to replace or supplement a tungsten liner.
D. Limited stress analysis of the nozzle structure.
E. Approximate weight analysis of cooled and uncooled nozzles.
F. The thermal effects of shutdown and restart on the nozzle wall.

We would like to express our appreciation to the Los Alamos Scientific Laboratory for making available their QAD IV Computer Program for the computation of gamma heating.

II. UNCOOLED NUCLEAR NOZZLE

The aim of this study was to determine the feasibility of an uncooled nozzle for the specified operating conditions. The term uncooled, as used here, refers to inactive cooling, such as by radiation to space, as distinguished from active, as exemplified by regenerative cooling.

The study is divided into two parts: the determination of gamma heating within the wall; and, the computation of the transient temperature distributions. Both the rate of gamma heating and the wall temperature distribution are functions of the wall configuration. An initial wall configuration was chosen and transient temperature distributions computed to determine its capability. The thermal design of the wall was changed, based on the results of this analysis and the process repeated until the design objective was achieved.

The method of computing gamma heating is reviewed in Appendix "B".

A. Heat Transfer

1. Material Considerations

In the design of a nozzle, the choice of materials for the component parts requires the matching of the respective properties and characteristics of proposed materials and the requirements of the parts. A basic consideration was that the materials selected and the design adopted could be fabricated, either at present or in the near future.

The requirements for attaining an uncooled nuclear nozzle are similar to those for uncooled chemical rocket nozzles with the exception of the effects of gamma heating. Solid propellant nozzles usually have a refractory liner in contact with the hot gas, an insulator to reduce the heat transferred through the wall, and an outer structural wall. The same general composite wall construction, Figure 1, is postulated for the uncooled nuclear nozzle concept. The liner must be impervious to hot hydrogen and sufficiently ductile to transmit internal pressure loads to the insulation. Of the refractories, tungsten appears most attractive for this application. Columbium and molybdenum

could not be given serious consideration because their melting points are too close to the contemplated operating temperature. Tantalum must be discounted on the basis of its susceptibility to hydrogen embrittlement. Pyrolytic graphite, while neither temperature limited nor subject to embrittlement, would react chemically with the hot hydrogen to form hydrocarbon gases.

The insulation material must have low thermal conductivity and be stable at operating temperature. It must have adequate compressive strength to transmit the pressure load to the external structure. Promising materials include the oxides BeO and ZrO_2 and pyrolytic graphite. Other more exotic materials are available, but were not considered in the initial analyses.

The structural wall must have strength at elevated temperatures and also be able to tolerate a higher temperature in the soak condition. The nickel base alloys look promising for this application.

The .2% offset yield strengths of high strength alloys that can be considered are listed in the following tabulation:

Alloy	.2% Offset Yield Psi	Temperature °F
Rene 41	84,000	1600
Hastelloy "W"	22,000	1800
Rene 41	25,000	1800
Udimet 700	40,000	1800
In-100	52,000	1800

Hastelloy "W" has been tentatively chosen for this component, primarily because of its excellent high temperature strength coupled with ease of fabrication. Although the other alloys have higher strength, they are more difficult to fabricate.

Tungsten presents several problem areas in the fabrication of large component parts: a) low temperature brittleness; and b) welding difficulty. Greater ductility and, hence, easier fabrication is realized in alloys such as tungsten-rhenium (WRe), and tungsten-molybdenum without much sacrifice in either strength or melting temperature.

Within the present state-of-the-art, the welding of tungsten parts to produce sizeable hardware is a problem. Joints produced by conventional fusion processes result in highly embrittled weld zones that cannot sustain nominal stresses. Development effort to restore forged, extruded or rolled properties in the recrystallized weld zones is indicated.

Successful joints have been achieved by diffusion bonding using Ni-Pd interface cements. These joints are limited to a temperature of about 5,000°F. Gas pressure bonding has also been used for welding small sized tungsten sheet. Parameters of 10,000 psi, 2,700°F, and three-hour cycle time result in fairly coarse grain structures. The process is presently limited to components up to 5 inches in diameter.

The brittle ductile transition temperature is of particular significance in the liners of nozzles subject to multiple starts. On start-up, transient thermal gradients exist between the gas side and insulation side of the tungsten. The cold side is placed in tension and, if the material has a high transition temperature, it will have no appreciable ductility until it reaches a temperature level of 300° to 400°F. The strains due to the thermal stresses alone can exceed the yielding capability of the cold, notch-sensitive tungsten. Greater ductility obtainable through higher purity, smaller grain size, or minor alloying can overcome this potential start-up problem.

Development effort is also being directed at raising recrystallization temperatures. Higher recrystallization temperatures imply longer operating times at higher temperatures before strength losses occur. This is of minor consideration in a design where the tungsten is not required to function as a structural member.

The pyrolytic graphite should not present any fabrication problems. It can be installed in several ways: a) deposited in place; b) laid up in the form of "molded" sections; and c) wound on as cloth or foil. The method used will depend on the nozzle design.

In the structural material, weldability is a prime requirement in order to limit the number of mechanical joints. The materials that were considered have been subjected to weld development and methods and standards have been established.

2. Method of Computing Nozzle Wall Temperature Distributions

The nozzle wall is subjected to the following modes of heat transfer: 1) convection on the gas contact surface; 2) conduction within the wall; 3) internal heat generation due to gamma ray attenuation; and 4) radiation to space. The general partial differential equation for this case can be written:

$$\frac{\partial^2 T}{\partial x^2} + \frac{\partial^2 T}{\partial y^2} + \frac{\partial^2 T}{\partial z^2} + \frac{q'''}{k} = \frac{\rho c}{k} \frac{\partial T}{\partial \theta} \qquad (6)$$

Where: $T(x, y, z, \theta)$ = Temperature at a point whose coordinates are x, y, and z, at time θ.

$q'''(x, y, z, \theta)$ = Rate of volumetric heat generation within the wall, BTU/HR-Cubic Foot, at a point whose coordinates are x, y, z, at time θ.

Wall Properties (assumed constant)

k = Thermal conductivity
ρ = Material density
c = Specific heat

This can be simplified by considering only one-dimensional heat transfer, normal to the wall surface. Both axial and circumferential conduction can be neglected since they are orders of magnitude lower than normal conduction. The differential equation now becomes:

$$\frac{\partial^2 T}{\partial x^2} + \frac{q'''}{k} = \frac{\rho c}{k} \frac{\partial T}{\partial \theta} \qquad (7)$$

If we consider a composite wall made up of three or more materials and apply the appropriate initial and boundary conditions, a closed form solution is virtually impossible to obtain. Numerical methods must, therefore, be used. The derivation of the finite difference approximation to Equation 7, the method of solution, and stability criteria are covered in Appendix "A". In brief, it consists of dividing up the wall into an integral number of slabs and using the derived equations to successfully build up the wall temperature distribution as a function of time.

3. Gamma Heating

The primary difference between a nuclear rocket nozzle and the nozzle of a chemically fuelled rocket is the energy deposition within the former. This is manifest in the internal generation of heat that is essentially independent of the temperature level of the working fluid. Thus, in a chemical system, the wall is limited to the gas recovery temperature, while in a nuclear system, the wall temperature can rise above that of the gas. The determination of the internal heat generation rate, due to gamma ray attenuation, therefore, is of utmost importance in this study.

a. Heating Rates Within Nozzle Walls

The method and procedures used to compute gamma heating rates are outlined in Appendix "B". In brief, the Los Alamos QAD IV Computer Program is used to obtain the gamma flux distribution within the wall and these values are converted into local heating rates. Results obtained for representative wall configurations are briefly reviewed in this section. A typical QAD IV output, the gamma flux at a receiver point, is presented in Figure 2.

The gamma flux distribution for the wall presented in Figure 1, is shown in Figure 3, for both upstream and throat sections. The flux is reduced by a factor of three, from the inside to the outside, due to attenuation by the intervening material. The throat values are approximately half of those upstream, due to the greater distance from the core and the shielding supplied by the convergent section. A buildup factor of one was used.

The effect of using the buildup factor of aluminum, which is equivalent to that of the core material, compared to a factor of one is evident from Figures 4 and 5. The flux values are 3 times as high when the aluminum was used.

The effect of tungsten liner thickness on the flux in the Hastelloy is also apparent. Increasing the tungsten from one-sixteenth of an inch to five-sixteenths cuts the flux in half.

The average energy level and the relation between the buildup factors β_a and β_e, used to convert the gamma fluxes into heating rates are indicated in Figure 6.

The gamma heating rates in a wall with a thick tungsten liner are presented in Figure 7. The attenuating effect of the thick liner on the heating rate is evident. The discontinuity of the curves is a result of the method of weighting the material nuclear properties. The volumetric rate of heat generation varies from 30 million BTU/Hr-ft^3 in the tungsten at the upstream section to one million in the Hastelloy. These rates will significantly affect the transient temperature distribution in the nozzle wall.

Figures 8 to 11 show the nuclear properties of the wall materials used in the calculations.

b. Tolerable Gamma Heating, Approximate Analysis

The heat generation within the nozzle due to gamma heating can nullify the effect of the insulation. The structural part of the wall can be raised above design temperature, even though conduction through the wall is reduced. In order to determine the order of magnitude of gamma heat generation that can be tolerated by the Hastelloy "W", an approximate analysis was made.

Consider the thermal insulation to be perfect and perform a steady-state heat balance on the Hastelloy. It is heated by internal heat generation, represented by:

$$q_{gen} = q'''\delta A$$

and cooled by radiation to space:

$$q_{rad} = \sigma \epsilon A T_w^4$$

The steady-state temperature, assuming a flat temperature profile is:

$$T_w = \left(\frac{q'''\delta}{\sigma \epsilon} \right)^{.25}$$

Where:

T_w = Steady state wall temperature °R

q''' = Volumetric rate of heat generation, BTU/Cu-Ft-Hr

σ = .171 X 10^{-8}, BTU/hr-ft^2-$°R^4$

ε = Wall emissivity = .8

δ = Wall thickness, feet

The wall temperature has been plotted in Figure 12 for variations in heat generation rate and wall thickness. It is dependent on both, and for a design limit of 1800°F, or 2260°R, the maximum heat generation rate is limited between one-quarter and one-half million BTU/hr-cu-ft.

Results of the QAD Program, presented in Figure 7, show that the gamma heating rate is greater than one million BTU/hr-cu-ft. Thus, gamma heating is seen as a potential problem area.

c. Methods of Reducing Gamma Heating

Gamma heating can be reduced by:

1. Shielding
2. Separation
3. Reducing the source power density

Shielding can be accomplished by increasing the tungsten thickness in the wall and by using auxiliary tungsten shields within the gas stream. The effect of thicker tungsten layers in the wall will be presented in another section.

To obtain a significant gamma reduction due to separation, great distances must be involved. Since the distance that can be utilized from the core to the nozzle is limited, this approach does not appear useful in the present application.

The source power density can be reduced by keeping the core size constant, but reducing the power output. Since this will affect the nuclear aspect of the core, this aspect will not be covered here. If we reduce the core power to 1,500 mw, the gamma heating rate will decrease in direct proportion by a factor of 10. The effect on wall temperature distribution will be covered in a subsequent section.

4. Transient Wall Temperature Distributions

Transient temperatures were computed within the wall at two sections: upstream where the gas coefficient is low; and at the throat where the highest coefficient exists. Core gas convection coefficients were computed by means of Bartz equation, presented in Appendix "C". The convection coefficients at the throat and upstream at an area ratio of 6.8 are respectively:

$$h_g^* = 4950 \text{ BTU/hr-ft}^2\text{-degree R}$$

$$h_g = 830 \text{ BTU/hr-ft}^2\text{-degree R}$$

In the quest for a wall that could tolerate a twenty-minute firing, the thickness of the wall materials was varied and the material arrangement was modified on the basis of the resulting gamma flux and temperature distribution. The more significant results will be discussed below.

The initial runs showed that a thin tungsten liner does not reduce the gamma heating rate significantly. The effect of the thickness of the tungsten liner on the gamma flux in the Hastelloy "W" can be seen on Figure 5. The gamma flux decreases as the tungsten is made thicker. On this basis, a liner nine-sixteenths (9/16) of an inch thick was chosen. It is visualized as made up of thin layers to reduce thermal shock. Only the initial layer need be gas tight.

The temperature distribution in the upstream section for the wall initially proposed with the tungsten thickness increased is shown on Figure 13. It is evident that the temperature limits of both the BeO and Hastelloy "W" are exceeded in 2 and 4 minutes respectively. It is instructive to examine the shape of the transient temperature distributions. Early in the firing, e.g., in the first two minutes, the liner temperature is already above that of the gas. The highest temperature within the insulation is at the tungsten interface and the outer structure is at a uniform temperature. As the firing continues, a peak starts to develop within the insulation and a noticeable slope appears in the outer structure. The peak is attributed to the accumulation of heat generated by gamma rays within the material, at a faster rate than it can be extracted by radiation at the rear surface or convection at the inner surface. It is evident that as the insulation is made thicker, the thermal resistance to either surface increases and the peak will become higher.

The slope of the temperature curve in the Hastelloy is due to the increased heat loss by radiation and to the heat that is being conducted through the insulation. At the end of twenty minutes, this temperature gradient is in excess of one thousand degrees (1000°).

The corresponding temperature distributions in the throat section are presented on Figure 14. Here the Hastelloy limit is exceeded in five minutes while the BeO becomes marginal late in the firing. The temperature peak within the insulation appears at a later time than it does upstream. The gradient in the outer structure is still evident.

The gamma heat generation rates for the above cases are shown on Figure 7. In the Hastelloy, it is approximately one million BTU/cu-ft-hr, which is much larger than can be tolerated as shown by the previous approximate calculation.

a. The Effects of Reduced Gamma Heating

In order to see the effects of reduced heat generation, the computed gamma was arbitrarily reduced to one-half, one-quarter, and one-tenth. Gamma reduction may be attained by reducing the core power density in the same proportion, e.g., by reducing the core total power while keeping its dimensions constant.

The resulting transient temperature distributions for the upstream section are presented on Figures 15a, 15b, and 15c. The temperature peak within the insulation decreases as the heat generation rate decreases, virtually disappearing at the one-quarter rate. The capability of the wall is increased in the following manner:

Gamma Rate	Wall Capabilities-Minutes
Full	4
Half	7
Quarter	9
Tenth	16

The corresponding results at the throat are similar to those at the upstream section. The wall capability at the throat is:

Gamma Rate	Wall Capability-Minutes
Full	5
Half	7
Quarter	9
Tenth	16

Another way to reduce the gamma heating rate is to shield the wall from the reactor core. This must be done with a minimum interference to the core gas flow. This concept is shown in Figure 16. The tungsten shield is retained by supports at the upstream end. It is kept concentric with the nozzle wall by longitudinal spacers. This arrangement is similar to that of the cooling liner in ramjet engines.

This method of shielding is potentially attractive since the shield is totally surrounded by the gas. Thus its temperature will not rise significantly above that of the gas, while if its thickness were added to the tungsten liner, the resulting total thermal resistance could be high enough that the tungsten design temperature could be exceeded at the insulation interface.

The effect of both single and double liners of various thicknesses is presented in Figure 17. The effect of reduced gamma is also indicated. A single quarter-inch shield is approximately equivalent to one-half gamma, while two three-eighth inch shields reduce the temperatures about the same as a reduction to one-quarter gamma. A single shield of greater thickness can reduce the temperature as effectively as multiple shields whose combined thickness is equal to that of the single shield. Supporting a shield operating at high temperature within a nozzle is not without problems. Also the difficulty increases as the number of shields increase. On this basis, a single thicker shield would be more desirable.

The wall construction was changed with pyrolytic graphite replacing the BeO, to take advantage of its higher temperature capability. The most promising combination also had a layer of tungsten within the wall. The transient temperature distributio

for this wall with full gamma is shown in Figure 18. This wall can withstand a six-minute firing, the critical material being the graphite. The Hastelloy remains below its design point for eight minutes.

The effects of reduced gamma were also investigated. The resulting temperatures in the upstream section are indicated in Figures 19a, 19b, and 19c.

The wall capabilities are:

Gamma Rate	Wall Capabilities-Minutes
Full	6
Half	14
Quarter	20
Tenth	>20

This wall is thus capable of withstanding a full twenty-minute firing, when the gamma rate is reduced to one-quarter or lower. Such a reduction can be attained by using either two three-eighth inch or one three-quarter inch shield.

The temperature distribution in the shielded wall, both upstream and at the throat, are shown in Figures 20A and 20B. The structural wall temperature is below 1600°F at both sections. It should be noted that the temperature profiles within the tungsten and the Hastelloy are flat, indicating that thermal stresses will be low. This configuration can withstand the twenty-minute firing with a margin for temperature rise during soak.

A heat balance was made on the upstream section of this wall to determine the relative magnitudes of the heat transfer modes involved. The half gamma case was considered after fourteen minutes of firing.

The balance included: 1) heat generation within the wall due to gamma heating; 2) heat transferred from the wall to the core

gas; 3) heat stored within the wall; and 4) heat radiated to space. The final balance shows:

Mode of Heat Transfer	BTU	Percent of q_{gen}
Gamma Heating Within Wall	= 297,000 BTU	100%
Convection to Core Gas	= 196,400 BTU	66%
Radiation to Space	= 5,800 BTU	2%
Stored in Wall	= 94,000 BTU	32%

It is evident that the sole source of energy is gamma heating while the more effective cooling method is convection to the gas stream. Although radiation to space is a numerically small quantity, it is sufficient to maintain the structural shell below its design temperature.

b. Effect of Gas Temperature Reduction

Runs were made with full gamma with the gas temperature reduced to 4000°R and 3500°R. The only effects were to reduce the internal peak temperature slightly; the structural shell was unaffected.

c. Effect of Gas Pressure Reduction

Heat transfer runs were made with the gas pressure reduced to 750 and 500 psia. In order to maintain thrust constant an increase in throat diameter is required. The gas convection coefficient is therefore, reduced by the .9 power of the pressure ratio. Again, the effects were only felt near the gas side surface. The Rene 41 was not affected.

d. Temperature Distribution in a Solid Tungsten Wall

A study was made to determine the effect of wall thickness on the temperature distribution of an uncooled solid tungsten wall. Both throat and upstream sections were considered. The resulting steady-state temperatures, achieved within several minutes of firing are shown in Figure 21.

The upstream section has a temperature peak that gets higher as the wall thickness is increased. It goes from 4700°R to 5500°R as the wall is varied from .75 inches to 3 inches. This effect is due to gamma heating and the increased thermal resistance from the interior to both surfaces where cooling is attained. Although the higher convective coefficient at the throat is sufficient to depress the peak, the strength of tungsten at the temperatures attained is not high enough to make the 4-inch wall structurally sound. The large temperature gradients within the tungsten are noteworthy. The resulting thermal stresses could not be tolerated. Thus the shielded, radiation-cooled wall uses the tungsten more effectively than it can be utilized in a single material wall.

III. LIMITED COOLING STUDY

A. General

The basic aim of the limited cooling study is to obtain a thin composite wall, cooling only the structural shell, with a minimum coolant flow. This is in contrast to usual regenerative cooling where all or most of the core flow is used to cool a wall made of a single material.

A wall consisting of a single material with moderate temperature capability would exhibit two undesirable effects if cooled on its outer diameter: first, the hot side temperature would have to be maintained below the allowable, resulting in a convective heat input from the gas; second, the temperature gradient within the wall, due to the high heat flux, will result in large thermal stresses. The first will require increased coolant flows. However, with an elevated gas temperature, and the high gas convection coefficients associated with high core pressures, adequate cooling may not be possible. The thermal stresses will limit the structural integrity of the wall.

In regenerative cooling studies of nuclear nozzles insulating coatings are considered to reduce the gas to wall temperature difference and the resulting heat flux. However, the requirements that a coating must meet for the nuclear nozzle are quite stringent and an adequate coating is not presently available. Appendix "D" contains a literature survey of coatings for this application. In place of a coating, a hydrogen barrier and a thin insulation were considered.

The resulting wall is postulated to be made of three materials; a thin tungsten liner as a hydrogen barrier; a thin layer of insulation; and a structural shell. The insulation is pyrolytic graphite, chosen for its high temperature capabilities. The structural shell is Hastelloy "W". Its nuclear and thermal properties are representative of the nickel alloys. It will be convenient to simulate other alloys by merely varying the wall thickness as required by structural considerations.

B. The Effect of Coolant Location

The effect of the coolant location on the temperature distribution throughout the wall was investigated. The coolant was placed on the outside diameter, in the middle of the Hastelloy, and then at the Hastelloy pyrolytic graphite interface, as indicated in Figure 22.

1. Coolant on Outside Diameter

Initial computations were performed on the configuration with the coolant located at the outside diameter of the Hastelloy. The component thicknesses are .0625" tungsten, .250" pyrolytic graphite, and .750" Hastelloy. The rate of gamma heat generation is indicated on Figure 23. It ranges from 3 to 5 million BTU/HR-Cubic Foot within the Hastelloy compared to about 1 million for the uncooled wall with a .5625" liner without any shields.

The temperature distribution was computed for this wall as a function of coolant convection coefficient, ranging from 100 to 4000 BTU/HR-SQ.FT.-Degree. Two coolant temperatures were used; 800°R for pump turbine exhaust; 100°R for main stream flow. The resulting steady state temperature distribution, which is attained in one to three minutes of firing, is shown in Figure 24. The tungsten liner is above the gas temperature, 4500°R. The core gas therefore cools the wall. The peak within the pyrolytic graphite is due to gamma heating, and it exceeds the capability of the material. There is a significant temperature gradient, 2000°, within the Hastelloy.

The peak within the insulation indicates that the pyrolytic graphite is too thick. Another series of runs was therefore made with the insulation thickness reduced to .125 inches. The resulting temperature distributions are presented in Figure 25.

The wall hot side is still above the gas temperature, while the peak within the insulation has disappeared. The gradient within the structural shell has increased to 2500°.

2. Coolant in Middle of Hastelloy

One way to reduce the temperature gradient within the structural shell is to locate the coolant within the wall. Passages could be provided in any one of the components. However, there would be no advantage in locating the coolant in the tungsten since this would not significantly affect the structural shell temperature due to the insulation in between. The pyrolytic graphite could not be used as a coolant location since it would react with the hydrogen. The coolant was, therefore, located within the Hastelloy.

Heat transfer runs were made with the coolant in the middle of the Hastelloy. The resulting steady-state temperature distributions are shown in Figures 26 and 27 for 100°R and 800°R coolant, respectively. The temperature difference has been split, 800° on the section nearest the graphite and less than 200° on the outer section. The higher gradient over the inner Hastelloy section is due to the greater heat flux coming through the pyrolytic graphite.

The average temperature in the inner half of the Hastelloy is 250°F and 900°F for coolant temperatures of 100°R and 800°R respectively at convection coefficients of 1000 and higher. At these temperature levels, there are materials available with yield strengths over 200,000 psi.

3. Coolant at Pyrolytic Graphite - Hastelloy Interface

The effect of locating the coolant passages at the pyrolytic graphite - Hastelloy interface on the temperature gradient was also investigated. The resulting steady-state temperature distributions are presented in Figures 28 and 29. The total gradient is now 1100° across the Hastelloy. The temperature levels are significantly higher than in the previous case for the same coolant temperatures and convection coefficient. The

advantage of this configuration is that the temperature drop is spread across the total Hastelloy thickness, resulting in a lower gradient.

The results of the coolant location investigation indicate that the average structural wall temperature can be reduced by locating the coolant within the wall, not necessarily at its center. This is desirable since the strength of the structural material increases rapidly as the temperature is reduced in the operating range. This effect may even warrant the use of multiple cooling passages in critical areas to further reduce the mean wall temperature. For example, one passage could be at the Hastelloy - pyrolytic graphite interface, and another near the outside diameter in the same wall.

The location of the coolant within the wall will present a problem. The pressure loads would have to be transmitted across the passage in order to make effective use of the outer material. This could result in design and fabrication difficulties.

The temperature gradient is affected by the location of the coolant at the inside or outside diameter of the Hastelloy. In both cases, the coolest and strongest material is adjacent to the coolant. Structural considerations would, therefore, require that the coolant be placed on the outer diameter since this is the location of the maximum hoop stress.

On the basis of the above reasoning, the coolant was located on the outer diameter of the wall.

C. Effect of Hastelloy Thickness

Additional runs were made with the coolant on the outer diameter, to determine the effect of the Hastelloy thickness on the heat flux to the coolant and the wall temperature

distribution. Thicknesses of .50 and .25 inches were considered. Resulting wall temperature distributions are shown in Figures 30, 31, 32 and 33. The temperature gradient in the half-inch material is 1500° while it is 750° in the quarter-inch section. The gradient per inch is thus constant.

The temperature level is considerably reduced within the thinner section. This is evident if we consider 2260°R as an upper design temperature for Hastelloy. With a 800°R coolant, it is impossible to adequately cool a half-inch wall, with convection coefficients as high as 4000. On the other hand, a quarter-inch wall can be efectively cooled with a coefficient as low as 500. The same effect is also shown for the lower temperature coolant.

The effects of the coolant convection coefficient and Hastelloy thickness are indicated in Figure 34. The temperatures of both the hot and cooled surfaces of the Hastelloy drop sharply as the coolant convection coefficient is increased up to 1000 BTU/Hr-Sq-Ft-Degree, where there is a sharp "knee". The temperature does not decrease significantly as the coefficient is increased above 1000. The Hastelloy thickness has a major influence on its maximum temperature, e.g., an increase from .25 to .50 inches results in a 1000° rise,from 1100° to 2100°R, when the convection coefficient is 1000. The cooled surface temperature is insensitive to Hastelloy thickness.

The effect of wall thickness on the heat flux to the coolant is shown in Figure 35. The flux rises as the coefficient is increased, at low values of the coefficient, for all wall thicknesses. However, there is a sharp "knee" at 1000 BTU/Hr-Sq.Ft-Degree. At higher coefficients, the flux remains constant.

The value of the flux decreases as the Hastelloy thickness decreases. This is to be expected, since there is less gamma heating within a thinner wall. There is also a five percent variation in flux due to the coolant temperature change from 100° to 800°R. This effect may be neglected, as a first approximation to simplify the over-all coolant temperature rise calculation.

At this point several trends can be identified from the limited cooling studies:

1. It is advantageous to use as thin a structural wall as possible, to reduce the temperature level within the wall.

2. The heat flux to be removed is independent of the coolant convection coefficient, for coefficients over 1000.

3. The flux may be controlled by varying the insulation thickness. This effect is limited by the insulation temperature capability, since a temperature peak can be expected in thicker insulation sections. The local gas convection coefficient would also have to be considered.

D. Stress Analysis

Up to this point, "ball park" numbers were used for the thickness of the structural wall. This was done to determine the effects of other parameters on the wall temperature, which must be known to compute the wall thickness. In order to refine the thermal studies a simplified stress analysis was made. A more refined study is not warranted at this time.

The converging section of the nozzle was divided into five stations, from the entrance to the throat, as shown in Figure 36. The wall thickness required to resist hoop tension was computed for selected materials at several wall temperatures. A conservative allowable stress, 20% below the .2% yield, was assumed. Where the .2% yield strength was not available, the lower stress rupture data was used. Thermal stresses were neglected.

The materials considered and their physical properties are listed in Appendix "E". Computed wall thicknesses for the various materials and temperatures considered are also contained in the same appendix.

The variation in wall thickness for selected materials, at the several stations is shown in Figure 37. For Hastelloy "W" at 1800°F, Curve "F", it varies from 2.7 inches at station 1 to .3 inches at the throat. For tungsten at 3000°F, Curve "C", 12 inches are required at the inlet, and 1.5 inches at the throat.

Curves D and E are of particular interest. Curve D, for both Rene 41 at 1600°F and 7178-6T aluminum at room temperature goes from .726 inches at station 1 to .089 inches at the throat. The thermal and nuclear properties of Rene 41 are similar to those of Hastelloy "W" and since its thickness is less than the .750 inches used for the Hastelloy, all the results obtained for Hastelloy can be applied to this material. The structural temperature in the improved uncooled wall was below 1600°F. It is therefore possible to obtain a thin structural wall by using Rene 41 since its strength at 1600°F is about four times that of Hastelloy "W" at 1800°F.

Aluminum, 7178-6T, looks particularly attractive. It is a light material, resulting in less gamma heating than nickel base alloys for the same gamma flux. It also offers a weight advantage over the heavier alternate materials. The requirement that it be maintained below room temperature can be met with 100°R coolant. It cannot be used, in these thicknesses with 800°R coolant. The thickness of the same material at 400°F, is indicated by Curve "B". Twice the thickness is needed at 400°F compared to room temperature.

Curve "E" for maraging steel is also of interest. The thickness varies from .36 inches at station 1 to .044 inches at the throat. The use of this material can result in a thin wall, but it must be maintained at a relatively low temperature, below approximately 1500°F to prevent loss of strength, and cooled during shutdown. It does not present as large a potential weight saving as aluminum.

The wall thicknesses of Curve "D" are as follows:

Station	Dia. (Inches)	Thickness (Inches)
1	72	.726
2	60	.602
3	48	.479
4	36	.348
5	23	.089

The above values were used in all subsequent calculations. Rene 41 replaced Hastelloy "W" since a structural wall less than half as thick can be used. The structural wall of the uncooled nozzle was also considered to be Rene 41, of the thickness shown above.

It is noteworthy that the structural wall is less than .1 inches thick at station 5. In the supersonic regions, stations 6 to 10 Appendix "D", the thickness decreases rapidly. This is due to the rapid decrease in the local gas pressure, reducing the pressure loads. While the wall in this region may have to be reinforced locally to resist vibrations, the diverging section will be much lighter than the converging. Cooling will also be easier since gamma heating will be reduced: First, due to the thinner sections; and second, because the gamma rays will have to pass through the converging section wall to reach the structural shell. Therefore, subsequent studies were limited to the more critical region of the nozzle from the entrance to the throat.

E. Rene 41 Wall, Temperature Distribution

The steady state temperature distribution in the cooled Rene 41 wall, with a coolant convection coefficient of 2000 BTU/HR.-SQ.FT.-Degree, is indicated in Figures 38 and 39. When the 100°R coolant is used, Figure 38, the highest temperature within the structural wall is 1900°R, or 1440°F. The Rene 41 thickness could therefore be reduced since it was sized on the basis of 1600°F. A temperature gradient of 1500° exists at station 2.

With the 800°R coolant, Figure 39, the highest temperature is 2460°R or 2000°F, at station 2. This is due to two causes: first, the pyrolytic graphite is too thick at this station; and second, the gamma heating rate is high at this location. The pyrolytic graphite thickness can be optimized at each station, based on the rate of gamma heating. It was not done in this preliminary study in order to simplify the analysis.

F. Aluminum Wall - Temperature Distribution

The temperature distribution in the aluminum wall, at four stations is shown in Figure 40. The highest temperature is 500°R, or 40°F, below the design value of 75°F. The maximum temperature gradient is only 200°, which is only a fraction of that in the Rene 41 wall. This is due to the lower gamma heating rate in the aluminum wall and also the higher thermal conductivity of the aluminum. The lower gamma heating rate can be seen in Figure 41. It is about half that of the Rene 41 at the outer diameter and almost the same at the pyrolytic graphite interface. Although there is a greater difference in the energy absorption attenuation coefficients of the two materials, the method of "weighting" these factors for a composite wall reduces the difference in actual gamma fluxes.

G. Coolant Temperature Rise - Rene 41

The total coolant temperature rise, from stations 1 to 5, for 5% coolant flow was computed. A heat balance was made at each station and the flux determined. In computing the local heat flux the station to station coolant temperature rise was neglected. This is valid since a 700° coolant temperature rise, from 100°R to 800°R only changes the flux 5%. The flux was averaged between stations, and the station to station temperature rise computed. The results for both the 100°R and 800°R coolants are presented in Table IV.

The total coolant temperature rise is 31.5° and 28.2° for the 100°R and 800°R coolants, respectively. This is a moderate temperature increase. The heated coolant can be used for further cooling after flowing through the nozzle. Thus, the use of 5% total flow for cooling appears to be attractive.

H. Coolant Temperature Rise - Aluminum Wall

The coolant temperature rise was also computed for the aluminum wall. The results are presented in Table V. The total coolant temperature rise is 27.8°. This is slightly less than that obtained for the Rene 41 wall due to the lower gamma heating.

I. Coolant Passage

Attention was directed to the cooling passage. The physical dimensions required to attain convection coefficients of 2000 with 5% flow in an annulus were computed. The convection coefficient was computed by using a modified Colburn equation:

$$\frac{h\, d_e}{k} = a\,(Re)^m\,(Pr)^n$$

Where:

h = Convection coefficient

d_e = Equivalent diameter
$2\,\delta$ where, δ = Annular Height of Cooling Passage

Re = Fluid Reynolds Number

Pr = Fluid Prandtl Number

k = Fluid thermal conductivity

a, m, and n are constants taken as follows:

$a = .023$

$m = .8$

$n = .4$

The calculated annulus heights in inches, at the several stations are shown on Figure 42. The separate values for the two coolant temperatures are due to variation in coolant properties at their respective temperatures and pressures. It is noteworthy that the gap heights are practical, easily obtainable dimensions. Other coolant passages could be studied, such as tubes, helical or straight, but the annulus is believed to be representative.

IV. START-UP AND SHUTDOWN

A. Start-Up

A brief study was made to determine the thermal effects of start-up. Before start-up, the composite nozzle wall has a flat temperature profile at all sections. As the hydrogen flow is started and the reactor core activated, the hydrogen is rapidly heated to its design temperature, in turn heating the exposed surface of the nozzle. The tungsten liner temperature rises rapidly, but the structural wall is protected by the insulation and should show a thermal lag.

The temperature history for the Rene 41 wall, at station 3, is indicated in Figure 43. The wall was assumed to be at 560°R before start-up. The effect of any other initial temperature will be to shift the time scale. After .17 minutes, the tungsten is at 4500°R and there is a 300° gradient across the structural shell. The gradient continues to rise until steady state is attained. In .37 minutes it is 700°, in one minute 1100°, and at steady state, in two minutes, 1200°. The corresponding thermal stress builds up during this period and reaches its maximum at steady state.

The tungsten liner, exposed to local static pressure loads, at elevated temperatures, tends to expand. It is restrained by the insulation and the cooler structure. The liner will therefore remain in contact with the insulation and be constrained to expand with it during the first heating cycle.

B. Shutdown

When the reactor is shut down, the power does not drop instantaneously to zero, but due to the radioactivity of the fission products it continues at lower levels as time after shutdown increases. An empirical relation for the power decay of a reactor, which has been operating long enough to have the

fission products at an equilibrium value, is shown in Figure 44. The power drops to 7 percent of its normal operating value, in one second. It continues to drop at a slow rate, reaching 1.8 percent in one thousand seconds.

During shutdown the heat produced by gamma attenuation must be removed or the wall may exceed its temperature limitations. In the case of the Rene 41 structural wall the heat removal can be obtained by allowing the rear surface to radiate to space. This requires a good conduction path across the coolant passage, which is also required by structural considerations, to transmit the pressure loads.

The temperature history of a Rene 41 wall, at station 3, radiating to space, during the early shutdown period is presented in Figure 45. At time zero, the wall is at its steady state operating temperature. As the power decays, heat is conducted from the hotter tungsten liner and pyrolytic graphite to the structural shell. This continues for 150 seconds, until the rear surface temperature is high enough to radiate at a rate that is equal to the sum of the rates of conduction and heat generation.

The wall temperature now begins to drop as the generation rate is reduced due to the power decay. The highest temperature within the structural wall is 2200°R at 150 seconds, 2000°R at 500 seconds, and 1800°R at 1000 seconds after shutdown. The temperature profile flattens rapidly, going from a temperature difference of 1200° across the Rene 41 at time zero, to 100° at 150 seconds. Power shutdown is thus a period wherein the thermal stresses in the wall are relieved.

The tungsten liner temperature drops rapidly, from 4500°R at time zero to 2800°R at 150 seconds. In 1000 seconds it is below 2000°R.

The possibility exists that a gap may form between the liner and the pyrolytic graphite, after a start-stop cycle. On start-up, the liner heats up rapidly and tends to expand. It is restrained by the cooler, stronger outside structure and is thus hot upset. During cooldown it is not restrained and can contract more than it expanded.

A gap could thus form within the wall that might cause the tungsten liner to fail during the next operating period. Liner failure can be prevented by programming the start-up sequence, so that the liner is heated to a higher temperature where it is more elastic before full pressure is applied. The above potential failure mode should be checked by more detailed analysis.

The decay temperature history for the aluminum wall is presented in Figure 46. The coolant flow rate was reduced to .5 percent of operating core flow. The same trends shown in the case of the Rene 41 are evident. The temperature rises for the first 15 seconds after which time it drops. The aluminum is maintained well within its allowable temperature range. It may even be possible to further decrease the coolant flow rate during shutdown.

V. WEIGHT ANALYSIS

An analysis was made to obtain comparative weights for the uncooled and the cooled nozzles. The weight of the internal gamma shields in the uncooled case were charged to the wall. Two cooled nozzles were considered: one with a Rene 41 wall; the other with an aluminum wall. The thickness of the structural wall was assumed to be the same at a station for the three nozzles considered.

The comparative weights per lineal inch of nozzle, along the wall, are presented in Figure 47. The aluminum wall is about one half the weight of the Rene 41 cooled wall, upstream of station 4. Past this point the ratio approaches one, since the structural material thickness decreases and its weight no longer predominates. The uncooled wall is over ten times the weight of the aluminum wall, due to the thick tungsten components required to reduce gamma heating to a tolerable level. The detailed weight computations are contained in Appendix "F".

The total weight of a nozzle, from station 1 to 5, is proportional to the area under its curve in Figure 47. The abscissa is considered to represent the station to station distance, along the wall. The distance between stations was assumed to be equal, although that between 4 and 5 is actually slightly larger than the others. The effect of this assumption on the total weights can be neglected since this is the lightest part of the nozzle.

The areas were obtained by numerical integration. The total nozzle weights, up to the throat, are 6232, 880 and 450 lbs., for the uncooled, cooled Rene 41, and cooled aluminum respectively. The weight saving in going from the uncooled to the cooled Rene 41 wall is 5352 lbs. which is significant. The cooled aluminum wall shows a 430 lb. advantage over the cooled Rene 41.

These potential advantages may be deceiving. Thus although the aluminum wall is the lightest, it is limited to a 100°R coolant and also requires coolant flow during shutdown. The cooled Rene 41 wall can use both the 100°R and 800°R coolants and can be radiation cooled during power decay. The uncooled wall, while the heaviest presents the potential of simplifying the nozzle - reactor interface and making the nozzle independent of the balance of the system, since only a "dead" connection is required. A systems study should be made to evaluate the tradeoffs among the three nozzle walls.

VI. RESULTS AND CONCLUSIONS

A. General

1. Both the uncooled and partially cooled concepts appear feasible for the design conditions specified.

2. The simpler uncooled nozzle weighs substantially more than the limited cooled configuration. Uncooled nozzles would be comparatively more advantageous for applications with lower gamma flux and/or shorter firing durations.

3. No adequate coatings apparently are available to replace tungsten on the gas side of the wall.

B. Uncooled Nuclear Nozzle

1. An uncooled nuclear nozzle wall is feasible for a 20-minute firing duration. The wall must be internally shielded by two three-eighths inch tungsten shells to reduce gamma heating to a tolerable level. These shields effectively reduce gamma flux by a factor of four.

2. The uncooled wall, including internal shields, weighs 6232 lbs., from inlet to nozzle throat.

C. Partially Cooled Nuclear Nozzle

1. Two nozzle walls that can be adequately cooled with 5% of core flow have been evolved. They both consist of: .0625 in. of tungsten; .125 in. of pyrolytic graphite and a structural shell. In one case, the shell is Rene 41, in the other, 7178-6T aluminum. The materials are the same thickness, varying from .726 in. at the inlet to .089 at the throat.

2. The aluminum wall configuration weighs 450 lbs. from the inlet to the throat. The weight of the Rene 41 is 880 lbs.

3. The Rene 41 wall can be adequately cooled during shutdown by radiation to space.

4. The aluminum wall requires 100°R coolant. Ten percent of the limited cooling flow is needed during shutdown.

5. The partially cooled nozzle concept has growth potential for application to more severe mission requirements.

VII. RECOMMENDATIONS

The present study has indicated the initial feasibility of both the partially cooled and uncooled nuclear nozzle concepts for the design conditions specified. The partially cooled nozzle, however, is considerably lighter and has growth potential for application to more severe mission requirements. It appears warranted to make a more detailed study of this concept in order to more fully describe the advantages and limitations of the concept, and to pinpoint and define potential problems. In addition, because of the simplicity and other potential system advantages of an uncooled nozzle, it appears fruitful to explore and define the mission conditions where these advantages can be utilized at a reasonable nozzle weight. The following areas of investigation are therefore recommended:

A. Partially Cooled Nuclear Nozzle

1. Optimize the nozzle wall thickness and configuration.

2. Conduct tradeoff studies between cooled nozzles of different construction.

3. Undertake material investigations aimed toward solution of fabrication problems, such as tungsten joining and utilization of composite material segmented construction.

4. Investigate the diffusion rate of hydrogen through tungsten at elevated temperatures and related material interface problems.

5. Study and design joints, seals, cooling passages and other mechanical details.

6. Conduct a detail study of start-stop conditions and associated potential mechanical problems.

B. Uncooled Nuclear Nozzle

1. Evaluate mission conditions at which a nozzle of reasonable weight can be utilized.

2. Conduct tradeoff studies with an equivalent nozzle of partially cooled construction.

APPENDIX A

METHOD OF COMPUTING TRANSIENT TEMPERATURES WITHIN THE NOZZLE WALL

INTRODUCTION

The nuclear nozzle wall is subjected to: 1) Newtonian heating at the gas interface; 2) conduction within the wall; 3) internal heat generation due to gamma attenuation; and 4) radiation to space. The partial differential equation for the temperature, for the one-dimensional case, becomes:

$$\frac{\partial^2 T}{\partial x^2} + \frac{q'''}{k} = \frac{1}{\alpha}\frac{\partial T}{\partial \theta} \qquad \text{(A-1)}$$

where: x = Space coordinate, feet

θ = Time in hours

$T(x,\theta)$ = Temperature within wall, at location x, and Time θ.

α = Wall material thermal diffusivity

$= k/\rho c$

Wall Material Properties

k = Thermal conductivity

ρ = Density

c = Specific heat

This appendix will describe the method of solving the finite difference approximation of Equation A-1, with the appropriate boundary conditions.

Division of Section:

The finite difference equations can be developed from simple heat balances. In brief, the method consists of dividing the wall up into thin slabs and considering heat balances on each slab during an elemental time period, $\Delta\theta$. The temperature of each slab is assumed to remain stationary for the period $\Delta\theta$, and all temperature changes take place instantaneously at the end of this period. This procedure is repeated until the temperature at all points for $n\Delta\theta$ time steps are computed.

In a composite wall, radiating to space, four types of equations will be required, for the physical situations: 1) at a heated surface; 2) within one material; 3) at an interface between adjacent materials; and 4) at the radiating surface. These equations will now be developed.

Consider the nozzle wall as a flat slab, and divide the first material in the cross section into an integral number of spaces, Δx apart. Number each point obtained consecutively, from the gas side, as indicated in Figure A-1. Now consider each point, or node as the limit of a small slab, Δx wide, extending $\Delta x/_2$ to either side, as its volume shrinks to a point.

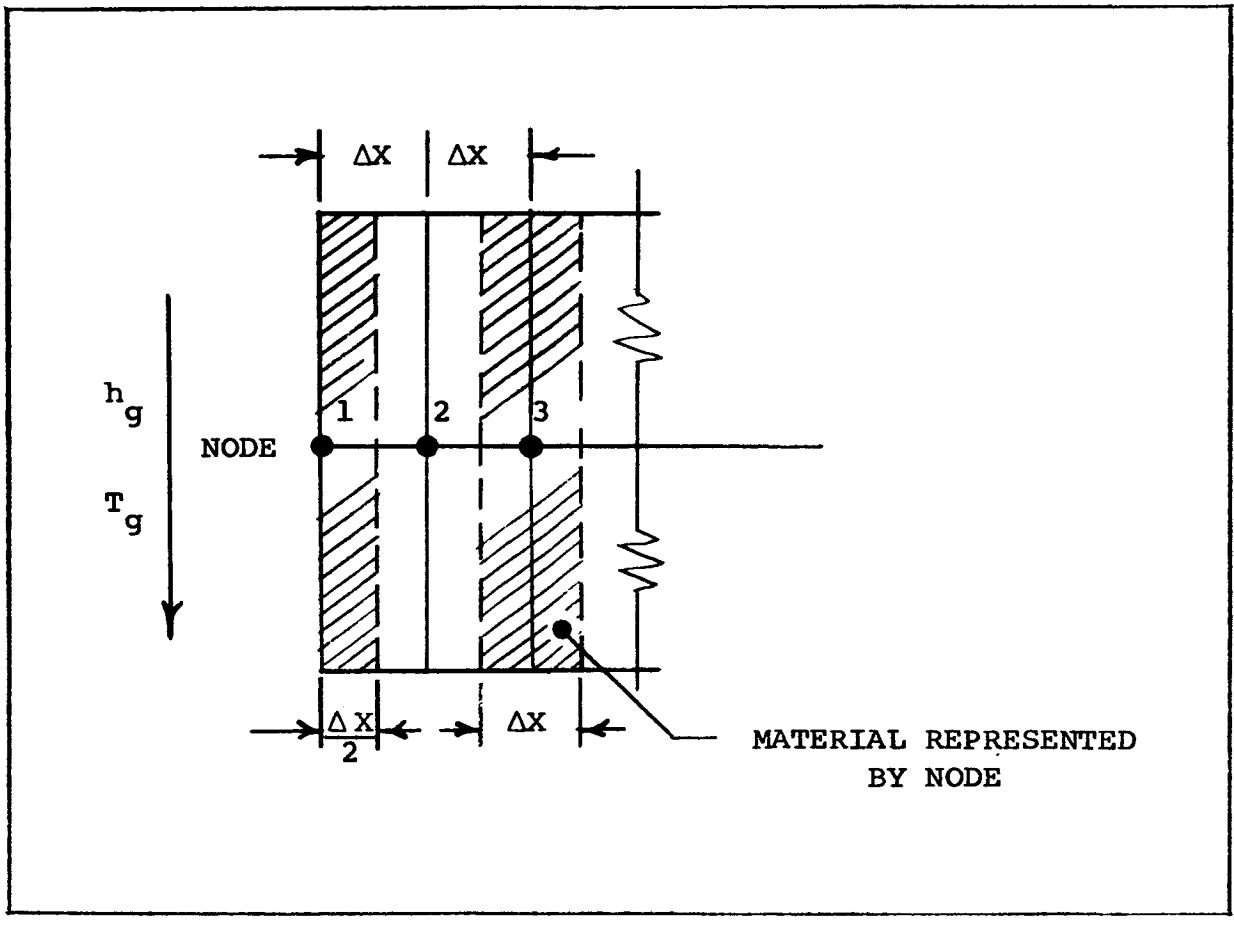

FIGURE A-1

SECTION THROUGH NOZZLE WALL
SHOWING DIVISIONS INTO NODES

Surface Equation:

A heat balance on the surface slab, node 1, during this period will contain the following terms:

1. Convection from the core gas:

$$\Delta q_{conv} = h_g A \left[T_g - T_1\right] \Delta\theta$$

2. Conduction from node 2:

$$\Delta q_{cond} = \frac{k}{\Delta x} A \left[T_2 - T_1\right] \Delta\theta$$

3. Heat generation within slab 1:

$$\Delta q_{gen} = q''' \frac{A \Delta x \Delta \theta}{2}$$

4. Heat stored:

$$\Delta q_{stored} = \rho \frac{c A \Delta x}{2} \left[T_1' - T_1\right]$$

Where: T_g = Gas temperature

h_g = Gas convection coefficient

T_1 = Node 1 temperature at start of time period, θ.

T_1' = Temperature at Node 1 at time $\theta + \Delta\theta$.

The heat balance may be written:

$$\Delta q_{conv} + \Delta q_{cond} + \Delta q_{gen} = \Delta q_{stored}$$

Now by defining the following non-dimensional groups:

$$N = \frac{h_g \Delta x}{k}, \text{ Nusselt Number}$$

$$M = \frac{\rho c}{k} \frac{(\Delta x)^2}{\Delta \theta} = (\text{Fourier Number})^{-1}$$

And solving for the surface temperature, T_1' at the next time increment, the following relation is obtained:

$$T_1' = \frac{2N}{M} T_g + \frac{2}{M}\left[\frac{M}{2} - 1 - N\right] T_1 + \frac{2}{M} T_2 + q''' \frac{(\Delta x)^2}{km} \qquad (A-2)$$

Interior Equation:

In a similar manner, a heat balance on an interior node, within one material results in:

$$T_n' = \frac{T_{n-1}}{M} + \frac{1}{M}\left[M-2\right] T_n + \frac{T_{n+1}}{M} + q''' \frac{(\Delta x)^2}{kM} \qquad (A-3)$$

Where: n = Node in question

n-1 = Previous Node, to the left

n+1 = Succeeding Node, to the right

Interface Equation:

At an interface between material "a" and "b", the interface node, is made up of two half slabs, $\Delta x_a/2$ and $\Delta x_b/2$. The

interface equation can be derived as:

$$T_n' = \frac{2}{S} T_{n-1} + \frac{1}{S}\left[S-2R-2\right] T_n + \frac{2R}{S} T_{n+1} + \left[\frac{P_a + P_b R}{S}\right] \quad \text{(A-4)}$$

Where: n = Interface Node
n-1 = Adjacent Node in material "a"
n+1 = Adjacent Node in material "b"
R = Relative resistance = $\left[\frac{k}{\Delta x}\right]_b \left[\frac{\Delta x}{k}\right]_a$

$S = M_a + RM_b$

$P_a = \left[\frac{(\Delta x)^2 q'''}{k}\right]_a$

$P_b = \left[\frac{(\Delta x)^2 q'''}{k}\right]_b$

Subscripts: "a" and "b" refer to the respective materials.

Final Node:

The node on the wall cool side radiates to space. Assuming space is at zero degrees Rankine, a heat balance at this node results in:

$$T_n' = \frac{2 T_{n-1}}{M} + \frac{2}{M}\left[\frac{M}{2} - 1 - \frac{\sigma \varepsilon T_n^3}{k} \Delta x\right] T_n + \frac{\Delta x^2}{kM} q''' \quad \text{(A-5)}$$

Where: n = Final Node
σ = .171 X 10^{-8} BTU/hr-ft^2-°R^4
ε = Wall Emissivity

By using the equations on the following page, based on wall properties and slab geometry, the transient temperature can be built up, one time step at a time. The procedure is too long for hand computation, and an existing ARDE-PORTLAND 704 computer program is used.

Stability of Solution:

The several equations are of the form:

$$T'_n = AT_{n-1} + BT_n + CT_{n+1} + D$$

Where the coefficients A, B and C operate on the known temperatures at adjacent nodes, to compute the temperatures at a node at a future time. Now since physical considerations require that the coefficients do not become negative, this is the basis for a stable solution.

Thus at a surface node, equation (A-2), $B = \frac{2}{M}\left[\frac{M}{2} - 1 - N\right]$ requires that $M \geqslant 2+2N$.

Within a given material, equation (A-3), $B = \frac{1}{M}\left[M-2\right]$ and $M \geqslant 2$.

Other criteria are obtained from the interface and radiating node equations. In any given problem, all these criteria must be satisfied in order to obtain a stable solution.

Procedure

The material on the gas side is tentatively divided into an integral number of slabs Δx wide, and a value of "M" chosen to satisfy the stability criterion of equation (A-2). The time step, $\Delta\theta$, is now established, since:

$$\Delta\theta = \frac{(\Delta x)^2}{\alpha M}$$

This time step must be used for all the other material in the wall, to obtain a valid solution. Therefore, the following relation must apply:

$$\left(\frac{(\Delta x)^2}{\alpha M}\right) = \left(\frac{(\Delta x)^2}{\alpha M}\right)_a = \left(\frac{(\Delta x)^2}{\alpha M}\right)_b = \left(\frac{(\Delta x)^2}{\alpha M}\right)_i$$

Where the unsubscripted values refer to the first material, while "a", "b",.....and "i" refer to the subsequent materials within the wall. The above equation determines the ratios of Δx, α , and M for each material, and together with the stability criteria, dictate the number of nodes to be used.

APPENDIX B

GAMMA HEATING

SUMMARY

This section briefly reviews the methods and procedures used to determine the rate of gamma heating within nuclear nozzle walls. The local rate of energy deposition at selected points is obtained by means of the Los Alamos QAD IV Computer Program. This data is converted into local heating rates by the use of the appropriate wall material nuclear properties and buildup factors. The resulting distribution of gamma heating is presented for a representative wall.

The Gamma Ray Energy Fluxes

In order to obtain the geometrical distribution of the rate of energy deposition in the walls of the nozzle, we require a method for calculating the gamma ray fluxes and their energy distribution or, the integrated energy flux, Γ (mev/cm^2 sec) at points within the walls due to radiation from the distributed reactor source. These energy fluxes were obtained by using the Los Alamos QAD IV computer program which is briefly described below.

The Los Alamos QAD IV Program

The QAD is a 704/7090 computer program which calculates the gamma radiation from a distributed source (in our case, the reactor) and through attenuating materials, whose boundaries can be described by quadratic surfaces. Provision is made for specifying a distributed source which is then divided into a number of point isotropic sources of discrete energy groups and normalized to give the desired total power. The program determines the line-of-sight distances through each attenuating material from a source point to a detector point, then uses exponential attenuation (with energy dependent mass attenuation coefficients) and a single buildup factor. This process is continued for each source point and for all energy groups; finally, these contributions are summed for each detector point. This program, as well as a preliminary description, was made available to Arde-Portland by the Los Alamos Scientific Laboratory through the NASA Lewis Research Center.

The energy dependent gamma attenuation coefficients for the materials in the system (reactor and nozzle walls) can be specified for the different regions. By introducing fractional and absolute densities, the attenuation coefficients for mixtures or chemical combinations of materials in different regions are automatically determined by the program according to the formula

$$\frac{\mu}{\rho} = \frac{1}{\rho} \sum \left(\frac{\mu}{\rho}\right)_i \rho_i \qquad (1)$$

Where $\frac{\mu}{\rho}$ (cm^2/gm) is the mass attenuation coefficient of the mixture or composition and ρ_i the fractional density of material i, where $\rho = \sum_i \rho_i$

The energy buildup factor in the program is computed from the polynomial expression

$$\beta_E(\mu t, E) = \sum_{i=0}^{3} \beta_i(E)(\mu t)^i \qquad (2)$$

Where the polynomial coefficients, β_i, are energy dependent and μt is the attenuation length or mean free path. The coefficients for the polynomial fit are given in General Electric Apex 510.

Since the program provides for the use of only one buildup factor, the appropriate choice of this factor requires some care. This will be discussed below.

A schematic section of the nuclear nozzle is shown in Figure 1. The wall is of multi-layered construction with receiver points indicated where the rates of energy deposition are to be computed.

A typical QAD IV printout is presented in Figure 2. The receiver points are identified with the flux for each of the energy groups indicated, and summed. Two sets of values are shown: 1) minimum, where a buildup factor of one is used; 2) maximum, using a specified buildup factor.

The Calculation of Heating Due to Gamma Rays

The rate of heat deposition at a point in the nozzle wall from scattered and unscattered gamma radiation is given by

$$\dot{q}''' = 1.55 \times 10^{-9} \mu_a \beta_a(\mu t, E) \Gamma \qquad (3)$$

Where μ_a (cm^{-1}) is the energy absorption attentuation coefficient (energy dependent) at the point in the material, $\beta_a(\mu t, E)$ is the energy absorption buildup factor chosen for the photon energy E, material and the number of relaxation lengths μt. Γ is the energy flux (mev/cm^2- sec) for the unscattered gamma ray flux at the point. The use of the buildup factor $\beta_a(\mu t, E)$ accounts for the scattered radiation.

In the application of Equation 3 to the calculation of the rate of heating at any point in the nozzle wall, the following procedure was used to evaluate the terms. The number of mean free paths μt to a point was calculated by traversing the wall normally to the point in question. This, of course, is only an approximation for all the line-of-sight paths from the source points. However, since $\beta_a(\mu t, E)$ does not vary greatly for small values of μt the approximation is not unreasonable. $\beta_a(\mu t, E)$ is also dependent on the attenuating material (or Z value) and was determined as follows. The attenuation coefficients were calculated on the assumption that the multilayered material along the path of the radiation could be replaced by a homogeneous material of the same composition. By comparison of a μ/ρ vs. E plot with a similar plot for materials of known Z values, the best material (or Z value) is determined. The same procedure was used in determining, β_E, the energy buildup factors.

The Buildup Factors

It has already been pointed out that the QAD program makes provisions for a single buildup factor. If this is the energy buildup factor β_E, it will account for the scattered radiation, since the line-of-sight method computes only the direct or unscattered component.

In the selection of this factor, some choice or compromises must be made since the reactor materials and nozzle walls require distinctly different buildup factors. For reasons which are explained below, the buildup factor, β_e, which was used in the QAD program was selected as most appropriate to the attenuating material in the reactor. One reason is that the number of mean free paths through the reactor materials is larger than through the thin nozzle walls. Furthermore, as may be seen from Equation 3, Γ in this equation is the unscattered energy flux. It is, therefore, necessary to derive from the energy fluxes given by the QAD program the unscattered energy fluxes required in Equation 3. This means that we must remove the influence of the energy buildup factor, β_e, from the QAD data (but only for the path through the nozzle walls). The selection of β_e for the program should, therefore, be primarily concerned with the reactor materials only. On the basis of the method discussed in the previous section, the nuclear properties of aluminum are a close approximation of those of the reactor materials. A buildup factor of aluminum was therefore used.

The effect of using this buildup factor, compared to a factor of one can be seen by comparing Figures 4 and 5. Figure 4 shows gamma flux distributions, using a buildup factor of unity while gamma fluxes in the same wall with an aluminum buildup factor are presented in Figure 5. It is evident that the local values are increased by a factor of three.

It might be noted from Equation 3 that actually an interchange in buildup factors (β_a for β_e) is required.

These problems lead to the necessity of determining the average energy of the radiation at points in the nozzle wall since their buildup factors (as well as the other nuclear constants) are energy dependent.

The Gamma Ray Energy At A Point In The Nozzle Wall

The energy absorption and mass attenuation coefficients in Equation 3, as well as $\beta_a(\mu t, E)$, are energy dependent and

it is, therefore, necessary to devise a means for determining the average energy of the radiation at a point in the nozzle wall. This has been done in two ways.

The QAD program prints out the gamma ray energy flux for a designated number of discrete energies (in this case, 10 groups), as well as the total energy flux. Hence,

$$\sum_{i=1}^{10} \left(\frac{\Gamma}{E}\right)_i = \frac{\Gamma_{TOTAL}}{E_{AV}} \qquad (4)$$

This gives E_{AV}, the average energy of the radiation at the point.

Equation 4, though simple, is, however, in practice, complicated by the fact that the energy fluxes, Γ_i in this equation, represent both the scattered and unscattered radiation and were calculated by means of an unrepresentative buildup factor β_E. E_{av} is then a somewhat dubious value, though it is probably not too unreasonable as an approximation. To check this, another method was used.

A simplified version of how this average energy is calculated by this second method is now given. We assume that at two neighboring points in the same material, the relation between the energy fluxes is approximately

$$\Gamma_2 = \Gamma_1 e^{\mu(E)\Delta t} \qquad (5)$$

where Δt is the known distance between the two points. From this $\mu(E)$ and hence E, the energy in the interval Δt can be approximated. In this way, values of E_{av} are obtained at points within the wall that are believed to have some validity.

Figure 6 shows the variation of the buildup factors β_E, β_a and E in a typical nuclear nozzle wall. It should be noted that the ratio of buildup factors, β_a/β_E is approximately equal to 1.1, throughout the nozzle wall. This suggests a simple way to correct the QAD results by interchanging β_a for β_E, namely by multiplying by 1.1.

Nuclear Data

The mass attenuation and energy absorption coefficient were taken from the literature, mostly from LA-2237. The values used for several elements are indicated in Figures 8 and 9. Those for alloys and compounds were derived by using Equation 1 and are shown in Figures 10 and 11.

The wall materials and their densities are presented in Table 1. Table II lists their gamma attenuation coefficients.

APPENDIX C

METHOD OF CALCULATING
CORE GAS CONVECTION COEFFICIENTS

CALCULATION OF CORE GAS CONVECTION COEFFICIENTS

An equation for the core gas convection coefficient, in convergent - divergent nozzles was derived in the following reference:

Bartz, D.R., "A Simple Equation For Rapid Estimation of Rocket Nozzle Convective Heat Transfer Coefficients" Jet Propulsion, Vol. 27, Number 1, Pgs. 49-51. (Jan.1957)

The equation is:

$$h_g = \left[\left(\frac{.026}{d_*^{.2}}\right)\left(\frac{\mu^{.2} C_p}{P_r^{.6}}\right)\left(\frac{P_c\, g}{C^*}\right)^{.8}\left(\frac{d_*}{r_c}\right)^{.1}\right]\left(\frac{A^*}{A}\right)^{.9}\sigma$$

where:

h_g = Local Convection Coefficient BTU/IN^2-Sec-°

d_* = Throat Diameter - Inches

μ = Gas Viscosity - Lbs/In.Sec.

C_p = Gas Specific Heat - BTU/LB-°

P_r = Gas Prandtl No. = $C_p \mu / k$ (Non Dim.)

k = Gas Thermal Conductivity

p_c = Chamber Pressure - Lbs/In^2

g = Gravitational Const. = 32.2 Ft./Sec^2

C^* = Nozzle Characteristic Velocity - Ft/Sec

r_c = Throat Radius of Curvature = d_*

A^* = Cross Sectional Flow Area at Throat - In^2

A = Local Cross Sectional Flow Area

σ = Correction Factor For Variation of Gas Properties Across the Boundary Layer

$$\sigma = \frac{1}{\left[\frac{1}{2}\frac{T_w}{T_o}\left(1+\frac{\gamma-1}{2}M^2\right)+\frac{1}{2}\right]^{.8-\omega/5}\left[1+\frac{\gamma-1}{2}M^2\right]^{\omega/5}}$$

T_w = Local Wall Temperature °R

T_o = Combustion Temperature (Stagnation) °R

M = Local Mach Number

γ = Ratio of Specific Heats, Dimensionless

ω = Temperature Exponent in Viscosity Equation

$(\mu \sim T^{\omega})$ = .60

The equation is based on the observation, by Bartz, that is his,

"An Approximate Solution of Compressible Trubulent Boundary-Layer Development and Convective Heat Transfer in Convergent-Divergent Nozzles". Trans. ASME, Nov. 1955.

The dominant variable factor, (under certain conditions), in the mass flow rate per unit area, and that the variations in velocity and temperature boundary layer thickness exert only secondary influences. The resulting relation is made non-dimensional, and after simplification, the equation presented on Sheet 1 is obtained.

The term within the square brackets, on the right hand side of the equation is a constant for any given nozzle, and so the local value of hg varies as $(A^*/A)^{.9} \times \sigma$

Since $(A^*/A)^{.9}\sigma \cong 1$ at the throat, $\gamma = 1.34$

then $h_g = h_g^*$

where: h_g^* = Throat Convection Coefficient for the given nozzle

Now $h_g^* = \left[\left(\frac{.026}{d_*^{.2}}\right)\left(\frac{\mu^{.2}c_p}{P_r^{.6}}\right)\left(\frac{P_c g}{C^*}\right)^{.8}\left(\frac{d_*}{r_c}\right)^{.1}\right]$

$= \left[(\alpha)\ (\beta)\ (\delta)^{.8}\ (r)^{.1}\right]$

Where each term corresponds directly to the term in the equation above.

Examining Each Term:

α is proportional to $d_*^{-.2}$

β depends on the gas properties μ, C_p, P_r

$\delta = \frac{P_c g}{C^*} = \frac{\dot{\omega}}{A_t} = \frac{f(M)}{\sqrt{T}} P_c$, where:

$\dot{\omega}$ = nozzle flow - Lbs/Sec

A_t = A* = Throat Area -IN^2

$f(M)$ = Mach Number Function ($\sin \frac{P}{P_c}$)

= Constant for γ = Const.

$\delta^{.8}$ is proportional to $(P_c)^{.8}$ when

Combustion Temperature, T is Const.

$\Gamma \cong 1$ and may be neglected

To Recapitulate: h_g^* is proport. to $\left[\frac{P_c^{.8}}{d_*^{.2}}\right]$

For Nozzles With:

1. Similar Combustion Gases (μ, C_p, P_r)
2. Similar Combustion Temperature
3. γ = Constant or close to each other

The transport properties for 4500°R hydrogen[+] are:

$$k = .524 \text{ BTU/HR-FT-}^\circ\text{R}$$

$$C_p = 4.241 \text{ BTU/LB-}^\circ\text{R}$$

$$\mu = 25.0 \times 10^{-6} \text{ LBS/FT-SEC.}$$

The computed convection coefficients at the throat and upstream at an area ratio of 6.8 are respectively:

$$h_g^* = 4950 \text{ BTU/HR-FT}^2\text{-degree R}$$

$$h_g = 830 \text{ BTU/HR-FT}^2\text{-degree R}$$

THE EFFECT OF A CHANGE IN CHAMBER PRESSURE, P_c, ON THE CONVECTION COEFFICIENT, h_g^*

In a given nozzle h_g^* is proportional to $\frac{P_c^{.8}}{d_*^{.2}}$

If the chamber pressure is changed, a change in gas flow rate will result. For a moderate pressure variation, there will be no change in specific impulse, and the throat area will have to be adjusted to maintain thrust constant

$$\frac{\dot{W}}{A} = \mathcal{F}\frac{(M)}{\sqrt{T}} P_c \text{ , or } \dot{W} \text{ is proportional to } d^2 P_c$$

for constant $\dot{W}$, d_* is proportional to $\frac{1}{P_c^{.5}}$

and h_g^* is proportional to $\frac{P_c^{.8}}{\frac{1}{P_c^{.1}}} = P_c^{.9}$

[+] Durham, F.D., and Orndorff, J.D., "Nuclear Propulsion, Handbook of Astronautics", Koelle, H.H. ed. McGraw-Hill Book Company, 1961, Chapter 21.1

APPENDIX D

COATINGS TO REPLACE TUNGSTEN LINER

COATINGS TO REPLACE TUNGSTEN LINER

Summary

In general, refractory ceramic material offer little hope as replacements for the tungsten liner under the stringent operating conditions. Of the materials discussed, only the borides may possibly retain sufficient structural integrity to withstand the required temperature. The chemical interaction of the borides with carbon will have to be investigated and barrier layers developed to prevent the formation of low melting point intermetallic compounds. It is very probable that refractory carbides will form at the coating - graphite interface. Their inability to resist the thermal shock of three heating - cooling cycles would be a limitation. However, the materials may be so arranged that a stable carbide is formed.

Literature Search*

A literature search was made to identify materials that showed potential as substitutes for the tungsten liner. The wall was visualized as: (1) an outer structural metal shell; (2) an insulation, such as pyrolytic graphite; and (3) a coating material on the graphite to contact the hot hydrogen.

Required material properties for this application, include: (1) structural stability at the operating temperature, over 4500°F; (2) chemical stability, when in contact with 4500°F hydrogen, for three 20 minutes periods; (3) thermal shock resistance to withstand three heating-cooling cycles.

Candidate materials for this application can be initially screened by considering their melting points. Materials with melting points around 4532°F or 2500°C, are not expected to have sufficient structural integrity in their plastic condition at the operating temperature to withstand the scrubbing action of the high velocity hydrogen.

- - - - - - -

* A brief bibliography is included at the end of this Appendix.

Silicides and Beryllides

On this basis, the silicides and beryllides can be eliminated since none of these materials for which data exists remain solid over 4500°F. For example, tantalum disilicide, $TaSi_2$, the silicide with the highest melting point, liquefies at 4352°F. Molybdenum and tungsten disilicides follow with melting points around 3632°F. The beryllides follow, melting under 3632°F, with the possible exception of hafnium beryllide, Hf_2Be_{21}, for which incomplete data exists.

Classes of materials that pass the melting point criterion are the oxides, borides, carbides, and nitrides.

Oxides

Oxide	Melting Point °C	Melting Point °F
Beryllia (BeO)	2550	4622
Calcia (CaO)	2600	4712
Ceria (CeO_2)	2600	4712
Zirconia (ZrO_2)	2677	4851
Hafnia (HfO_2)	2777	5031
Magnesia (MgO)	2800	5072
Thoria (ThO_2)	3300	5972

The oxides can be eliminated on the basis of the other requirements. For example, calcia lacks structural and chemical stability, while thoria and ceria have poor thermal shock resistance. Although beryllia, thoria, and zirconia are the most stable at elevated temperatures, they cannot be expected to withstand the severe reducing environment of 4500°F hydrogen on one surface, and the same temperature graphite on the other. The oxides thus offer little hope as substitutes for tungsten in this application.

Borides	Melting Point °C	°F
Titanium Boride (TiB_2)	2980	5396
Zirconium Boride (ZrB_2)	3040	5504
Hafnium Boride (HfB_2)	3250	5882
Tantalum Boride (TaB_2)	>3100	>5612

The borides, as a group, demonstrate high stability under reducing atmospheres. However, their stability in the presence of high temperature carbon has not been clearly demonstrated. Useful strength above 3992°F has not been indicated. Their lack of low temperature ductility, as exemplified by the need for diamond grinding finishing operations, pose potential fabrication problems. Present fabrication methods have resulted in simple shapes up to 1.5 ft. in diameter and height. The borides should have reasonably good thermal shock resistance, especially when compared to other ceramics. The borides definitely hold more promise as a coating material than do the oxides.

Carbides	Melting Point °C	°F
Silicon Carbide (SiC)	2850	5162
Boron Carbide (BoC)	2450	4442
Hafnium Carbide (HfC)	3890	7034
Columbium Carbide (CbC)	3500	6332
Tantalum Carbide (TaC)	3880	7016
Titanium Carbide (TiC)	3100	5612
Zirconium Carbide (ZrC)	3530	6386
Tungsten Carbide (WC)	2870	5198
4 Tantalum Carbide. 1 Hafnium Carbide (4TaC:1HfC)	3942	7128

Carbides have higher melting temperatures than any other materials. However, they are synthesized materials and, therefore, exact stoichiometry is not always attainable and reproducible to yield the attractive high melting point compounds. Their extreme hardness and lack of ductility make fabrication difficult. Poor thermal shock resistance also limits their usefulness under thermal cycling conditions. Meager specific data exists regarding their chemical stability with 4500°F hydrogen, but it is reasonable to assume that reactions forming unstable hydrides and hydrocarbons would occur. Eutectic reactions between carbides and graphite do occur at temperatures above 4000°F.

Nitrides	Melting Point	
Nitride	°C	°F
Boron Nitride (BN)	3000	5432
Titanium Nitride (TiN)	2940	5324
Zirconium Nitride (ZrN)	2980	5396
Hafnium Nitride (HfN)	3310	5990
Tantalum Nitride (TaN)	2890	5234

The use of nitrides has been limited because they are extremely brittle, difficult to sinter, and fairly volatile. Hence very little data exists in the temperature range of interest. Stability is greatest in nitrogen environments and loss of stability and stoichiometry of the synthesized nitride compounds is to be expected when exposed to 4500°F hydrogen and graphite.

Bibliography

High Temperature Materials

Campbell, I.E., "High Temperature Technology", New York: John Wiley and Sons, Inc., 1956.

Schwarzkopf, P., and Kieffer, R., "Refractory Hard Metals", New York: MacMillan Co., 1953.

Latva, J.D., "Selection and Fabrication of Nonmetallics - Oxides, Beryllides and Silicides", Metals Progress, Nov. 1962.

Latva, J.D., "Selection and Fabrication of Ceramics and Intermetallics", Metals Progress, Oct. 1962.

Hauck, J.E., "Guide to Refractory Ceramics", Materials in Design Engineering, 1963.

Hausner, F., and Friedemann, H., "High Temperature Compounds Data Book", General Astrometals Corp., July, 1962.

APPENDIX E

STRESS ANALYSIS - NOZZLE WALL THICKNESS DETERMINATION

INTRODUCTION

A simplified stress analysis was made to determine the thickness of the structural wall of the nuclear nozzle. This section covers the methods used, lists the properties of materials of interest at several temperatures, and presents wall thicknesses for the various materials.

METHOD

Consider the nozzle shown below. Neglect thermal stresses and assume that the internal pressure forces are resisted by the outer structural shell. The resulting hoop stress at a station in a thin wall is equal to:

$$s = \frac{PR}{t}$$

where: s = local hoop stress, psi
P = local static pressure, psi
R = local radius, normal to the surface
t = local wall thickness

Now make the conservative assumption that the allowable stress is 20% below .2% yield at the temperature of interest.

The required wall thickness is:

$$t = \frac{PR}{s_a} = \frac{PR \times 1.2}{Y}$$

where: s_a = allowable stress, psi
Y = .2% yield stress of wall material

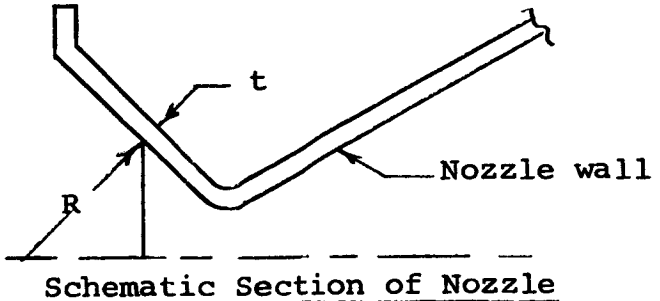

Schematic Section of Nozzle

MATERIAL PROPERTIES

The structural properties of the materials considered for the nozzle wall are listed in the following tables. Both the ultimate tensile and the .2% offset yield strengths fall as the temperature is increased, the offset yield at a lower rate. The yield strength varies by a factor of 3 for Rene 41 from room temperature to 1700°F, from 155 ksi to 50 ksi. Hastelloy "W" has a yield that drops from 39 ksi at 1000°F to 22 ksi at 1800°F.

There are also lower temperature high strength materials such as 300K maraging steel and 7178-6T aluminum. The yield of the maraging steel goes from 295 ksi at 25° to 168 ksi at 1000°F. For aluminum, it drops from 84 ksi at 75° to 45 ksi at 400°F.

NOZZLE WALL THICKNESS

The resulting wall thicknesses for the materials considered are tabulated in this section. The thickness for several selected materials at the stations indicated in Figure 36, are presented in Figure 37. For Hastelloy "W" at 1800°F, Curve "F", it varies from 2.7 inches at Station 1 to .3 inches at the throat. For tungsten at 3000°F, Curve "C", 12 inches are required at the inlet, and 1.5 inches at the throat.

Curves "D" and "E" are of particular interest. Curve "D", for both Rene 41 at 1600°F and 7178-6T aluminum at room temperature goes from .726 inches at Station 1 to .089 inches at the throat. Aluminum 7178-6T looks particularly attractive. It is a light material, resulting in less gamma heating than nickel base alloys for the same gamma flux. It also offers a weight advantage over the heavier alternate materials.

Curve "E" for maraging steel is also of interest. The thickness varies from .36 inches at Station 1 to .044 inches at the throat. The use of this material can result in a thin wall, but it must be maintained at a relatively low temperature, below approximately 1500°F to prevent loss of strength, and cooled during shutdown.

MATERIAL PROPERTIES

HIGH STRENGTH MATERIALS

MATERIAL	TEMP.	UTS*	.2% Y**	E
18% 300 KSI Maraging Steel	25	295	293	
	500	263	254	
	1000	180	168	
Allegheny Ludlum R 41 (Fe-Ni) (Rene 41)	RT	205	155	31.6
	500	203	150	29.6
	1000	202	145	27.3
	1500	130	125	24.0
	1700	55	50	21.8
	1800			
Allegheny Ludlum AF 71 (Fe)	RT	150	105	28.8
	500	130	105	27.5
	1000	110	95	22.5
	1500	50	45	20.5
	1600	40	37	
	1800	?	?	
UNI TEMP L-605	RT	160.7	85	35.3
	500	148	67	
	1000	130.6	53.9	
	1500	55.3	44.9	
	1800	29.2	27.5	
Allegheny Ludlum V 36 (Co-CR-Ni)	RT	145	82	32.5
	500	138	72	31
	1000	120	60	27.5
	1500	68	50	24
	1800	25	23	22
Haynes Alloy #25	RT	146	67.2	32.6×10^6
	500	127.6	44	29.8
	1000	115.7	35.8	27
	1500	57.5	36.5	23.7
	1800	34.4	23.1	21.2
Hastelloy X	RT	113.2	55.8	
	500	100	47	23
	1000	93	42.5	22
	1500	50	34	19.5
	1800	21	17	

* Ultimate Tensile Strength

** .2% Offset Yield Strength

E Young's Modulus

MATERIAL	TEMP.	UTS	.2% Y	E
Hastelloy "W"	1000	101.4	39.3	30.75×10^6
	1400	70.0	37.8	
	1600	59.8	35.8	
	1800	38.2	22.1	
Hastelloy C	RT	129.5		28.5
	500	117		
	1000	106	48	
	1500	50.7		
	1800	21		
Aluminum 7178-6T	75	92.9	83.9	
	212	86.5	76.9	
	300	69.0	62.0	
	400	49.5	45.0	

MATERIALS THAT ARE READILY FABRICATED

301 Stainless Steel	RT	92	40	
	500	83.5	32	
	1000	76.5	25.5	
	1500	32.5	19	
	1800	16	9	
INCONEL X	RT	162	92	31
	500	158	90	
	1000	140	84	
	1500	52	44	
	1800	9	5.5	

HIGH TEMPERATURE MATERIALS

Tungsten (A)	2500	56	46	SOURCE (A)#
	3000	35	27	
	3500	14	9	
Tungsten (B)	2500	44	38	SOURCE (B)#
	3000	28	22.5	
	3500	13	7.5	
Tungsten (C)	2500	35	30	SOURCE (C)#
	3000	24	6	
	3500	16	5	

Tungsten Properties from Hughes Tool Company - Aircraft Division

MATERIAL	TEMP.	UTS .2% Y	E
Tungsten + 2% TH O_2		Stress Rupt. 1/2 Hr.	
	2500	38	
	2700	24	
Tungsten		Stress Rupt. 1/2 Hr.	
	2700	16	
	3000	10	
Tungsten - Tant. (90TA + 10W)		Stress Rupt. 4 Minutes	
	2500	22	
	3000	19	
	3200	15	
	3800	8.5	
Columb.-Tant.- Tungsten		Stress Rupt. 4 Minutes	
	2730	12.5	
	2970	8	
	3200	6.5	
	3500	4.5	
Columb.-Tant.- Molybd.		Stress Rupt. 4 Minutes	
	2400	14	
	2750	13	
	2800	10 1/2	
	3000	8	

MATERIAL: ALUMINUM 7178-6T

MATERIAL: HASTELLOY "W"

STATION	75 S=69916	212 S=64083	300 S=51666	400 S=37500	1000 S=32749	1400 S=31499	1600 S=29833	1800 S=18416
1	.726	.793	.984	1.355	1.552	1.613	1.703	2.759
2	.602	.658	.816	1.125	1.288	1.339	1.414	2.290
3	.479	.523	.649	.894	1.023	1.064	1.123	1.870
4	.348	.380	.472	.650	.744	.774	.817	1.323
5	.089	.097	.120	.165	.189	.197	.208	.337

MATERIAL THICKNESS AS A FUNCTION OF NOZZLE STATION AND WALL TEMPERATURE

MATERIAL: HAYNES ALLOY #25

STATION	SLANT RADIUS INCHES	LOCAL STATIC PRESSURE	STRENGTH AT TEMP.	S^{500}=36670	S^{1000}=29830	S^{1500}=30410	S^{1800}=19250
1	50.92	998	t=.907	t=1.386	t=1.704	t=1.671	t=2.640
2	42.43	994	.753	1.150	1.414	1.387	2.191
3	33.95	987	.598	.914	1.123	1.102	1.741
4	25.46	959	.436	.666	.819	.803	1.268
5	11.50	539	.111	.169	.208	.204	.322

	MATERIAL: HASTELLOY X					MATERIAL: ALLEGHENY LUDLUM V-36				
STATION	RT S=46500	500 S=39170	1000 S=35420	1500 S=28330	1800 S=14170	RT S=68330	500 S=60000	1000 S=50000	1500 S=41650	1800 S=19170
1	t=1.093	t=1.297	t=1.435	t=1.794	t=3.586	t= .744	t= .847	t=1.016	t=1.220	t=2.651
2	.907	1.077	1.191	1.489	2.976	.617	.703	.844	1.013	2.200
3	.721	.855	.946	1.183	2.365	.490	.559	.670	.805	1.748
4	.525	.623	.689	.862	1.723	.357	.407	.488	.586	1.274
5	.133	.158	.175	.219	.437	.091	.103	.124	.149	.323

	MATERIAL: UNITEMP. L 605					MATERIAL: 18%-300 KSI MARAGING STEEL			
STATION	RT S=70850	500 S=55850	1000 S=44900	1500 S=37400	1800 S=22900	RT S=244000	500 S=212000	1000 S=140000	
1	t=.717	t=.910	t=1.132	t=1.359	t=2.219	t=.209	t=.240	t=.363	
2	.595	.755	.939	1.128	1.842	.173	.199	.301	
3	.473	.600	.746	.896	1.463	.137	.158	.239	
4	.345	.437	.544	.653	1.066	.100	.115	.174	
5	.087	.111	.138	.166	.271	.025	.029	.044	

NOT RECOMMENDED OVER 1000°F

SUBSONIC REGION RT TO 1800° (1000°) RANGE

SUBSONIC REGION 2500 - 3500°F

MATERIAL: TUNGSTEN (HIGHEST STRENGTH VALUE) SOURCE A

STATION	SLANT RADIUS INCHES	LOCAL STATIC PRESSURE	S^{2500}=38300	S^{3000}=22500	S^{3500}=7500	RADIUS X PRESSURE
1	50.92	998	t=1.327	t=2.258	t=6.776	50818.16
2	42.43	994	1.100	1.874	5.623	24175.42
3	33.95	987	.875	1.489	4.468	33508.65
4	25.46	959	.637	1.085	3.255	24416.14
5	11.50	539	.162	.275	.826	6198.50

MATERIAL: TUNGSTEN (LOWEST STRENGTH VALUE) SOURCE C

STATION	S^{2500}=25000	S^{3000}=5000	S^{3500}=4160
1	t=2.033	t=10.164	t=12.216
2	1.687	8.435	10.139
3	1.340	6.702	8.055
4	.977	4.883	5.869
5	.248	1.240	1.490

	MATERIAL: TUNGSTEN-TANTALUM		MATERIAL: COLUMBIUM-TANTALUM-TUNGSTEN			
STATION	2500 S=18300	3000 S=15800	3500 S=9200	2500 S=13500	3000 S=6650	3500 S=3750
1	t=2.776	t=3.216	t=5.523	t=3.764	t=7.642	t=13.551
2	2.304	2.669	4.584	3.124	6.342	11.246
3	1.831	2.121	3.642	2.482	5.039	8.935
4	1.334	1.545	2.654	1.809	3.671	6.511
5	.339	.392	.674	.459	.932	1.653

SUBSONIC REGION 2500 - 3500°F

MATERIAL: COLUMBIUM-TANTALUM-MOLYBD.

STATION	$s^{2500}=11650$	$s^{3000}=6650$	$s^{3500}=2500$
1	t=3.080	t=7.642	20.327
2	2.556	6.342	16.870
3	2.031	5.039	13.403
4	1.480	3.671	9.766
5	.376	.932	2.479
		SUPERSONIC REGION	
6	.177	.311	.826
7	.155	.202	.537
8	.062	.108	.288
9	.040	.070	.186
10	.026	.045	.119

MATERIAL: HAYNES #25 ALLOY

STATION	SLANT RADIUS INCHES	LOCAL STATIC PRESSURE	RT S=56000	500 S=36670	1000 S=29830	1500 S=30410	1800 S=19250	RADIUS X PRESSURE
6	15.53	133	t=.037	t=.056	t=.069	t=.068	t=.107	2065.49
7	18.63	72	t=.024	t=.037	t=.045	t=.044	t=.070	1341.36
8	24.84	29	.013	.020	.024	.024	.037	720.36
9	31.06	15	.008	.013	.016	.015	.024	465.90
10	37.27	8	.005	.008	.010	.010	.015	298.16

STATION	MATERIAL: HASTELLOY X RT S=46500	500 S=39170	1000 S=35420	1500 S=28330	1800 S=14170	MATERIAL: ALLEGHENY LUDLUM V-36 RT S=68330	500 S=60000	1000 S=50000	1500 S=41650	1800 S=19170
6	t=.044	t=.053	t=.058	t=.073	t=.146	t=.030	t=.034	t=.041	t=.050	t=.108
7	.029	.034	.038	.047	.095	.020	.022	.027	.032	.070
8	.015	.018	.020	.025	.051	.011	.012	.014	.017	.038
9	.010	.012	.013	.016	.033	.007	.008	.009	.011	.024
10	.006	.008	.008	.011	.021	.004	.005	.006	.007	.016

STATION	MATERIAL: UNITEMP L-605 RT S=70850	500 S=55850	1000 S=44900	1500 S=37400	1800 S=22900	MATERIAL: 18%-300 KSI MARAGING ST. RT S=244000	500 S=212000	1000 S=140000
6	t=.029	t=.037	t=.046	t=.055	t=.090	t=.008	t=.010	t=.015
7	.019	.024	.030	.036	.059	.005	.006	.010
8	.010	.013	.016	.019	.031	.003	.003	.005
9	.007	.008	.010	.012	.020	.002	.002	.003
10	.004	.005	.007	.008	.013	.001	.001	.002

SUPERSONIC REGION RT TO 1800° (1000°) RANGE

SUPERSONIC REGION

MATERIAL: TUNGSTEN (HIGHEST STRENGTH VALUE) SOURCE A

STATION	SLANT RADIUS INCHES	LOCAL STATIC PRESSURE	S^{2500}=38300	S^{3000}=22500	S^{3500}=7500	RADIUS X PRESSURE
6	15.53	133	t=.054	t=.092	t=.275	2065.49
7	18.63	72	.035	.060	.179	1341.36
8	24.84	29	.019	.032	.096	720.36
9	31.06	15	.012	.021	.062	465.90
10	37.27	8	.008	.013	.040	298.16

MATERIAL: TUNGSTEN (LOWEST STRENGTH VALUE) SOURCE C

STATION	S^{2500}=25000	S^{3000}=5000	S^{3500}=4160
6	t=.083	t=.413	t=.497
7	.054	.268	.322
8	.029	.144	.173
9	.019	.093	.112
10	.012	.060	.072

	MATERIAL: TUNGSTEN-TANTALUM			MATERIAL: COLUMBIUM-TANTALUM-TUNGSTEN		
STATION	2500 S=18300	3000 S=15800	3500 S=9200	2500 S=13500	3000 S=6650	3500 S=3750
6	t=.113	t=.131	t=.224	t=.153	t=.311	t=.551
7	.073	.085	.146	.099	.202	.358
8	.039	.046	.078	.053	.108	.192
9	.025	.029	.051	.035	.070	.124
10	.016	.019	.032	.022	.045	.080

APPENDIX F

WEIGHT ANALYSIS

INTRODUCTION

An analysis was made to obtain comparative weights for the uncooled and cooled nozzles. A unit weight was determined for a lineal inch of nozzle centered at each station. In the case of the uncooled walls, the internal gamma shields were taken as part of the wall. Two cooled nozzles were considered: one with a Rene 41 structural wall; the other with 7178-6T aluminum. The total weight of each wall from the inlet to the throat was also computed.

DISCUSSION

A summary of the unit weights is presented in Figure 47. At Station 1, the aluminum wall weighs 29 lbs. per lineal inch, the Rene 41 wall, 62 lbs. and the uncooled wall, 352 lbs. The relative weights are 1, 2, and 12, respectively. The weight of the cooled walls approach each other at the throat because the structural wall thickness has decreased so much that its weight no longer predominates. The great weight of the uncooled wall is due to the thick tungsten components required to reduce gamma heating.

The total weight of a nozzle, from Station 1 to 5, is proportional to the area under its curve in Figure 47. The abscissa is considered to represent the station to station distance along the wall. The distance between stations was assumed to be equal, although that between 4 and 5 is actually 8% larger than the others. The effect of this assumption on the total weights can be neglected since this is the lightest part of the nozzle.

The areas were obtained by numerical integration. The total nozzle weights, up to the throat, are 6232, 880 and 450 lbs., for the uncooled, cooled Rene 41, and cooled aluminum respectively. The weight saving in going from the uncooled to the cooled Rene 41 wall is 5352 lbs. which is significant. The cooled aluminum wall shows a 430 lb. advantage over the cooled Rene 41.

WEIGHT ANALYSIS

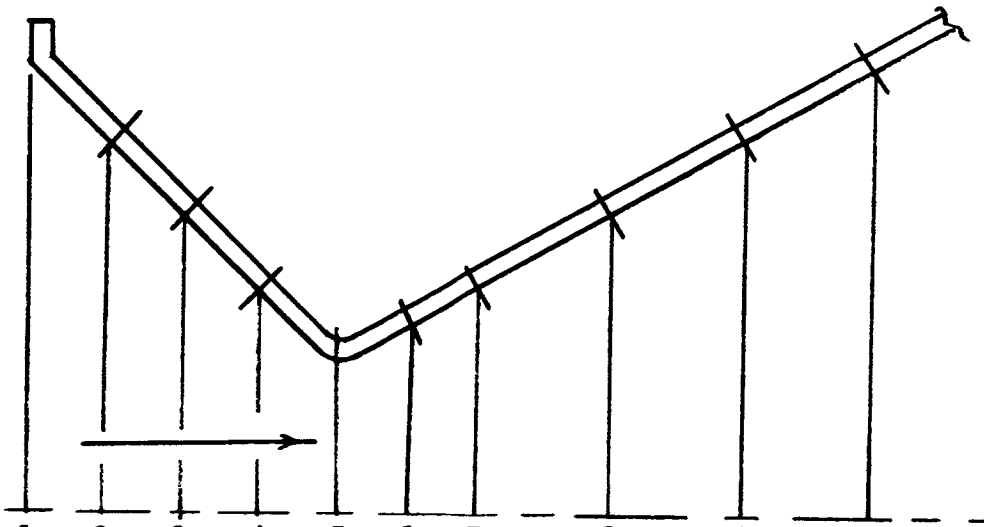

Stations	1	2	3	4	5	6	7	8	9	10
Radius-Inches	36	30	24	18	11.5	15	18	24	30	36

SCHEMATIC SECTION OF NOZZLE

PROCEDURE:

At each station consider a one-inch section of the nozzle centered at the station. Find the weight of each section for the cooled and uncooled walls.

COOLED NOZZLE

STATION 1

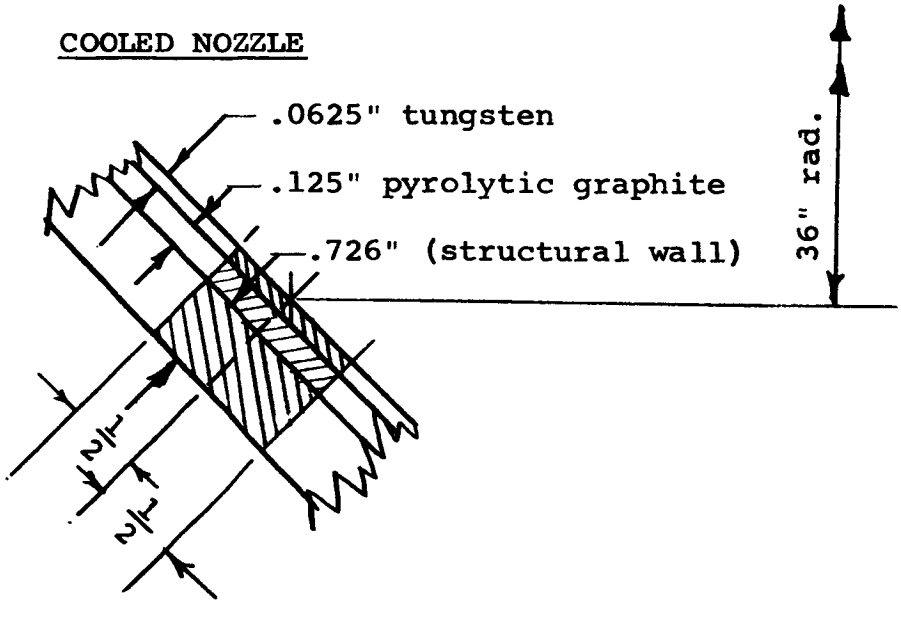

UNCOOLED NOZZLE:

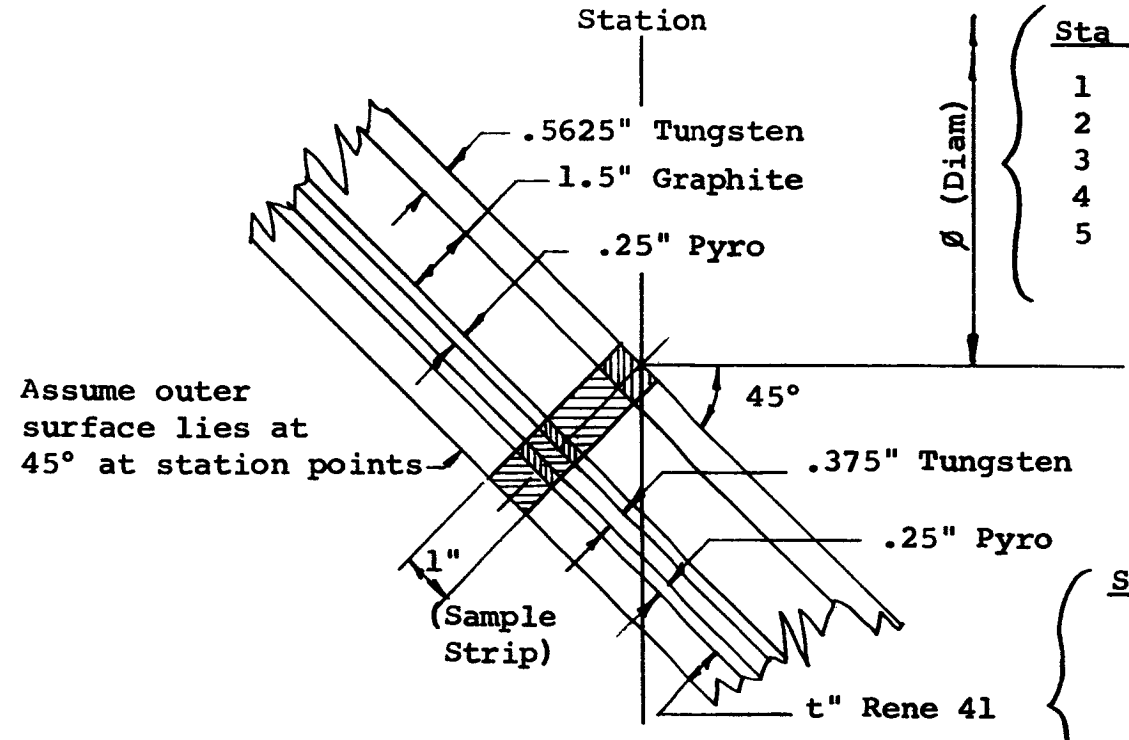

Sta	ø (in.)
1	72
2	60
3	48
4	36
5	23

Sta	t
1	.726
2	.602
3	.479
4	.348
5	.089

Tungsten Strips:-

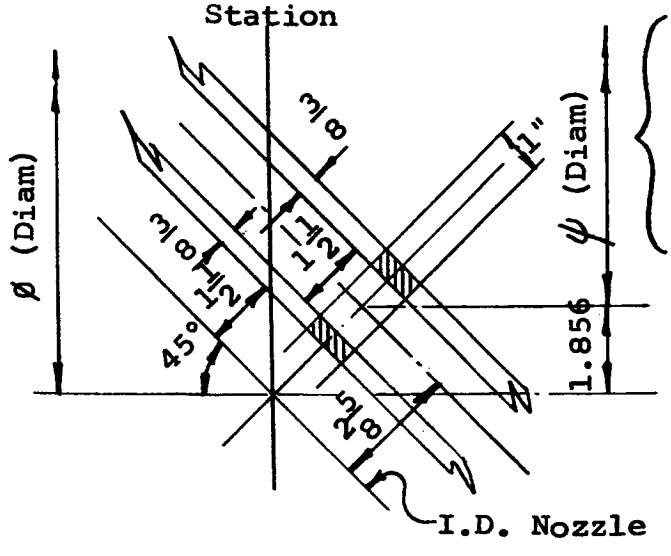

Sta	ψ
1	68.2877
2	56.2877
3	44.2877
4	32.2877

WEIGHT SUMMARY - COOLED NOZZLE (LBS/INCH)

	Sta. 1	Sta. 2	Sta. 3	Sta. 4	Sta. 5
Tungsten #1 (.695 lb/in^3)	9.8314	8.1938	6.5563	4.9187	3.1447
Pyro (.0792 lb/in^3)	2.2448	1.8716	1.4984	1.1252	.7208
Rene 41 (.298 lb/in^3)	49.4661	34.2048	21.7958	11.8952	1.9437
Alum 7178-6T (.1020 lb/in^3)	16.9313	11.7077	7.4603	4.0715	.6653
Total with Rene 41	61.5423	44.2702	29.8505	17.9391	5.8092
Total with Alum.	29.0075	21.7731	15.5150	10.1154	4.5308

WEIGHT SUMMARY - UNCOOLED NOZZLE (LBS/INCH)

Station 1	-	351.6596 Lbs.
2	-	285.7614
3	-	222.7191
4	-	162.1561
5	-	65.3088

TABLE I

MATERIAL	DENSITY IN gm/cm^3
Hastelloy "W"	9.03
Zirconium Oxide	5.60
Beryllium Oxide	2.70
Graphite	2.26
Uranium (235)	18.90
Tungsten	19.10
Pyrolytic Graphite	2.09
Rene 41	8.25
7178-6T Aluminum	2.82

TABLE II

GAMMA-RAY MASS ATTENUATION COEFFICIENTS μ, IN Cm^{-1}

MEV	Hast. "W"	ZrO_2	BeO	C	U^{235}	W
.5	.783	.452	.2245	.197	3.33	2.39
1.5	.438	.262	.1341	.117	1.045	.975
2.5	.353	.204	.1000	.089	.870	.800
3.5	.315	.180	.084	.074	.835	.780
4.5	.300	.170	.073	.065	.837	.780
5.5	.297	.165	.065	.058	.850	.790
6.5	.295	.162	.060	.054	.870	.805
7.5	.293	.161	.056	.050	.895	.825
8.5	.290	.161	.054	.047	.920	.850
9.5	.285	.162	.052	.045	.950	.877

TABLE III

MATERIAL	k	ρc	α	TEMP, °F	SOURCE
Tungsten	33.30	61.27	.5435	5000	1
Hastelloy "W"	9.50	51.11	.1859	1000	2
ZrO_2	1.17	75.00	.0156	4000	1
BeO^2	2.50	91.20	.0274	3500	1
Graphite	22.5	51.49	.4369	5000	3
Pyrolytic Graphite	.3	74.07	.0040	5000	3
Rene 41	10.8	55.61	.1942	1000	-
7178-6T Aluminum	70.15	40.54	1.7304	75	-

k = Thermal conductivity
BTU/hr-ft^2-°R/ft.

ρc = Volumetric Thermal Capacity
BTU/ft^3-degree

α = Thermal diffusivity
square ft./hour

Sources

1 ASD TDR 62-765
2 Union Carbide Bulletin
3 Super-Temp. Corp. Bulletin

TABLE IV

COOLANT TEMPERATURE RISE IN THE "RENE 41" WALL

100°R COOLANT

STATION	T_w	ΔT	$Q(10^3)$	$\bar{Q}10^3$	A	ΔT_c	T_c
1	234	134	268	350	12.422	9.4	100
2	316	216	432	432	10.188	9.5	109.4
3	316	216	432	398	7.933	6.8	118.9
4	282	182	364	425	6.283	5.8	125.7
5	343	243	486				131.5

$\Sigma = 31.5$

Where:

T_w = Wall temperature °R
Q = Local flux, BTU/Hr-Ft^2 of Wall
$\bar{Q}$ = Average flux between stations
A = Cooled area between stations, Ft^2
ΔT_c = Coolant temperature rise
T_c = Coolant temperature at a station
$\bar{C}_{p_{100}}$ = 3.1
$\dot{w}$ = 149,400 #/Hr.

800°R COOLANT

STATION	T_w	ΔT	$Q(10^3)$	$\bar{Q}10^3$	A	ΔT_c	T_c
1	926	126	252	336	12.422	8.5	100
2	1010	210	420	417	10.188	8.6	108.5
3	1007	207	414	379	7.933	6.1	117.1
4	972	172	344	391	6.283	5.0	123.2
5	1019	219	438				128.2

$\Sigma = 28.2$

Where:

T_w = Wall temperature °R
Q = Local flux, BTU/Hr-Ft^2 of wall
$\bar{Q}$ = Average flux between stations
A = Cooled area between stations, Ft^2
ΔT_c = Coolant temperature rise
T_c = Coolant temperature at a station
$\bar{C}_{p_{800}}$ = 3.3
$\dot{w}$ = 149,400 #/Hr.

TABLE V

COOLANT TEMPERATURE RISE IN THE 7178-6T ALUMINUM WALL

100°R COOLANT

STATION	T_w	ΔT	$Q(10^3)$	$\bar{Q}10^3$	A	ΔT_c	T_c
1	218	118	236	318	12.422	8.5	100
2	300	200	400	407	10.188	9.0	108.5
3	307	207	414	386	7.933	6.6	117.5
4	279	179	358	271	6.283	3.7	124.1
5	192	92	184				127.8

$\Sigma = 27.8$

Where:

T_w = Wall temperature °R
Q = Local flux, BTU/Hr-Ft^2 of Wall
$\bar{Q}$ = Average flux between stations
A = Cooled area between stations
ΔT_c = Coolant temperature rise
T_c = Coolant temperature at a station
$\bar{C}^c_{p_{100}}$ = 3.1

$\dot{w}$ = 149,400 #/Hr.

ARDE-PORTLAND UNCOOLED NUCLEAR NOZZLE

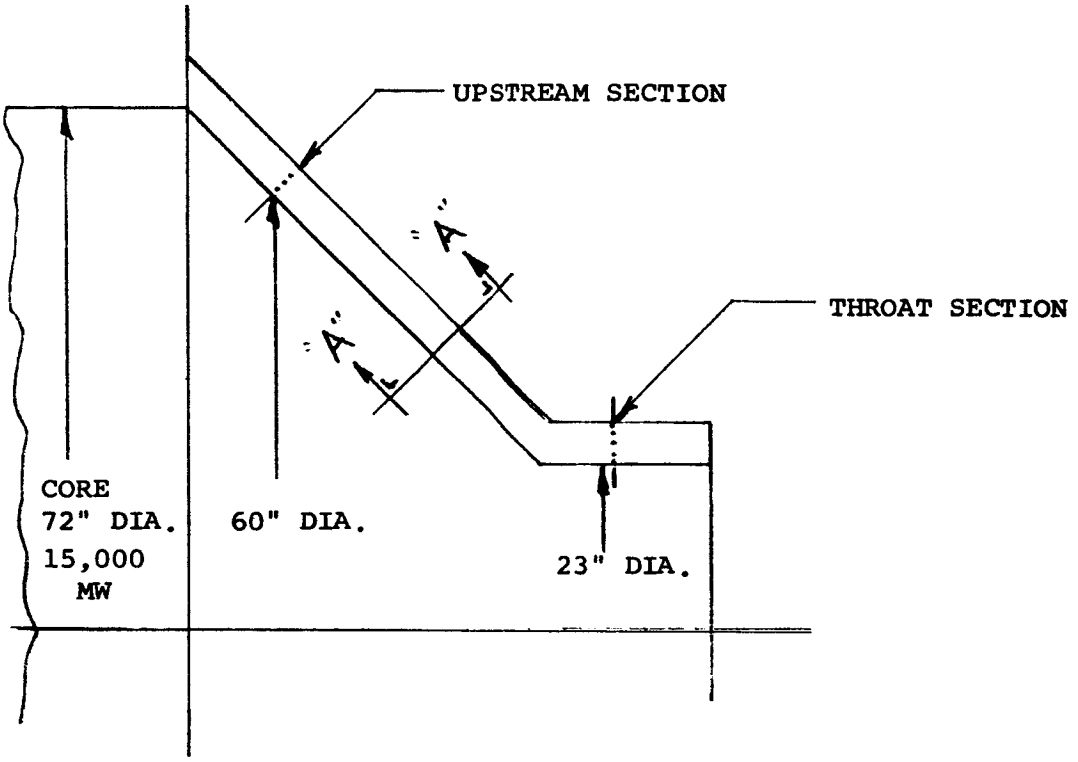

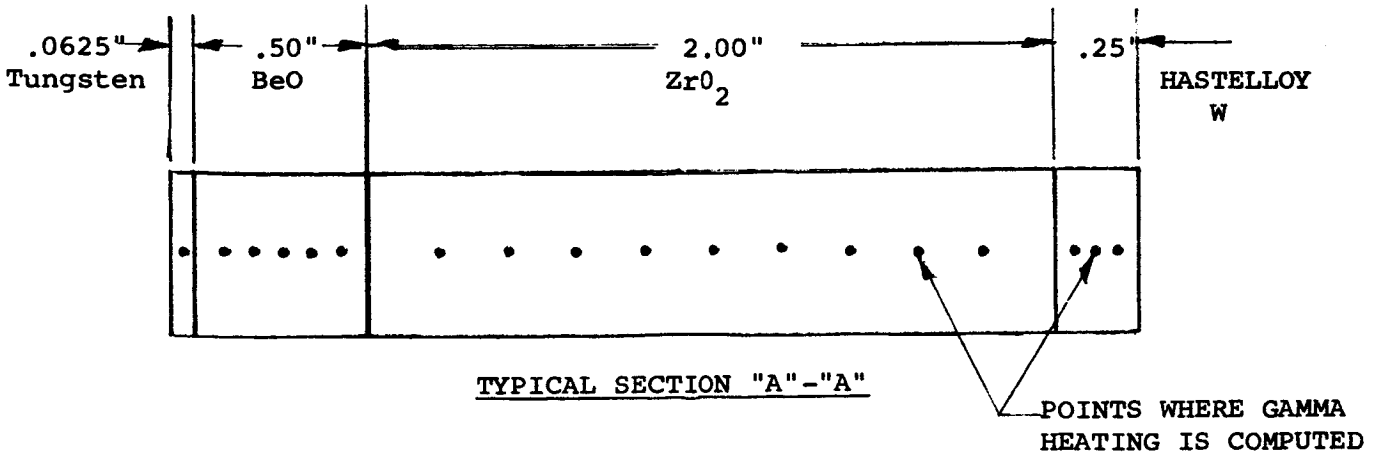

FIGURE 1

TYPICAL QAD IV RESULTS AT A RECEIVER POINT

RECEIVER POINT LOCATION

Radial Location = 76.00 cm
Axial Location = 15.04 cm

GAMMA FLUX Mev/sq cm-sec

ENERGY GROUP (Mev)	BUILDUP FACTOR=1	SPECIFIED BUILDUP FACTOR
1	7.3078E 10	3.2384E 12
2	2.6320E 13	1.6700E 14
3	4.4969E 13	1.7297E 14
4	2.9731E 13	9.0717E 13
5	1.6429E 13	4.3364E 13
6	6.0640E 12	1.4453E 13
7	2.6843E 12	5.9473E 12
8	9.0528E 11	1.8950E 12
9	1.6070E 11	3.2211E 11
10	5.6696E 10	1.0989E 11
TOTALS	1.2789E 14	5.001E 14

NOTE: 5.001E 14 = 5.001×10^{14}

FIGURE 2

ARDE-PORTLAND UNCOOLED NUCLEAR NOZZLE

GAMMA FLUX WITHIN THE NOZZLE WALL

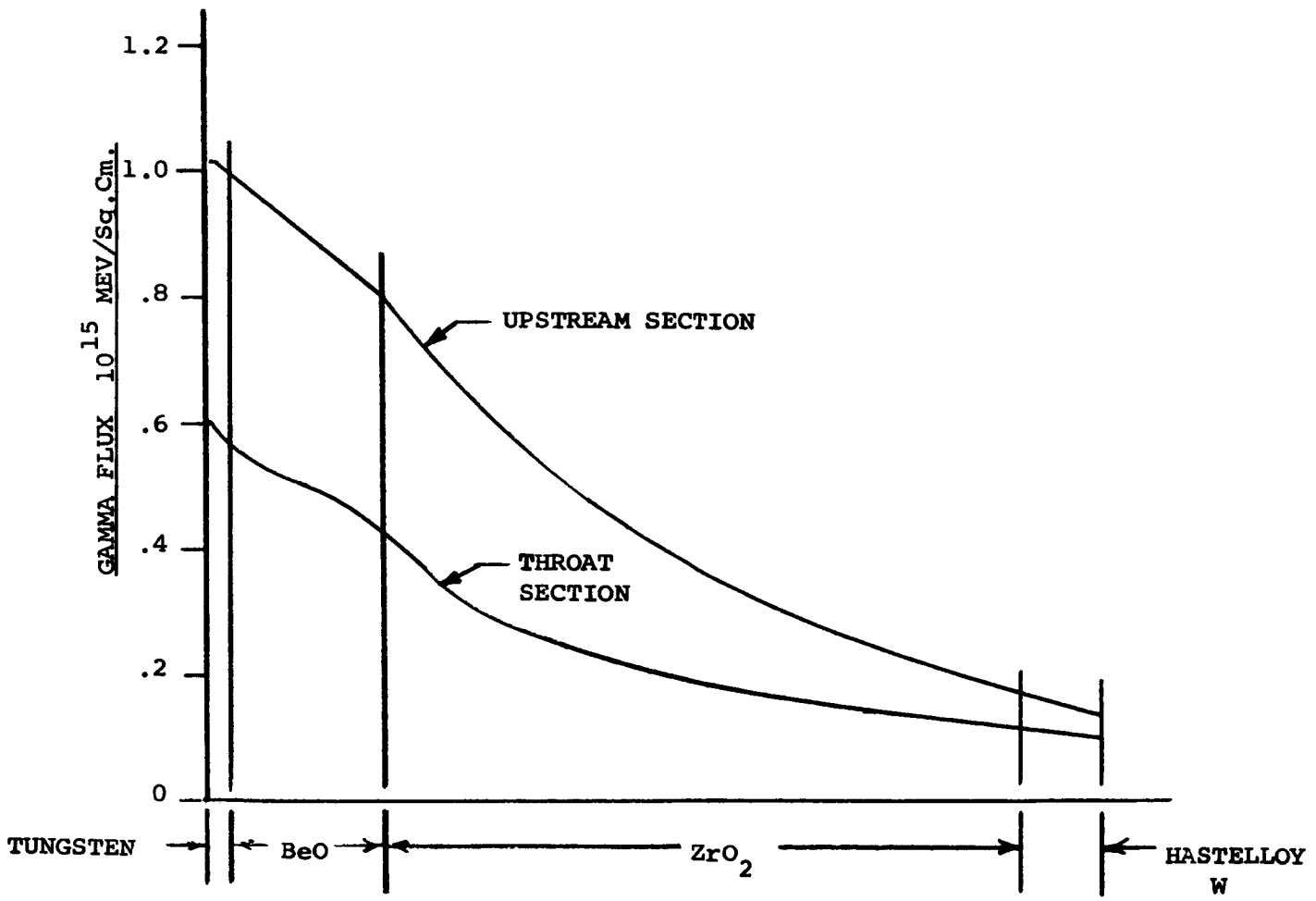

NOZZLE WALL

FIGURE 3

ARDE-PORTLAND NUCLEAR NOZZLE

EFFECT OF TUNGSTEN THICKNESS

ON GAMMA FLUX WITHIN WALL

UPSTREAM SECTION - BUILDUP FACTOR = 1

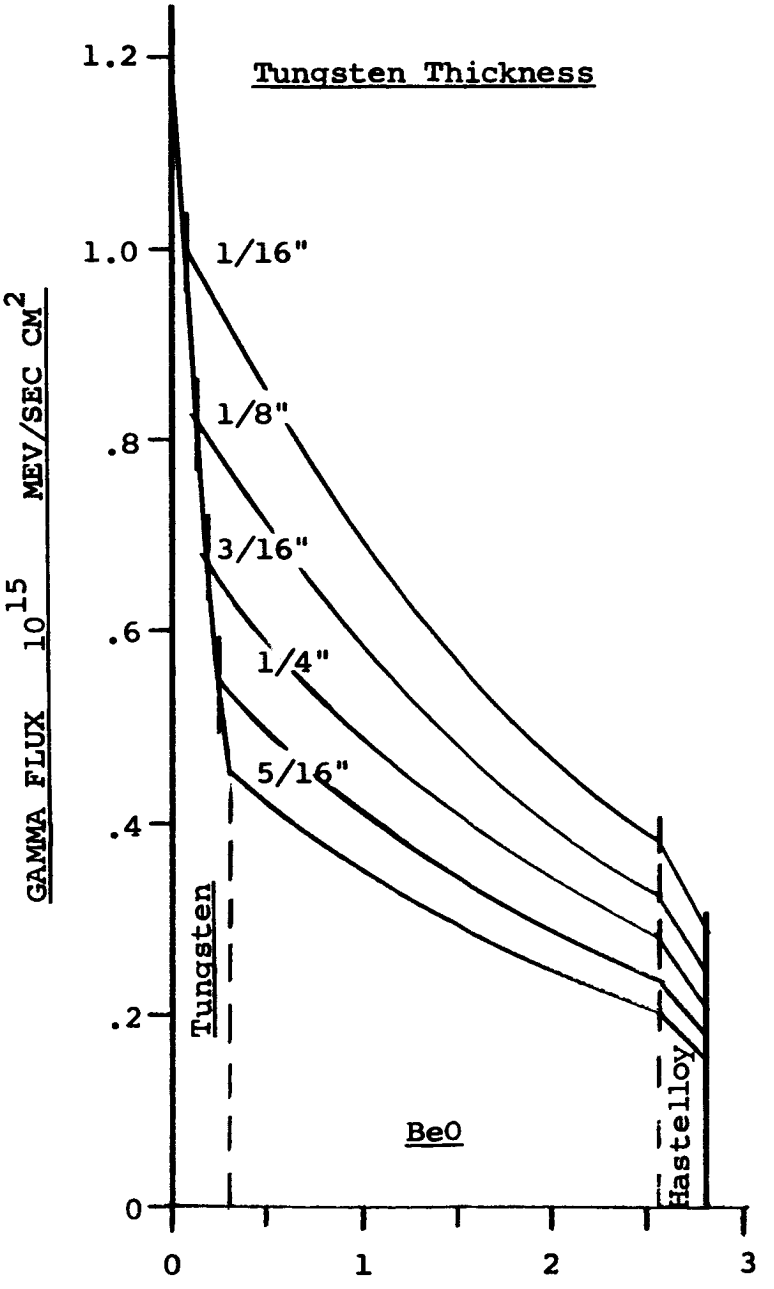

FIGURE 4

ARDE-PORTLAND NUCLEAR NOZZLE

EFFECT OF TUNGSTEN THICKNESS

ON GAMMA FLUX WITHIN WALL

UPSTREAM SECTION - BUILDUP FACTOR - ALUMINUM

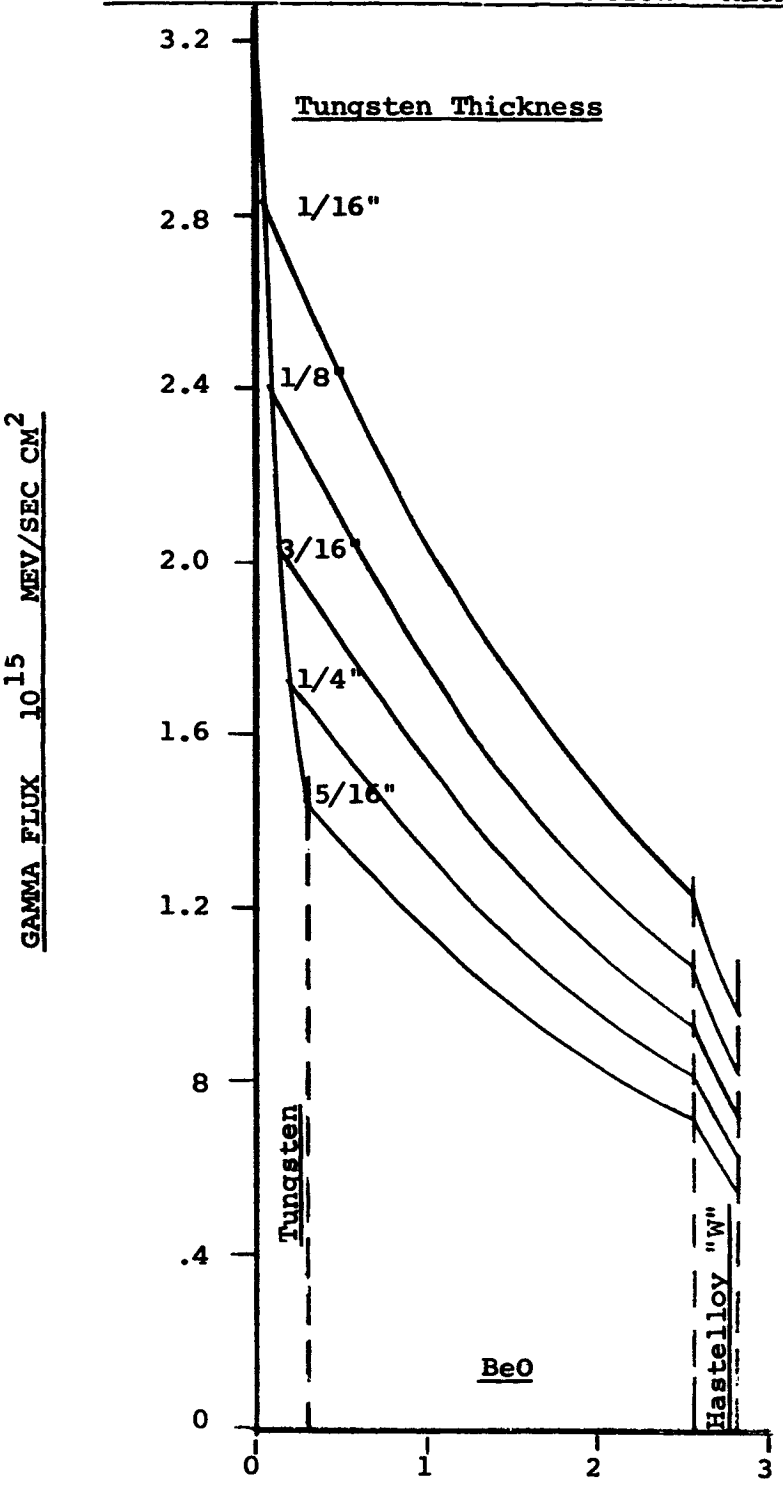

FIGURE 5

ARDE PORTLAND NUCLEAR NOZZLE

VARIATION OF ENERGY AND BUILDUP FACTORS WITHIN THE WALL

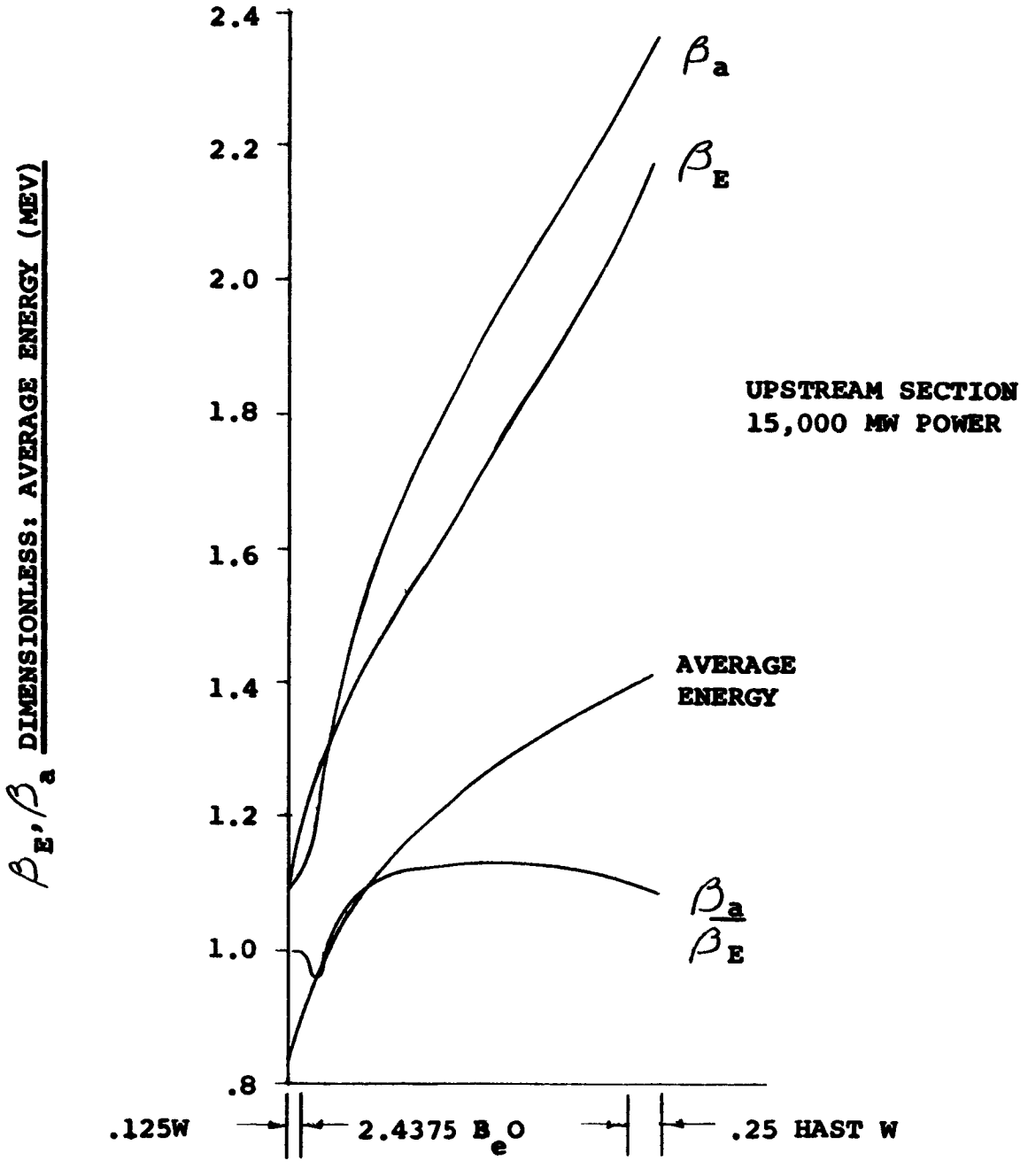

FIGURE 6

ARDE-PORTLAND UNCOOLED NUCLEAR NOZZLE

VOLUMETRIC GAMMA HEAT GENERATION WITHIN THE WALL

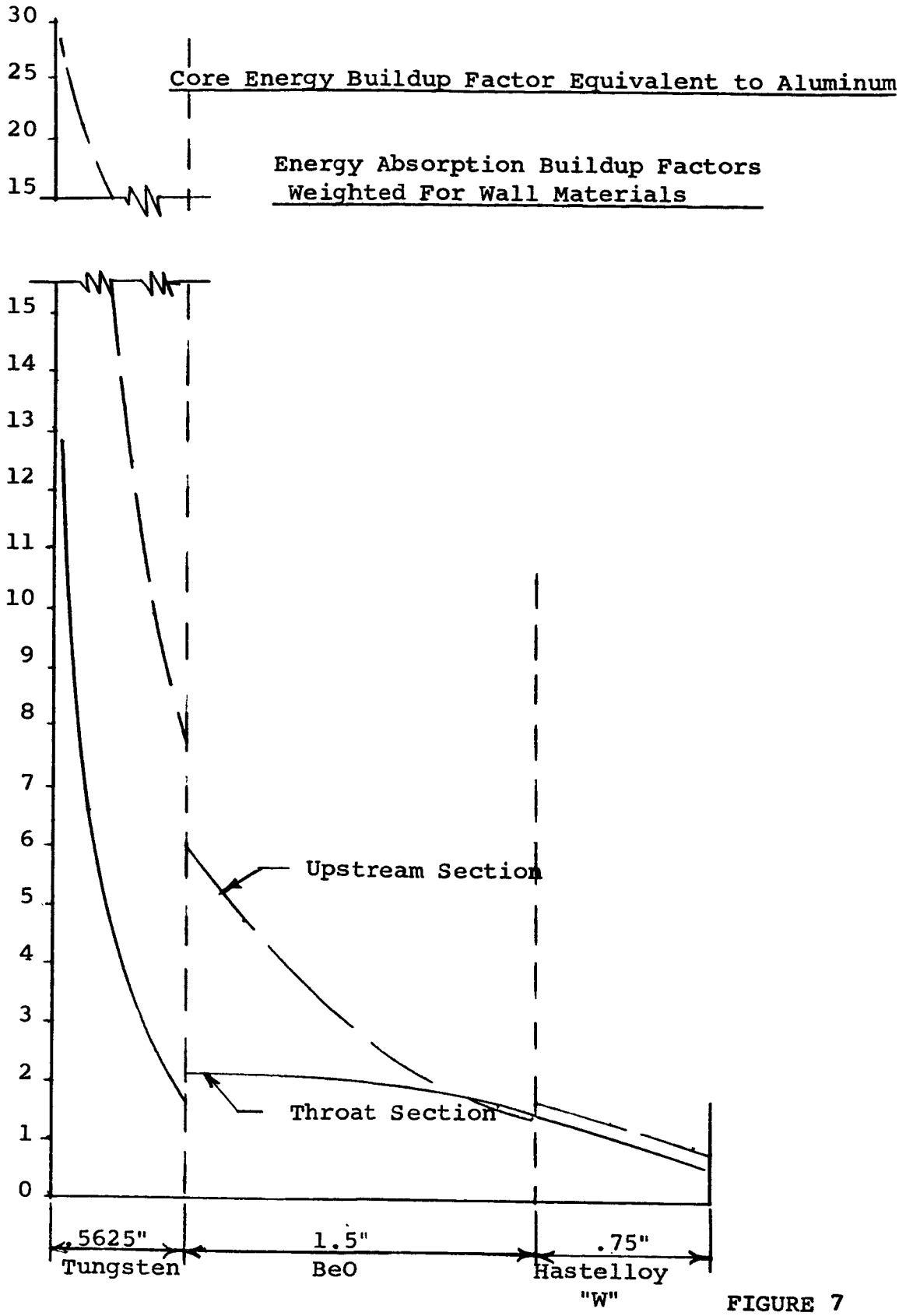

FIGURE 7

NOZZLE WALL

ENERGY ABSORPTION ATTENUATION COEFFICIENT FOR TUNGSTEN

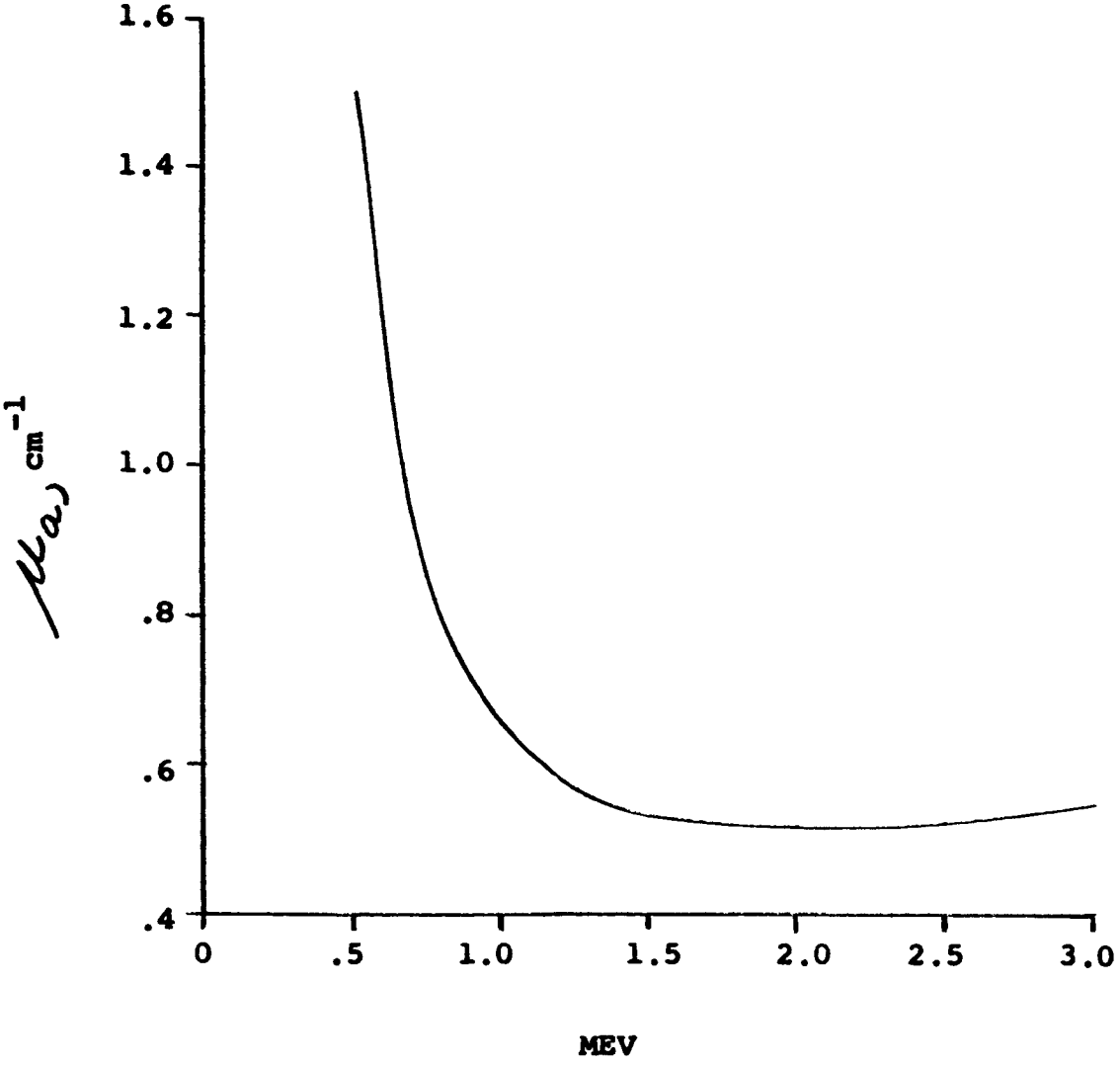

FIGURE 8

TYPICAL MASS ATTENUATION COEFFICIENTS

U^{235}, TUNGSTEN

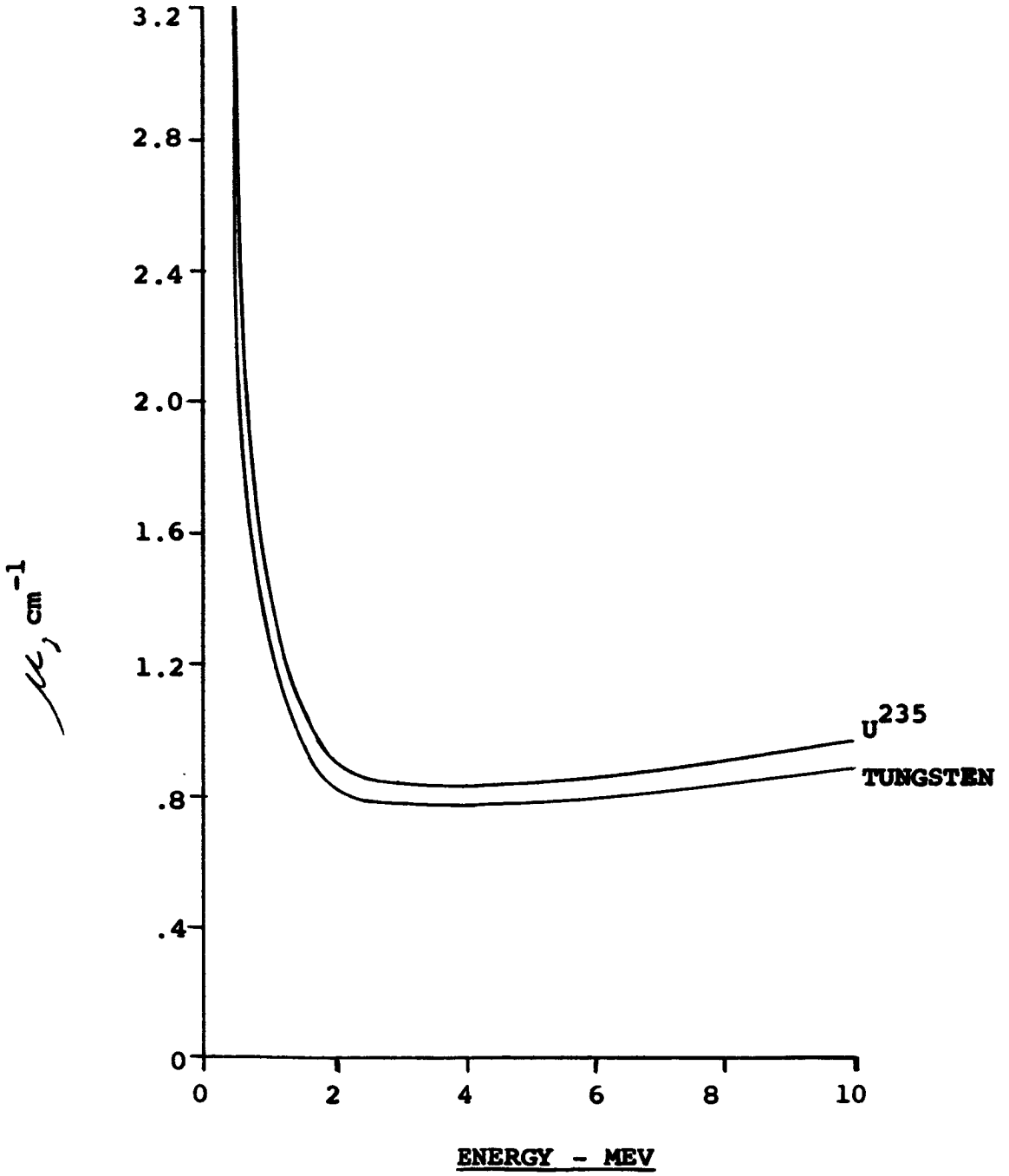

FIGURE 9

TYPICAL MASS ATTENUATION COEFFICIENTS

HAST "W", ZrO_2, BeO, Graphite

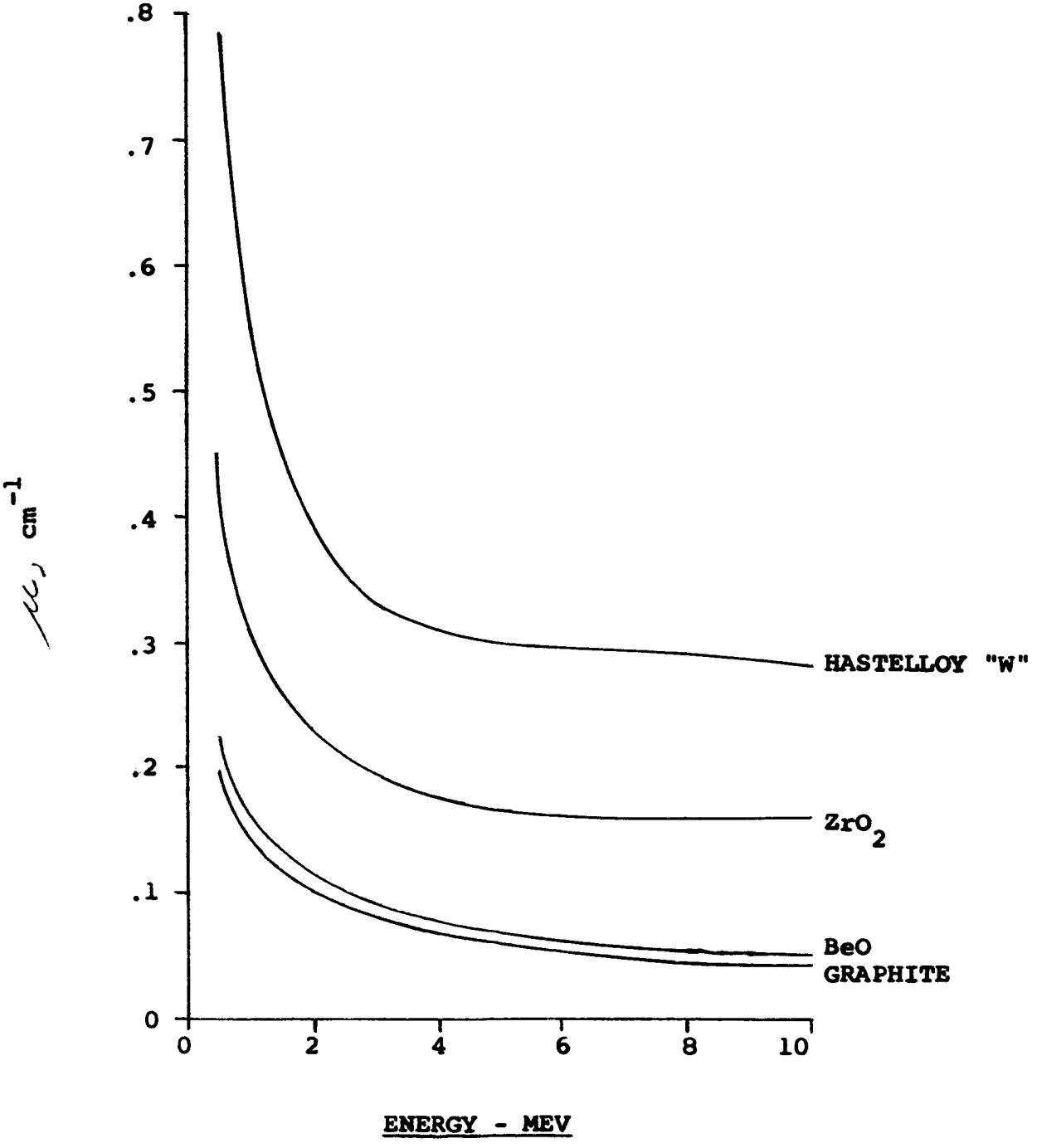

FIGURE 10

ENERGY ABSORPTION ATTENUATION

COEFFICIENT FOR NOZZLE WALL MATERIALS

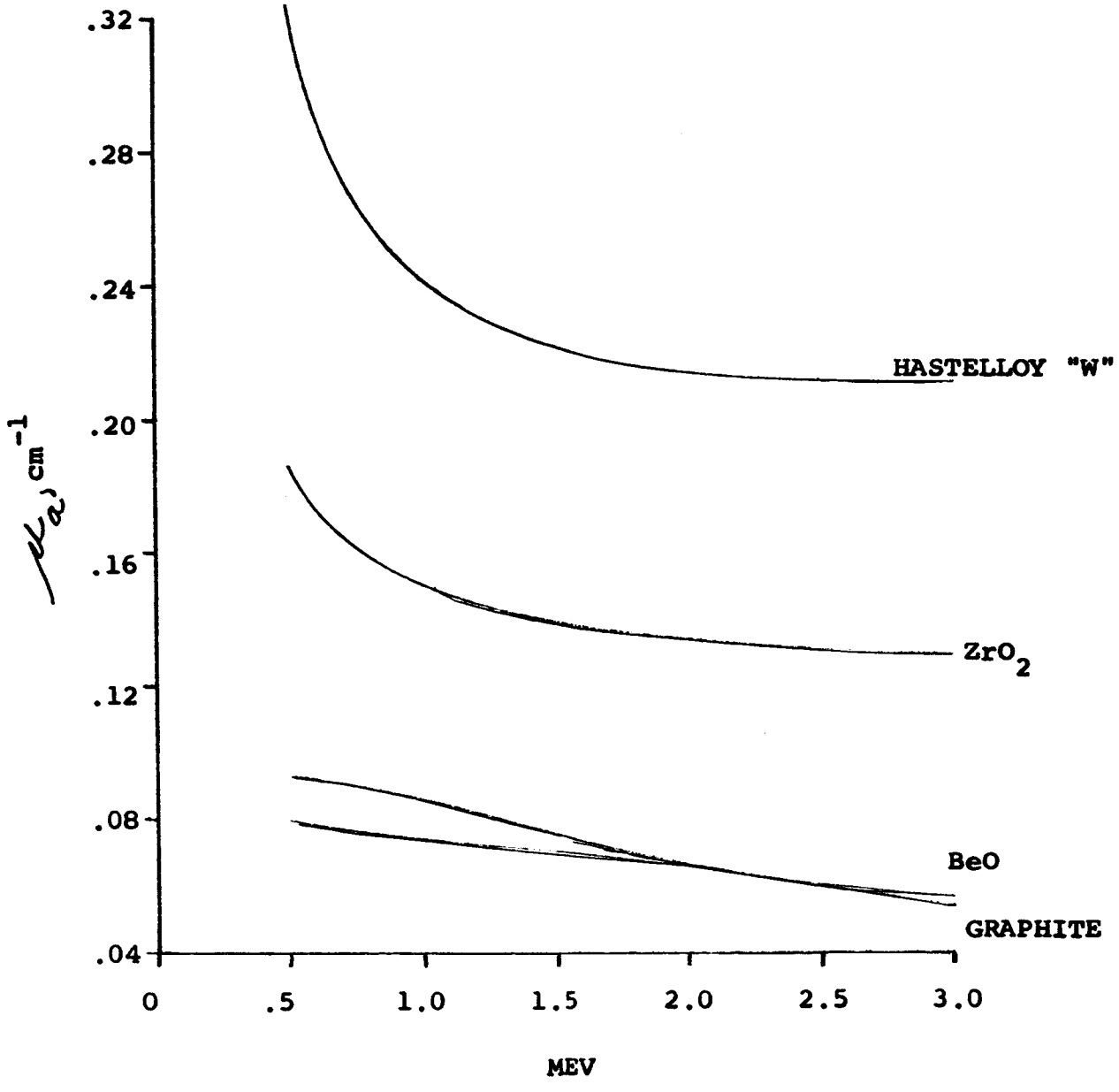

FIGURE 11

STEADY STATE TEMPERATURE

OF A

HEAT GENERATING WALL RADIATING TO SPACE

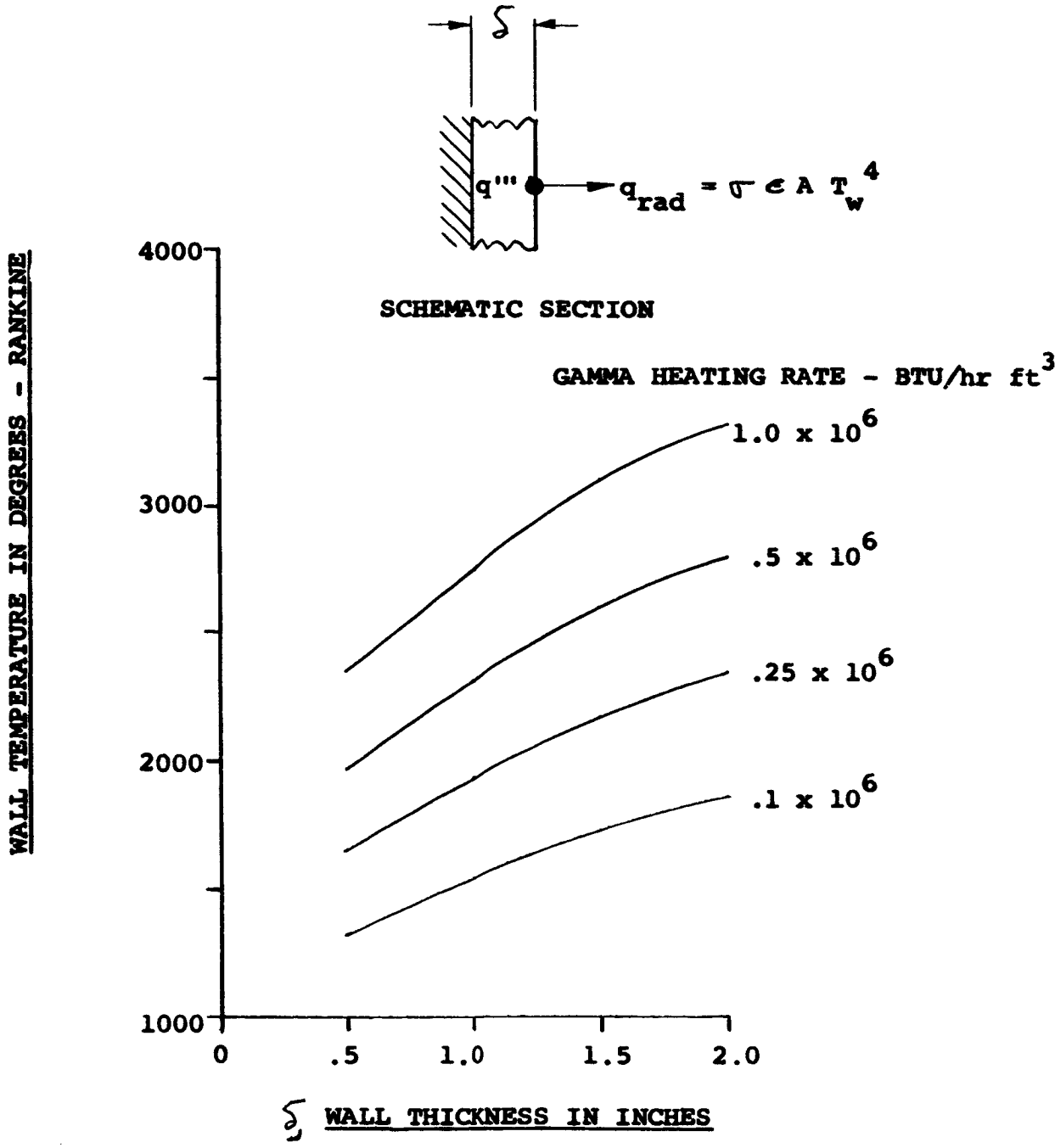

FIGURE 12

ARDE-PORTLAND UNCOOLED NUCLEAR NOZZLE

TRANSIENT TEMPERATURE DISTRIBUTION WITHIN WALL

UPSTREAM SECTION - 15,000 MW TOTAL POWER

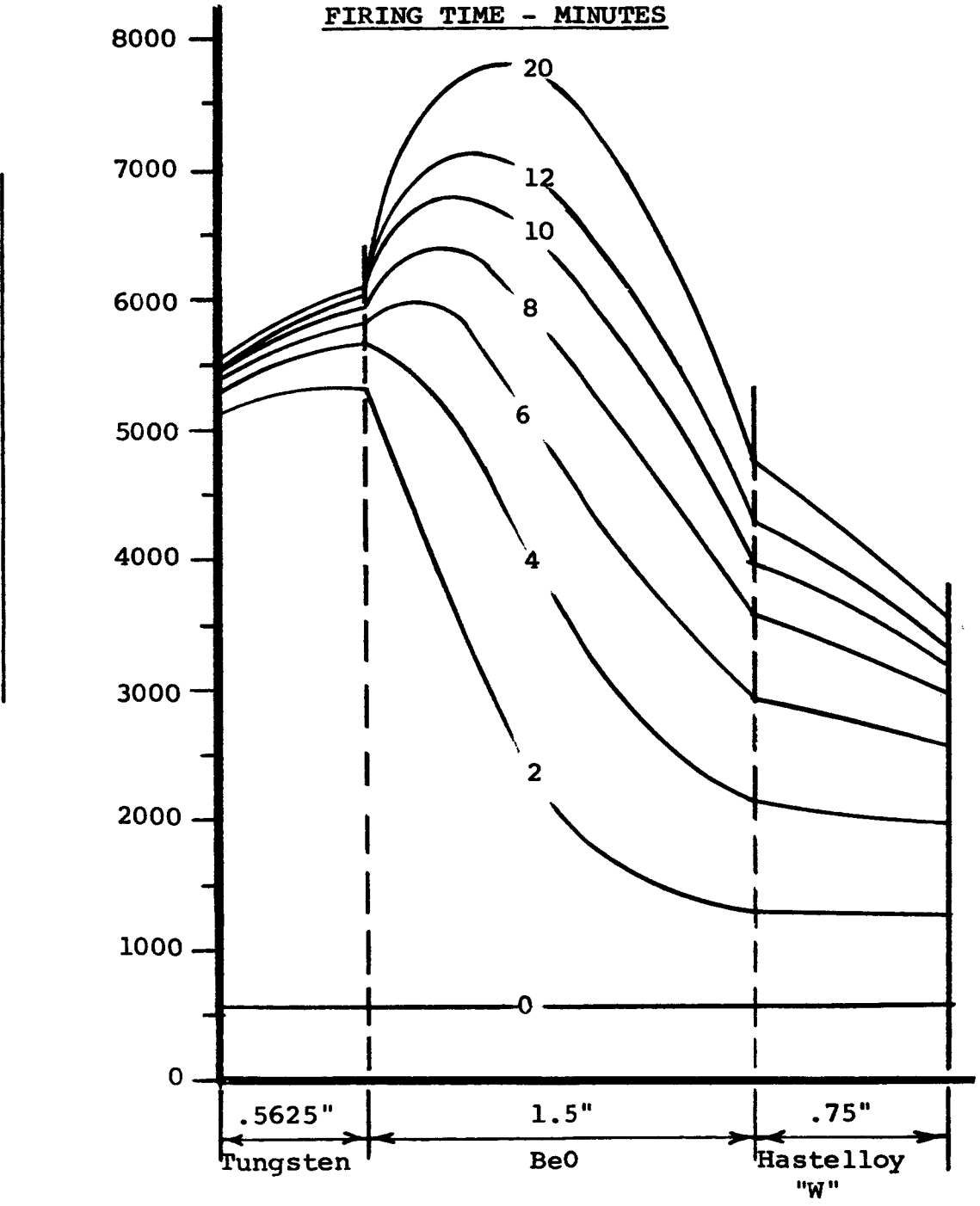

NOZZLE WALL

FIGURE 13

ARDE-PORTLAND UNCOOLED NUCLEAR NOZZLE

TRANSIENT TEMPERATURE DISTRIBUTION WITHIN WALL

THROAT SECTION - 15,000 MW TOTAL POWER

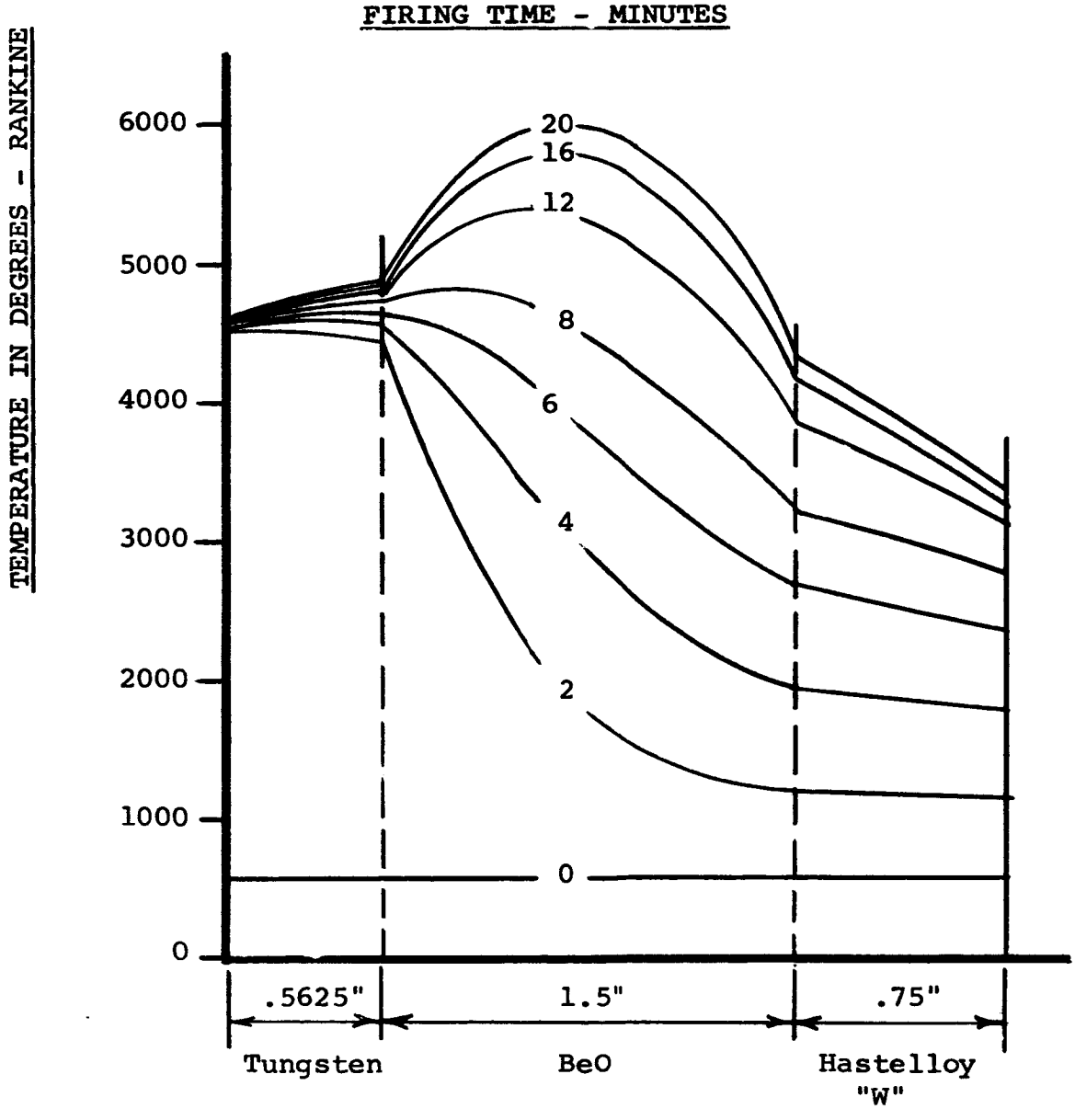

NOZZLE WALL

FIGURE 14

ARDE-PORTLAND UNCOOLED NUCLEAR NOZZLE

THE EFFECT OF VARIATION IN GAMMA HEATING ON

TRANSIENT TEMPERATURE DISTRIBUTION WITHIN WALL

UPSTREAM SECTION - 15,000 MW TOTAL POWER

50% of Calculated Gamma Heating Rate

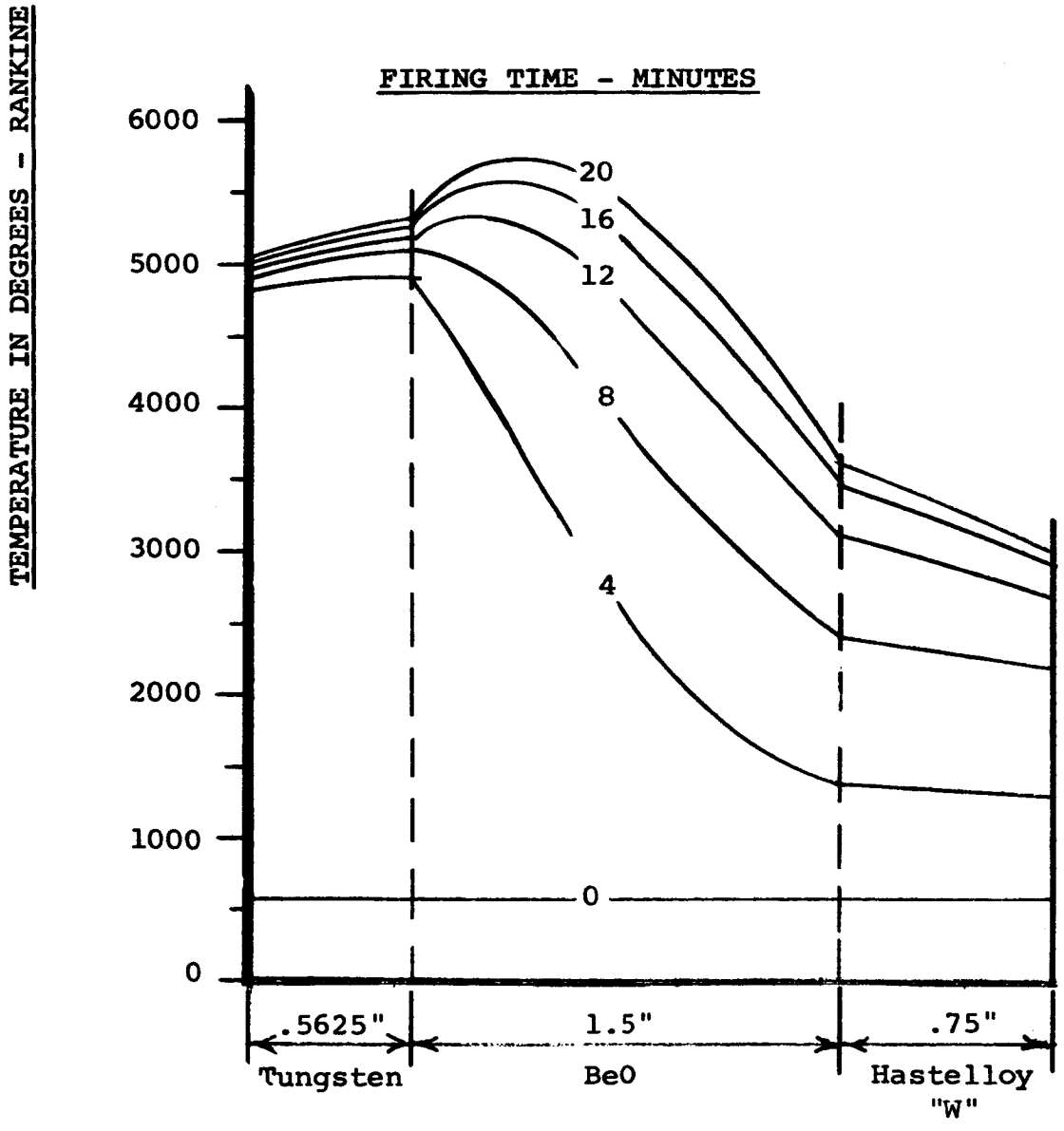

NOZZLE WALL

FIGURE 15a

ARDE-PORTLAND UNCOOLED NUCLEAR NOZZLE

THE EFFECT OF VARIATION IN GAMMA HEATING ON

TRANSIENT TEMPERATURE DISTRIBUTION WITHIN WALL

UPSTREAM SECTION - 15,000 MW TOTAL POWER

25% of Calculated Gamma Heating Rate

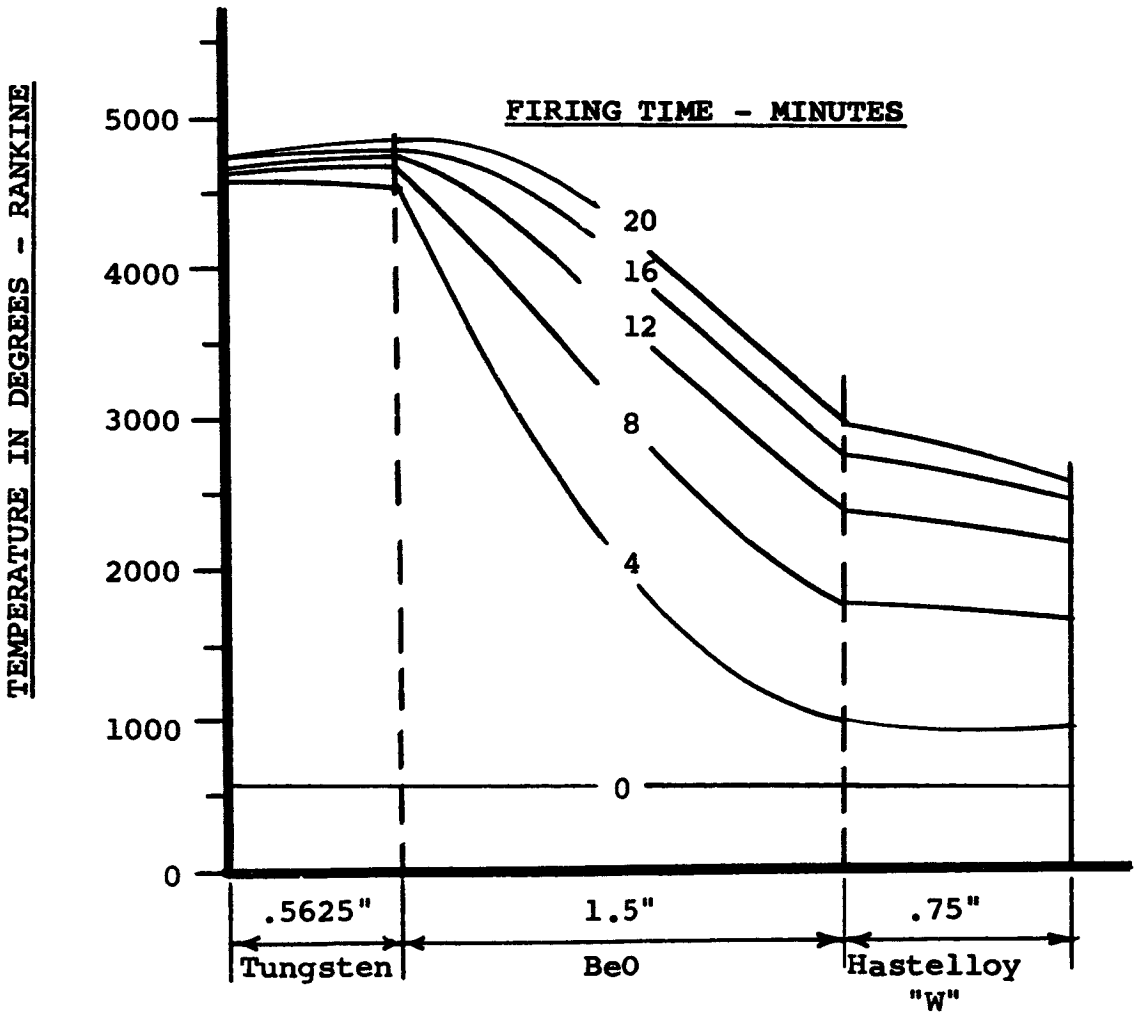

FIGURE 15b

ARDE-PORTLAND UNCOOLED NUCLEAR NOZZLE

THE EFFECT OF VARIATION IN GAMMA HEATING ON

TRANSIENT TEMPERATURE DISTRIBUTION WITHIN WALL

10% of Calculated Gamma Heating Rate

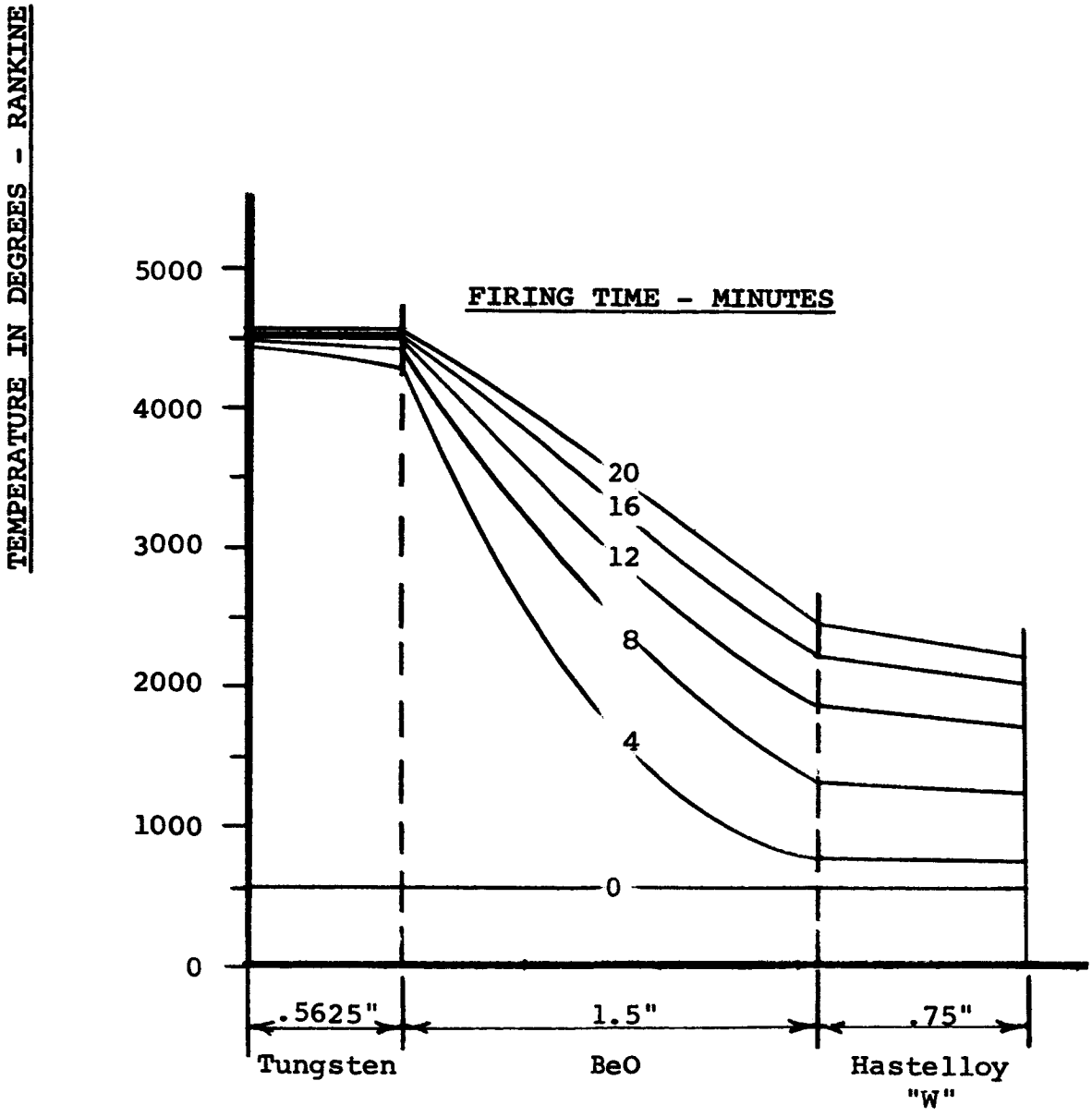

FIGURE 15c

CONCEPTUAL SKETCH OF UNCOOLED NOZZLE

INLET GAMMA SHIELD

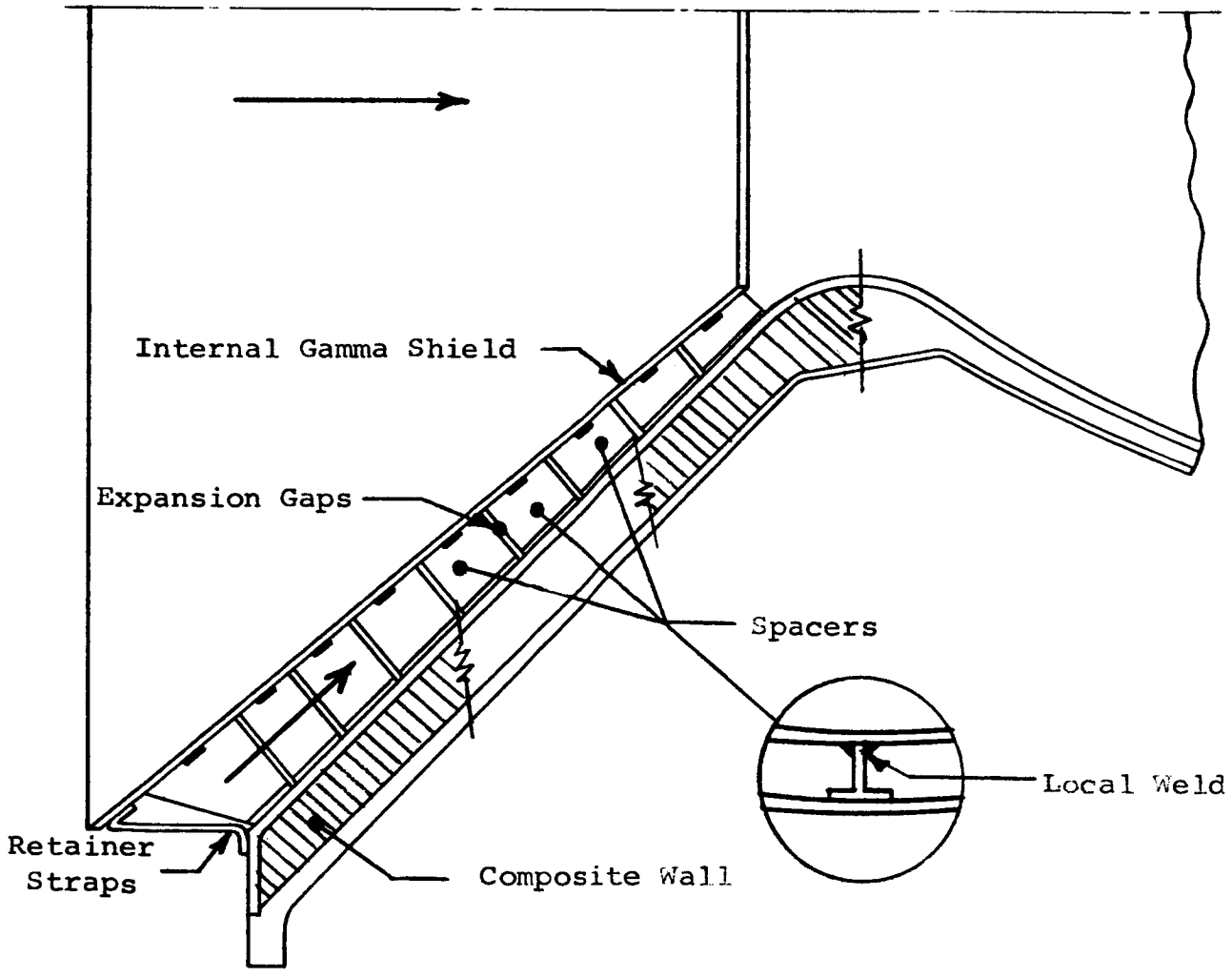

SCHEMATIC SECTION THROUGH NOZZLE WALL

ARDE-PORTLAND UNCOOLED NUCLEAR NOZZLE

EFFECTS OF GAMMA REDUCTION, AND SHIELD THICKNESS

ON THE WALL TEMPERATURE DISTRIBUTION

AFTER A 20 MINUTE FIRING

UPSTREAM SECTION - 15,000 MW

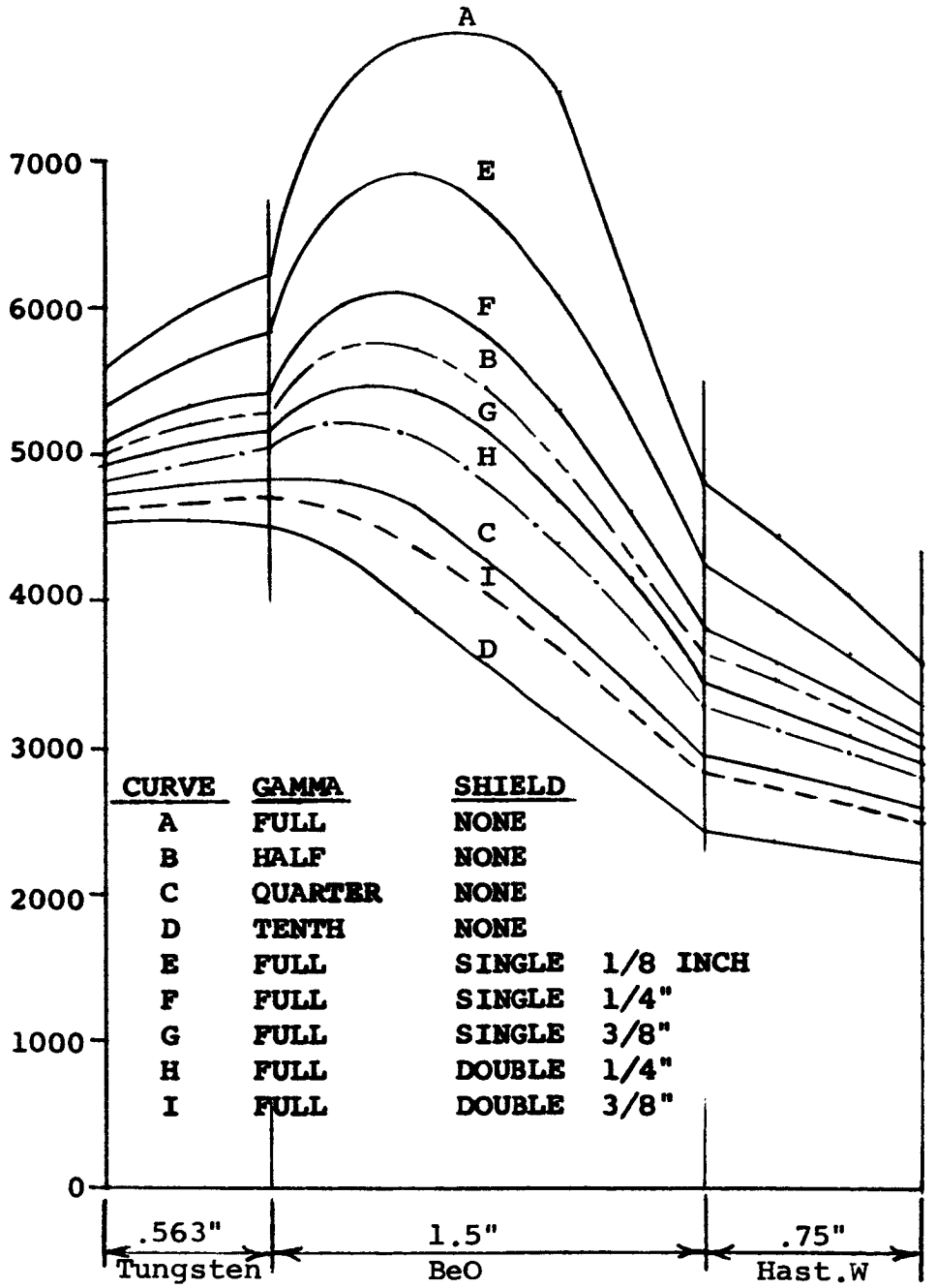

CURVE	GAMMA	SHIELD	
A	FULL	NONE	
B	HALF	NONE	
C	QUARTER	NONE	
D	TENTH	NONE	
E	FULL	SINGLE	1/8 INCH
F	FULL	SINGLE	1/4"
G	FULL	SINGLE	3/8"
H	FULL	DOUBLE	1/4"
I	FULL	DOUBLE	3/8"

FIGURE 17

ARDE-PORTLAND UNCOOLED NUCLEAR NOZZLE - IMPROVED WALL

TRANSIENT TEMPERATURE DISTRIBUTION - UPSTREAM SECTION

15,000 MW TOTAL POWER

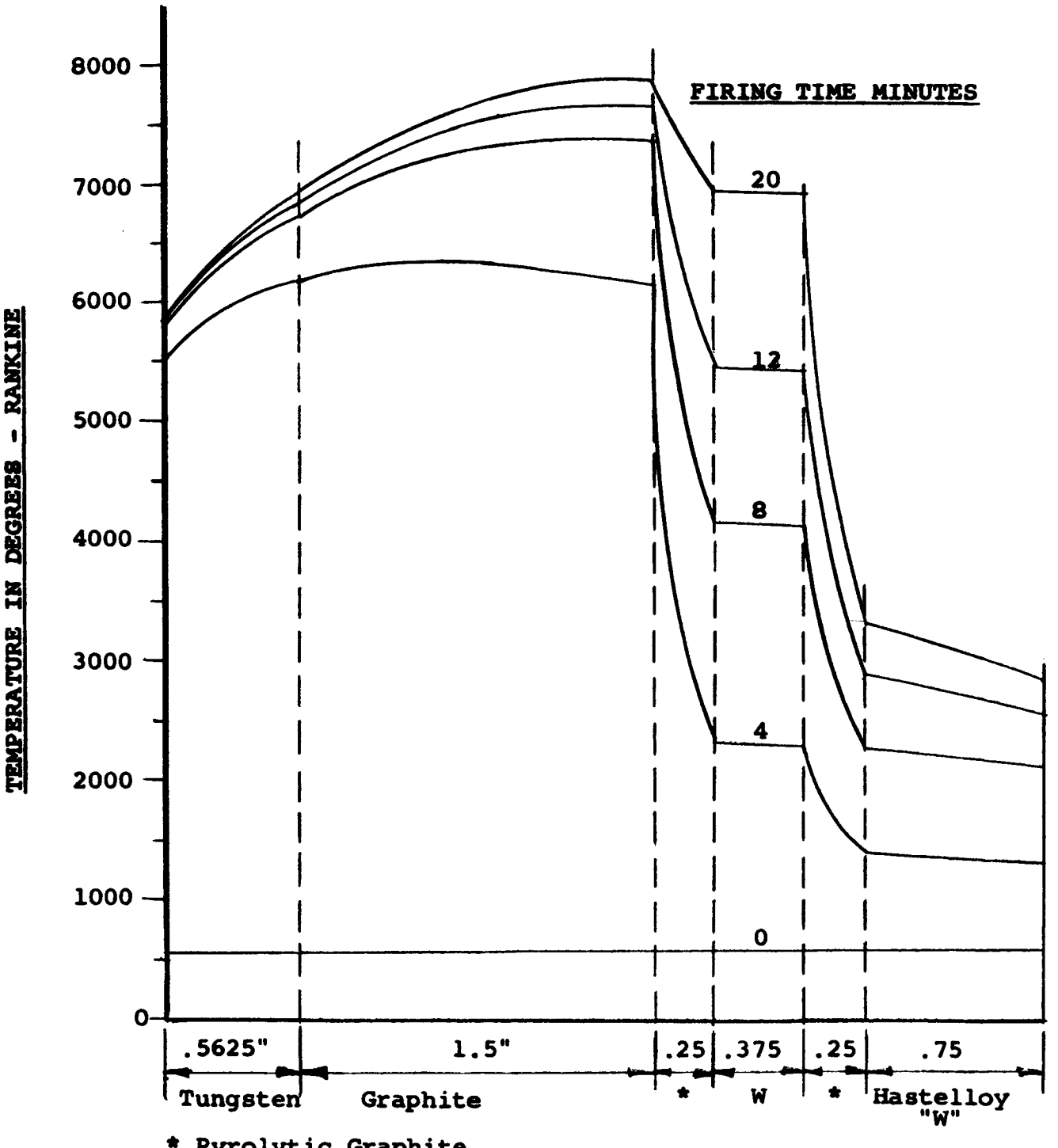

* Pyrolytic Graphite

NOZZLE WALL

FIGURE 18

ARDE-PORTLAND UNCOOLED NUCLEAR NOZZLE - IMPROVED WALL

THE EFFECT OF VARIATION IN GAMMA HEATING ON

TRANSIENT TEMPERATURE DISTRIBUTION - UPSTREAM SECTION

15,000 MW TOTAL POWER

50% OF CALCULATED GAMMA HEATING RATE

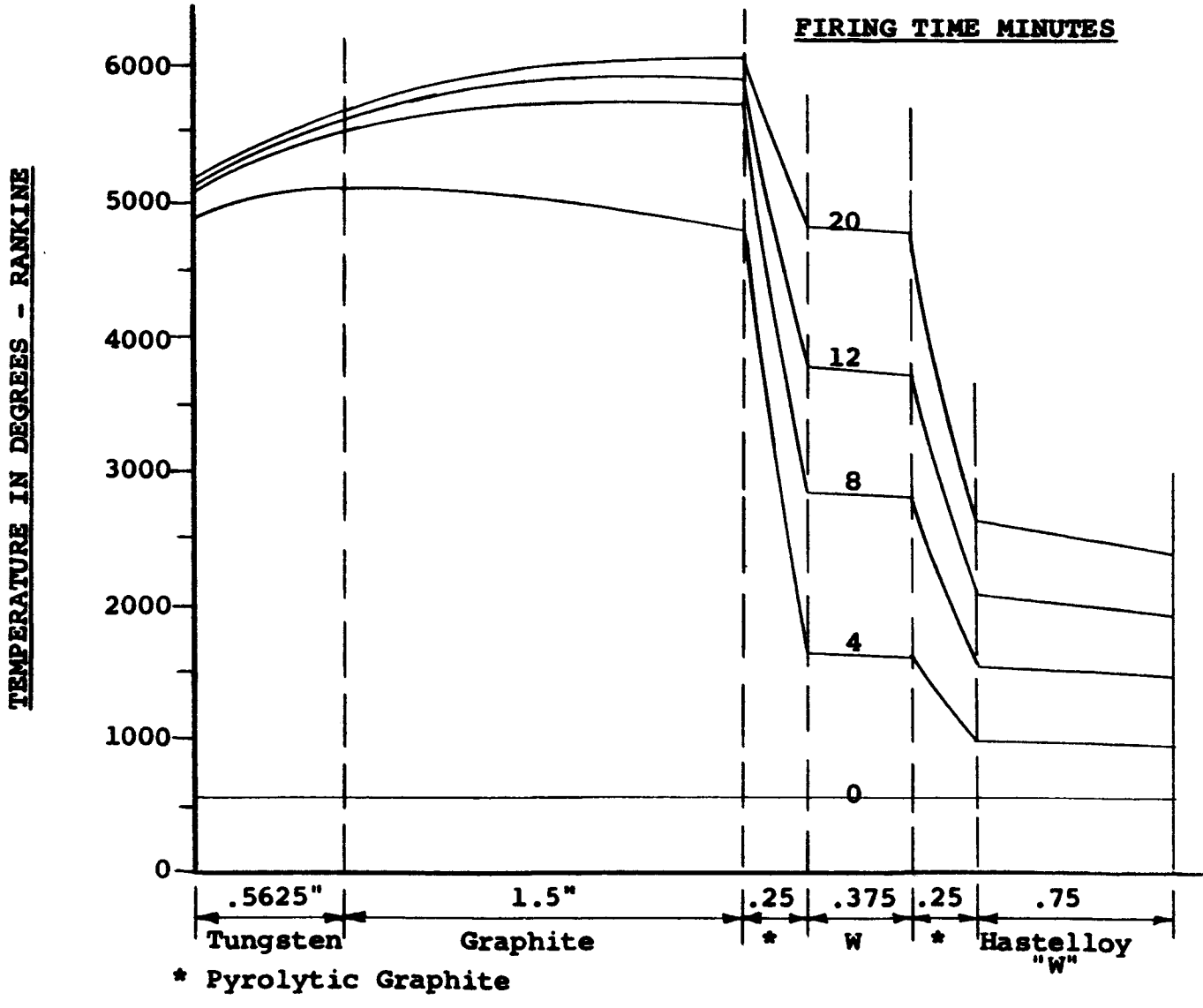

NOZZLE WALL

FIGURE 19a

ARDE-PORTLAND UNCOOLED NUCLEAR NOZZLE - IMPROVED WALL

THE EFFECT OF VARIATION IN GAMMA HEATING ON

TRANSIENT TEMPERATURE DISTRIBUTION - UPSTREAM SECTION

15,000 MW TOTAL POWER

25% OF CALCULATED GAMMA HEATING RATE

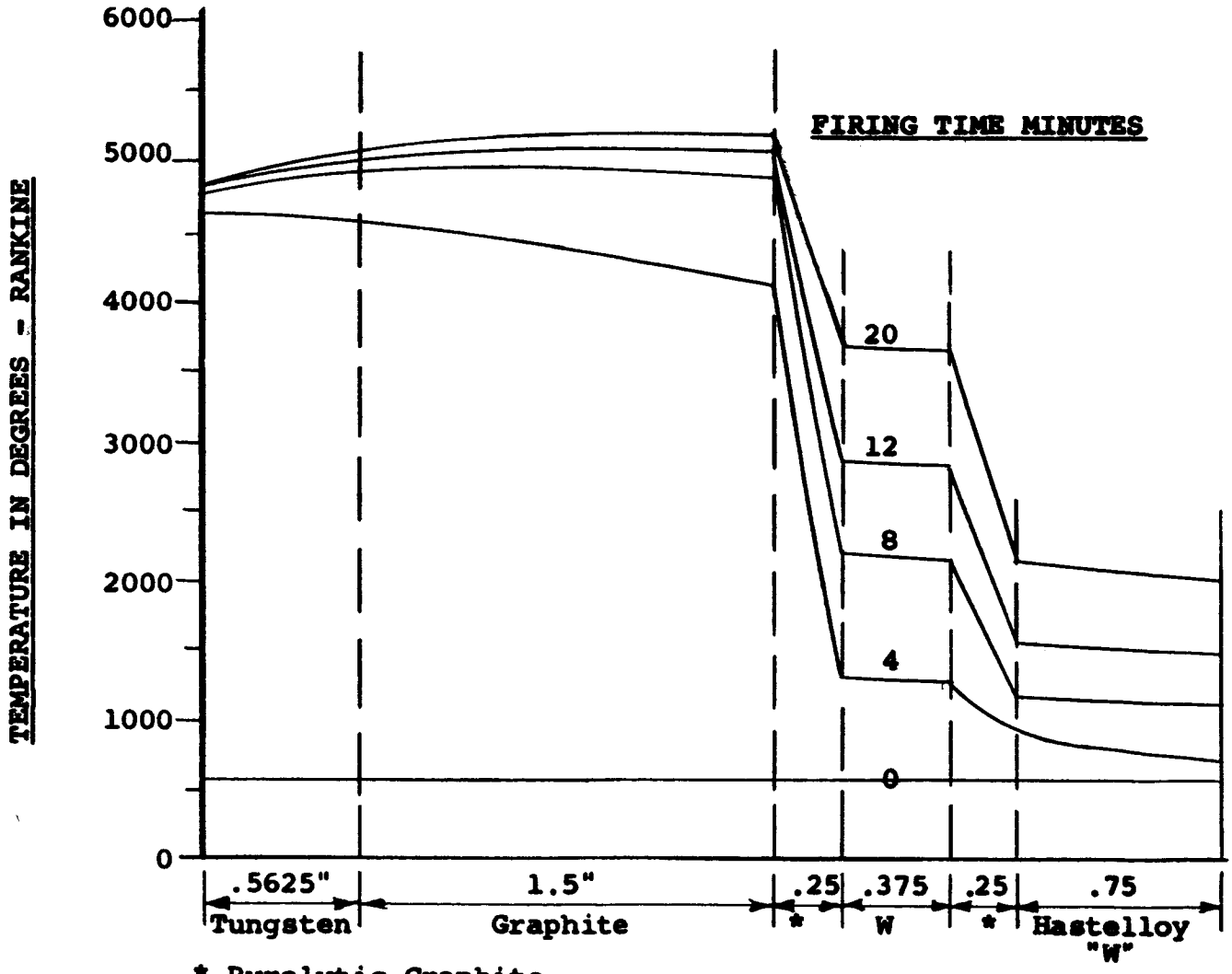

NOZZLE WALL

FIGURE 19b

ARDE-PORTLAND UNCOOLED NUCLEAR NOZZLE - IMPROVED WALL

THE EFFECT OF VARIATION IN GAMMA HEATING ON

TRANSIENT TEMPERATURE DISTRIBUTION - UPSTREAM SECTION

15,000 MW TOTAL POWER

10% OF CALCULATED GAMMA HEATING RATE

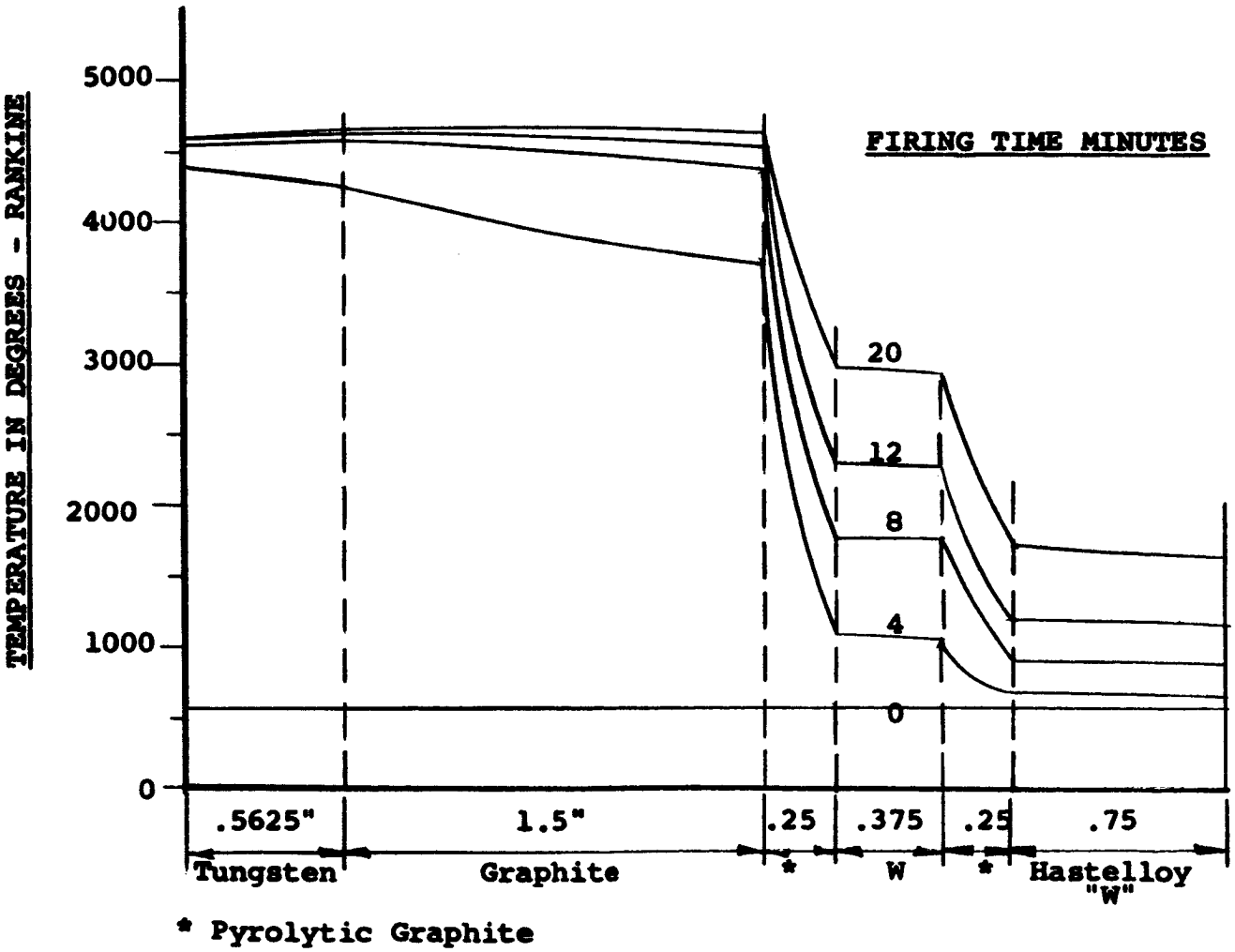

* Pyrolytic Graphite

NOZZLE WALL

FIGURE 19c

ARDE-PORTLAND UNCOOLED NUCLEAR NOZZLE - IMPROVED WALL

TRANSIENT TEMPERATURE DISTRIBUTION

UPSTREAM SECTION WITH TWO 3/8" SHIELDS

15,000 MW TOTAL POWER

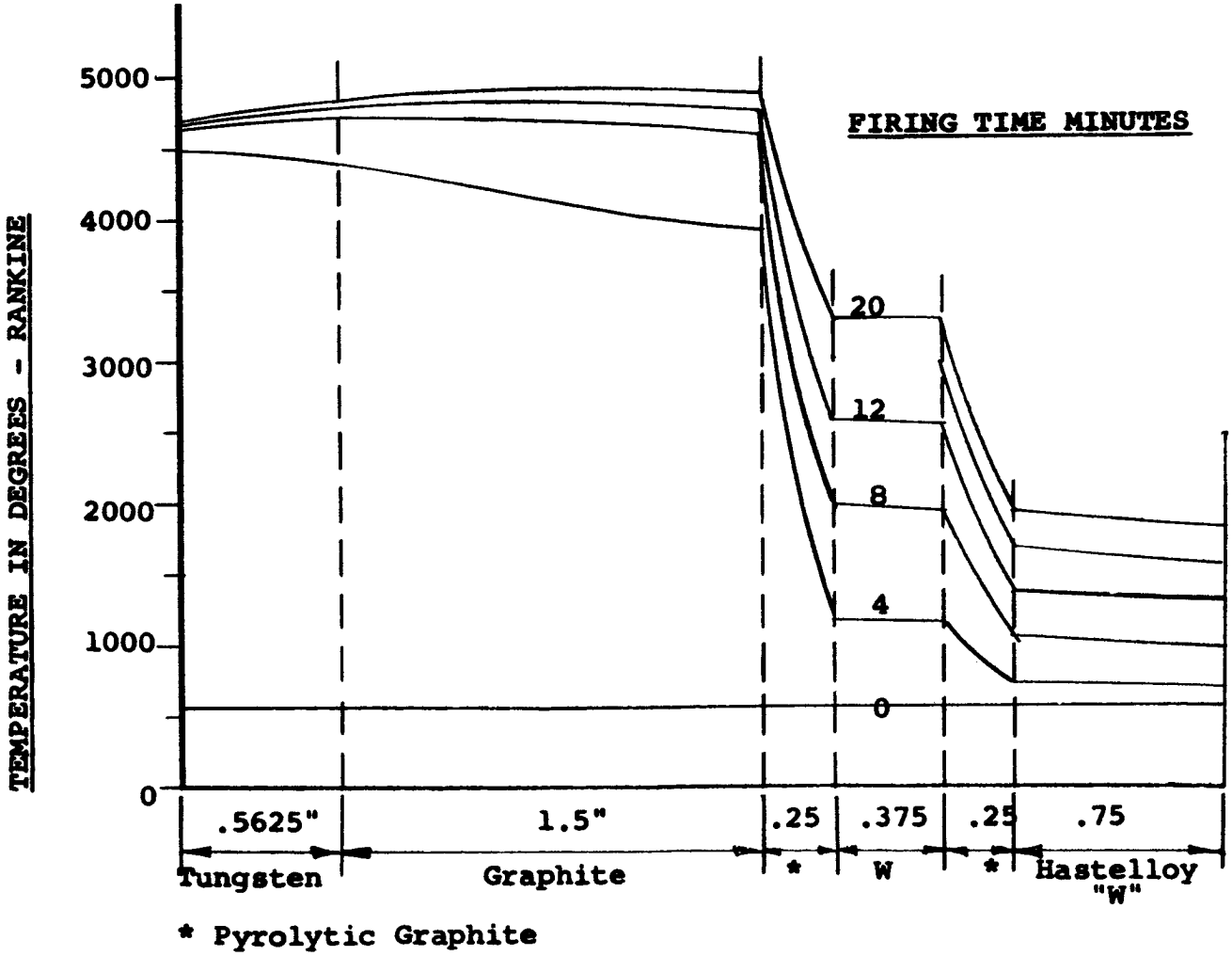

* Pyrolytic Graphite

NOZZLE WALL

FIGURE 20a

ARDE-PORTLAND UNCOOLED NUCLEAR NOZZLE - IMPROVED WALL

TRANSIENT TEMPERATURE DISTRIBUTION

THROAT SECTION WITH TWO 3/8" SHIELDS

15,000 MW TOTAL POWER

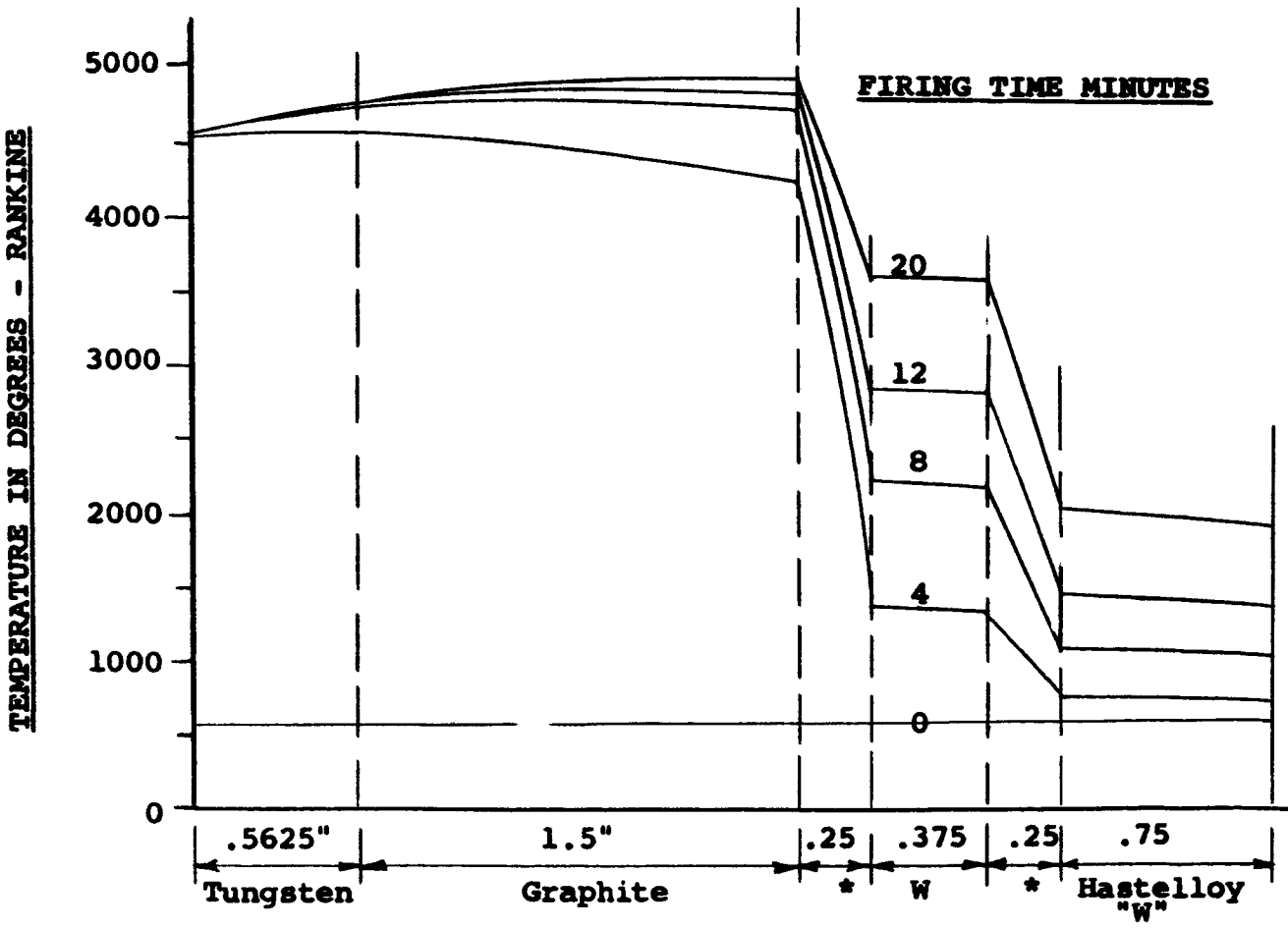

* Pyrolytic Graphite

NOZZLE WALL

FIGURE 20b

ARDE-PORTLAND NUCLEAR NOZZLE

EFFECT OF WALL THICKNESS

ON THE

STEADY STATE TEMPERATURE DISTRIBUTION

OF A SINGLE MATERIAL WALL - (W)

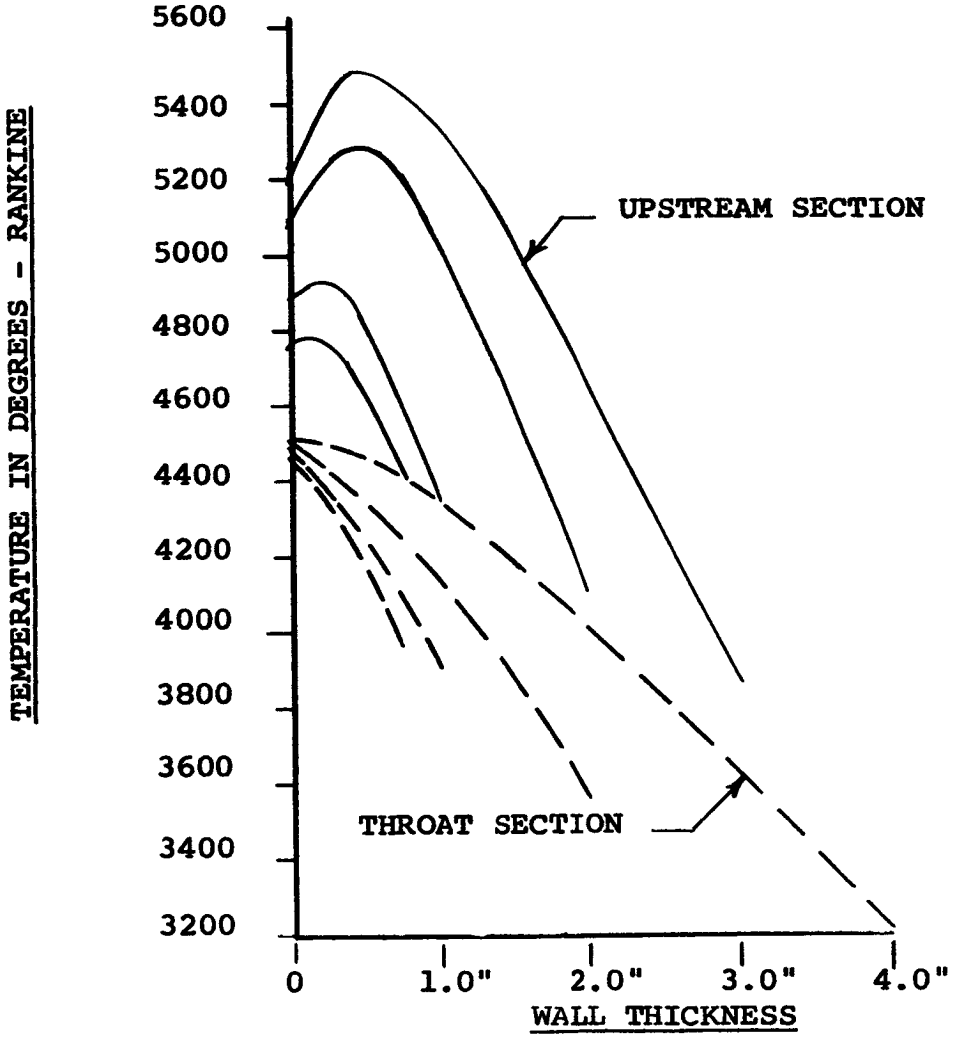

FIGURE 21

ARDE-PORTLAND NUCLEAR NOZZLE

LIMITED COOLING STUDY

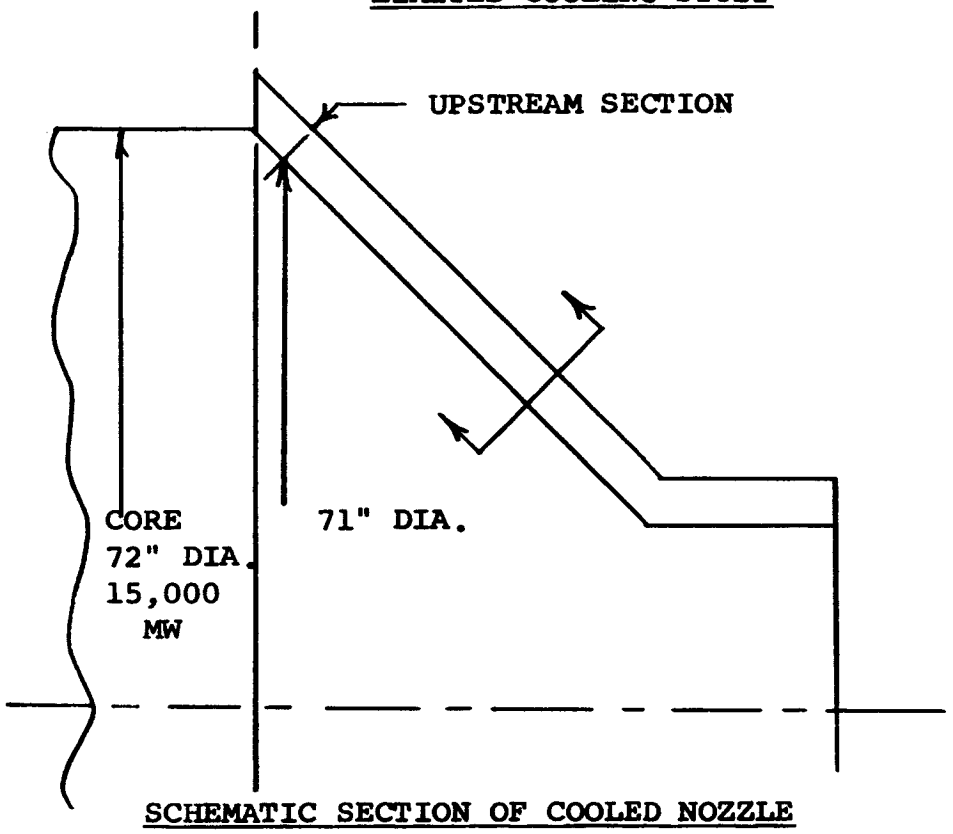

SCHEMATIC SECTION OF COOLED NOZZLE

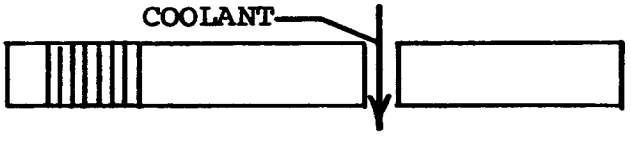

COOLANT IN MIDDLE OF HASTELLOY

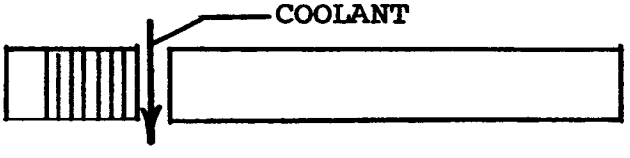

COOLANT AT HASTELLOY- PYROLYTIC INTERFACE

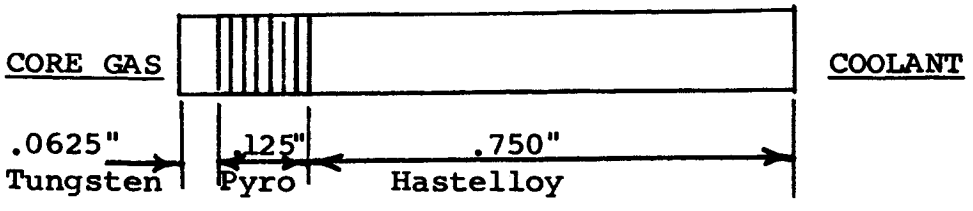

COOLANT AT OUTSIDE SURFACE

TYPICAL SECTION "A" - "A"

FIGURE 22

ARDE-PORTLAND NUCLEAR NOZZLE LIMITED COOLING STUDY

VOLUMETRIC GAMMA HEAT GENERATION WITHIN THE WALL

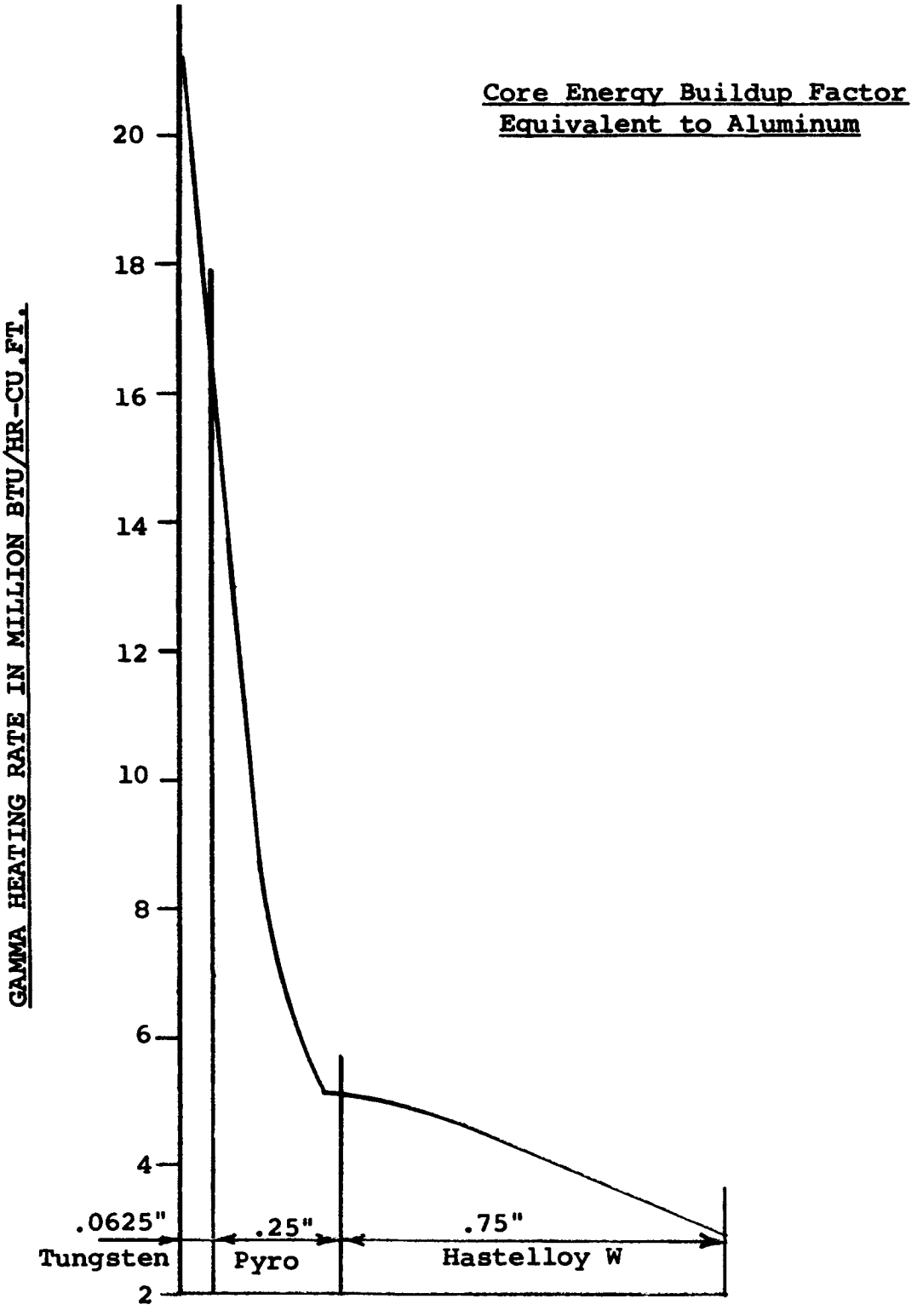

FIGURE 23

ARDE-PORTLAND NUCLEAR NOZZLE LIMITED COOLING STUDY

VARIATION OF STEADY STATE TEMPERATURE DISTRIBUTION AS A FUNCTION OF COOLANT TEMPERATURE AND CONVECTION COEFFICIENT

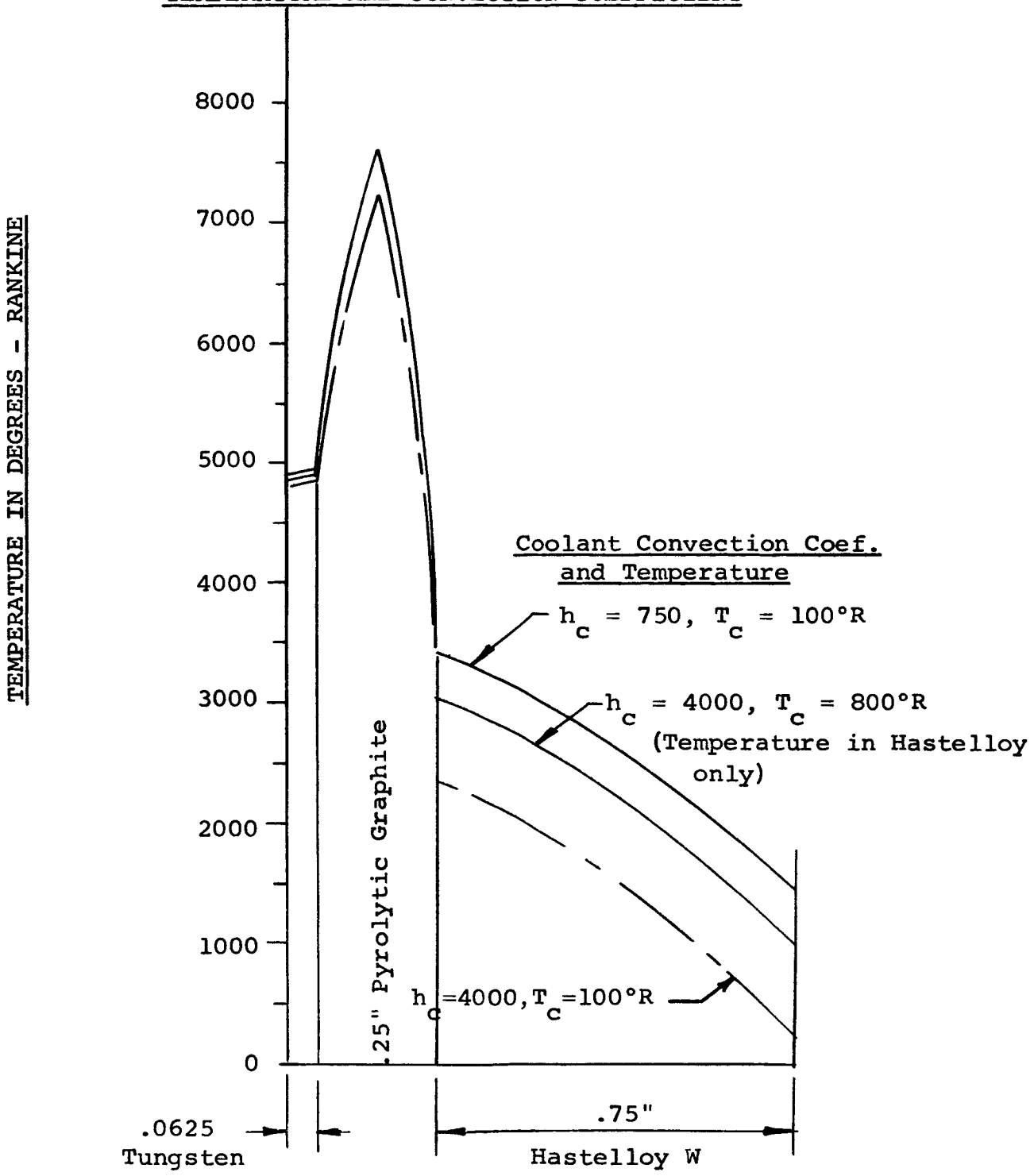

FIGURE 24

ARDE-PORTLAND NUCLEAR NOZZLE LIMITED COOLING STUDY

VARIATION OF STEADY STATE TEMPERATURE DISTRIBUTION AS A FUNCTION OF COOLANT TEMPERATURE AND CONVECTION COEFFICIENT

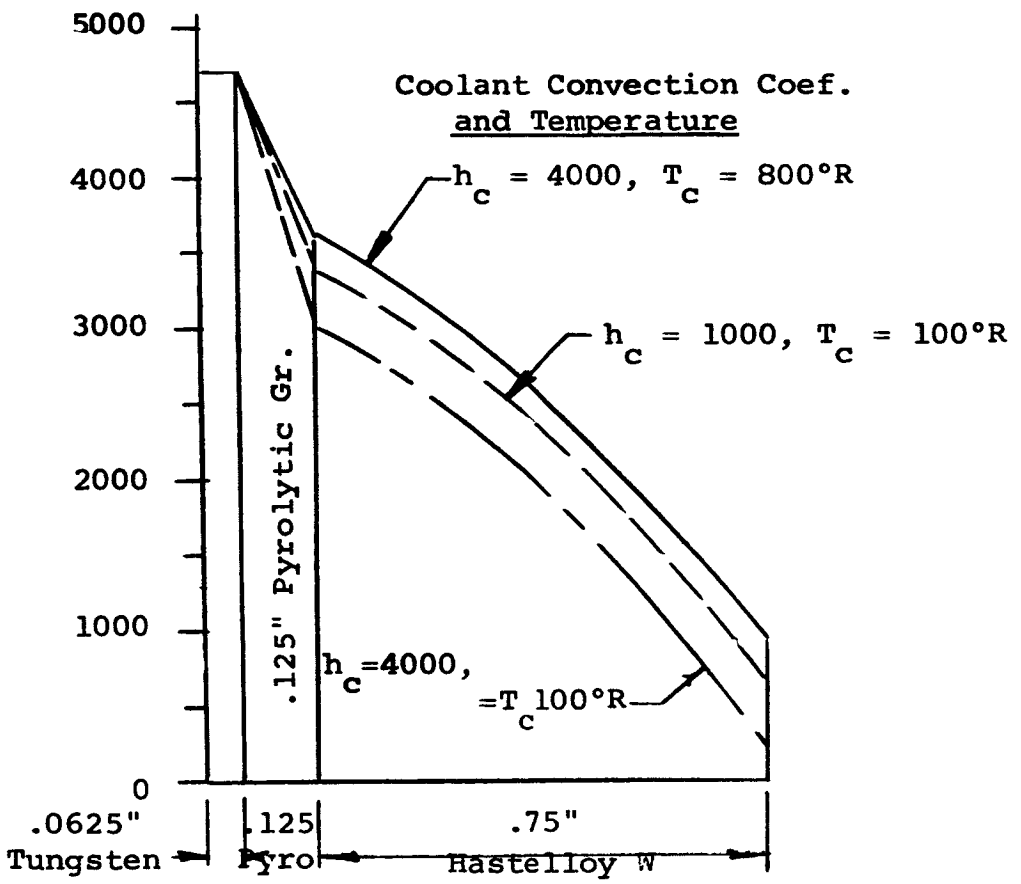

NOZZLE WALL

FIGURE 25

ARDE-PORTLAND NUCLEAR NOZZLE LIMITED COOLING STUDY

EFFECT OF COOLANT CONVECTION COEFFICIENT

ON STEADY STATE TEMPERATURE DISTRIBUTION

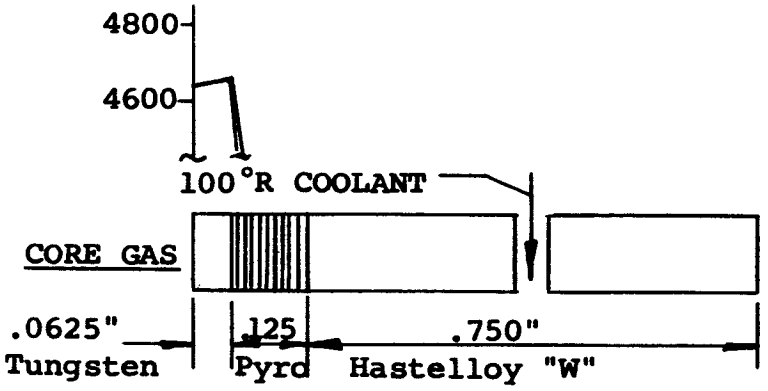

Schematic Section

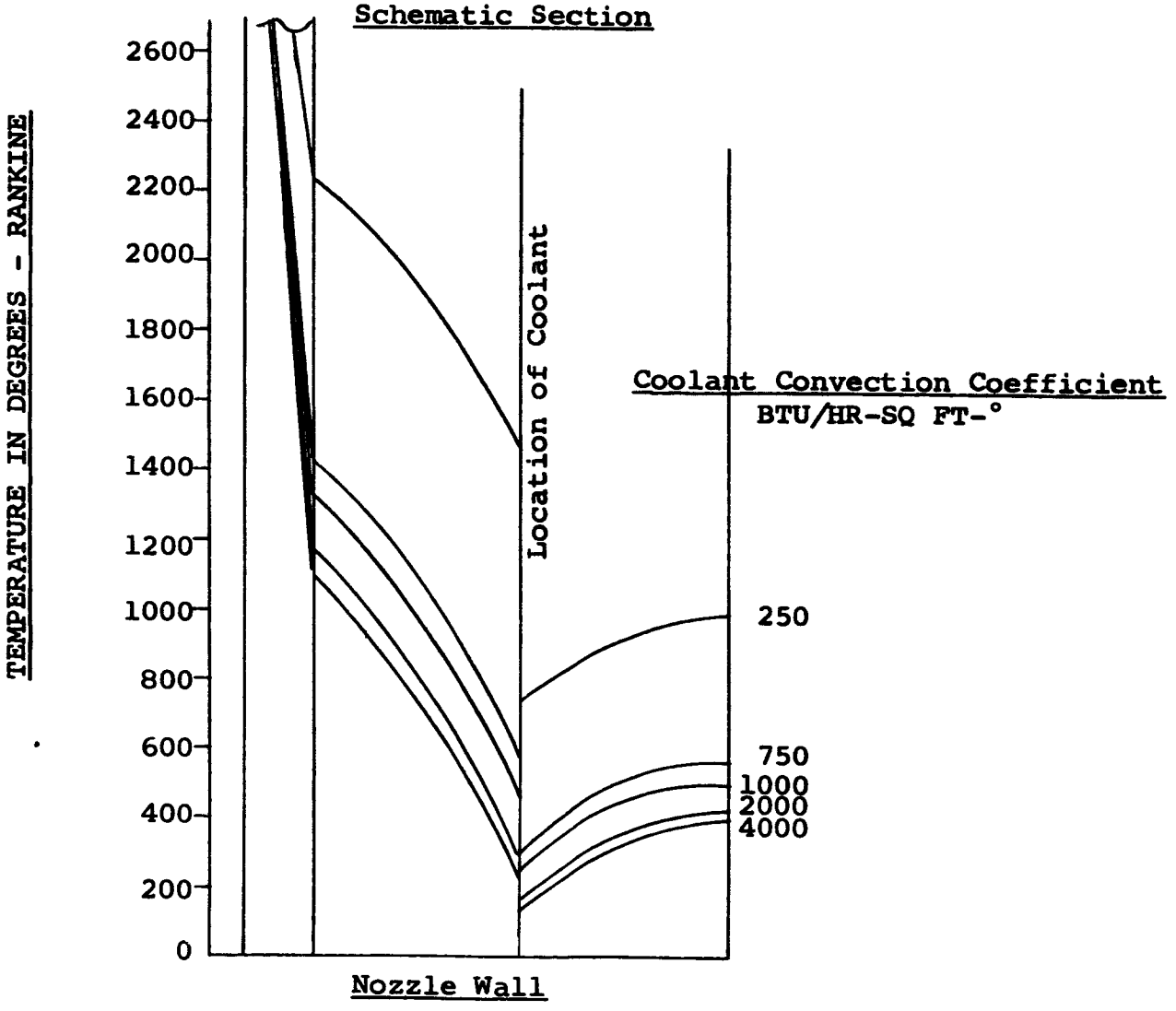

FIGURE 29

ARDE-PORTLAND NUCLEAR NOZZLE LIMITED COOLING STUDY

EFFECT OF COOLANT CONVECTION COEFFICIENT ON STEADY STATE TEMPERATURE DISTRIBUTION

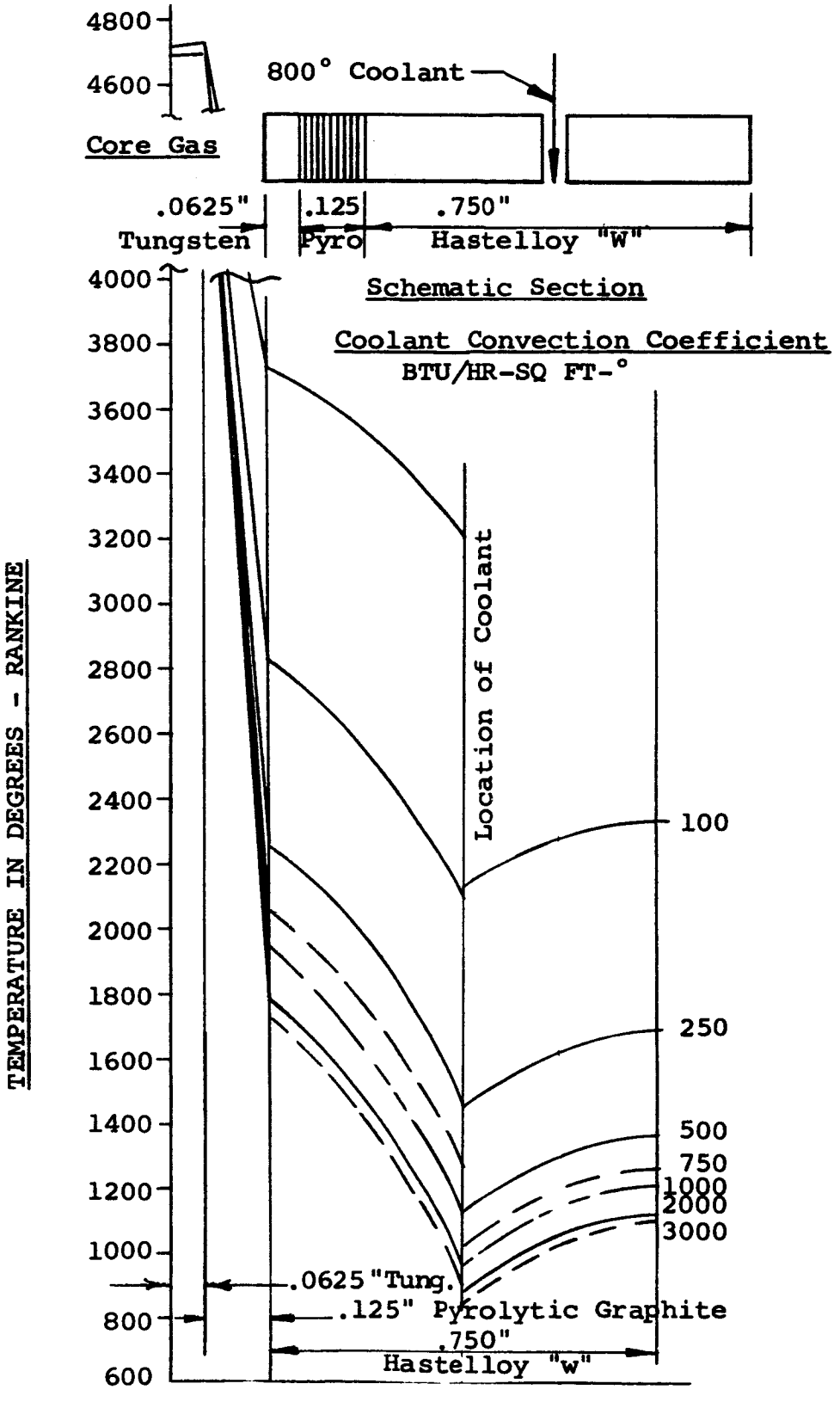

FIGURE 27

ARDE-PORTLAND NUCLEAR NOZZLE LIMITED COOLING STUDY

EFFECT OF COOLANT CONVECTION COEFFICIENT ON STEADY STATE TEMPERATURE DISTRIBUTION

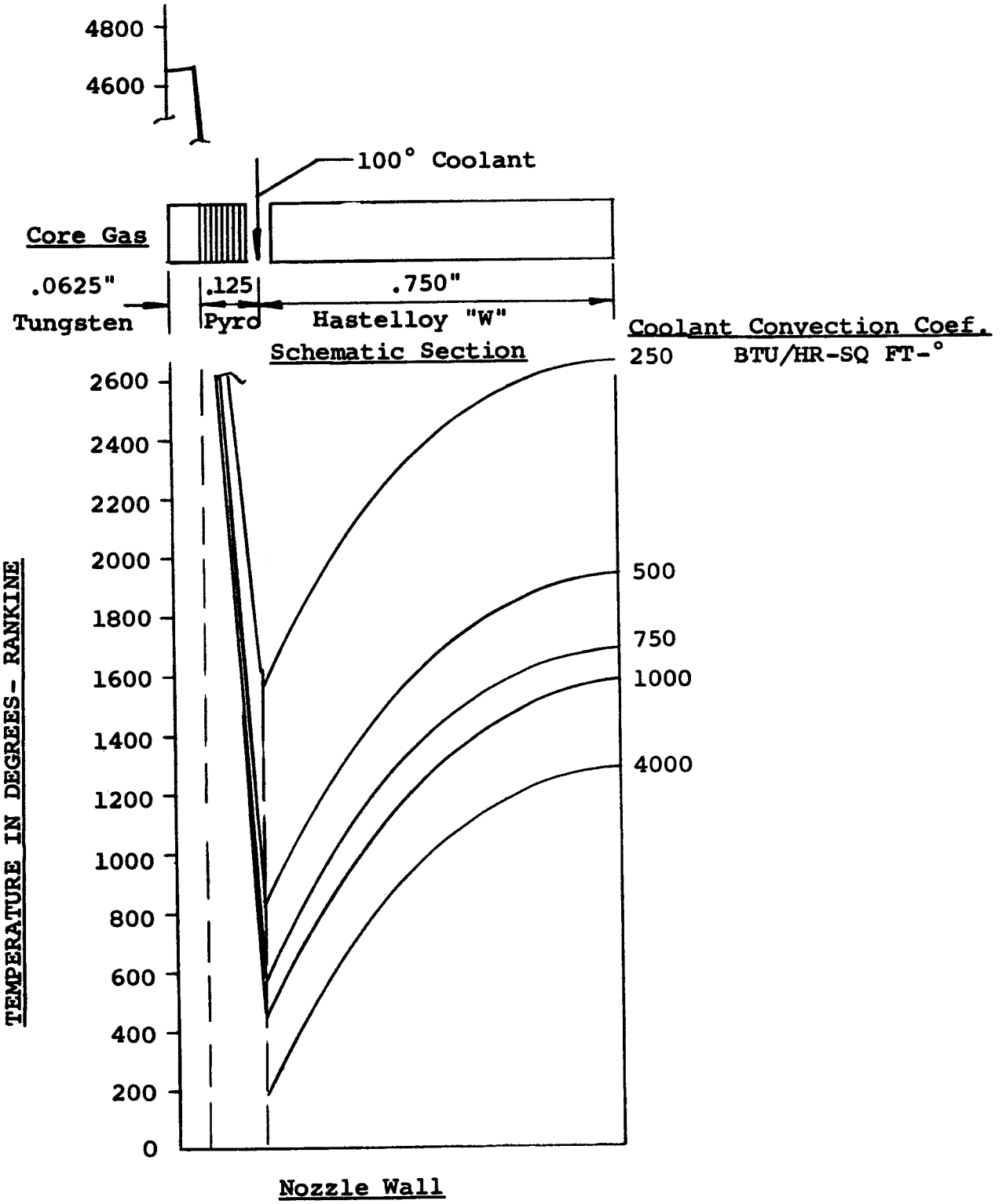

FIGURE 28

ARDE-PORTLAND NUCLEAR NOZZLE LIMITED COOLING STUDY
EFFECT OF COOLANT CONVECTION COEFFICIENT
ON STEADY STATE TEMPERATURE DISTRIBUTION

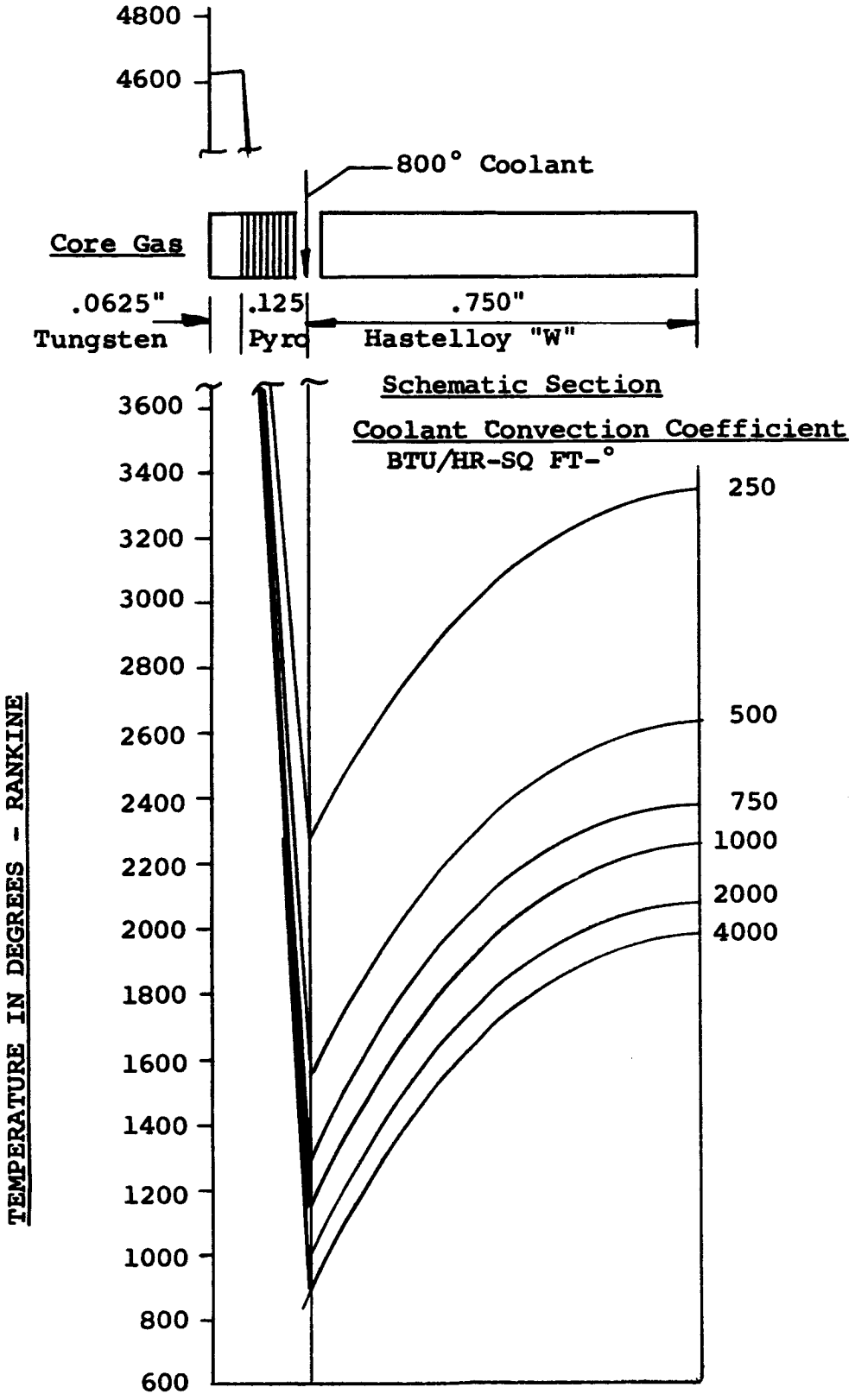

FIGURE 29

ARDE-PORTLAND NUCLEAR NOZZLE LIMITED COOLING STUDY

WALL TEMPERATURE DISTRIBUTION VS. COOLANT CONVECTION COEFFICIENT

COOLANT 100°R

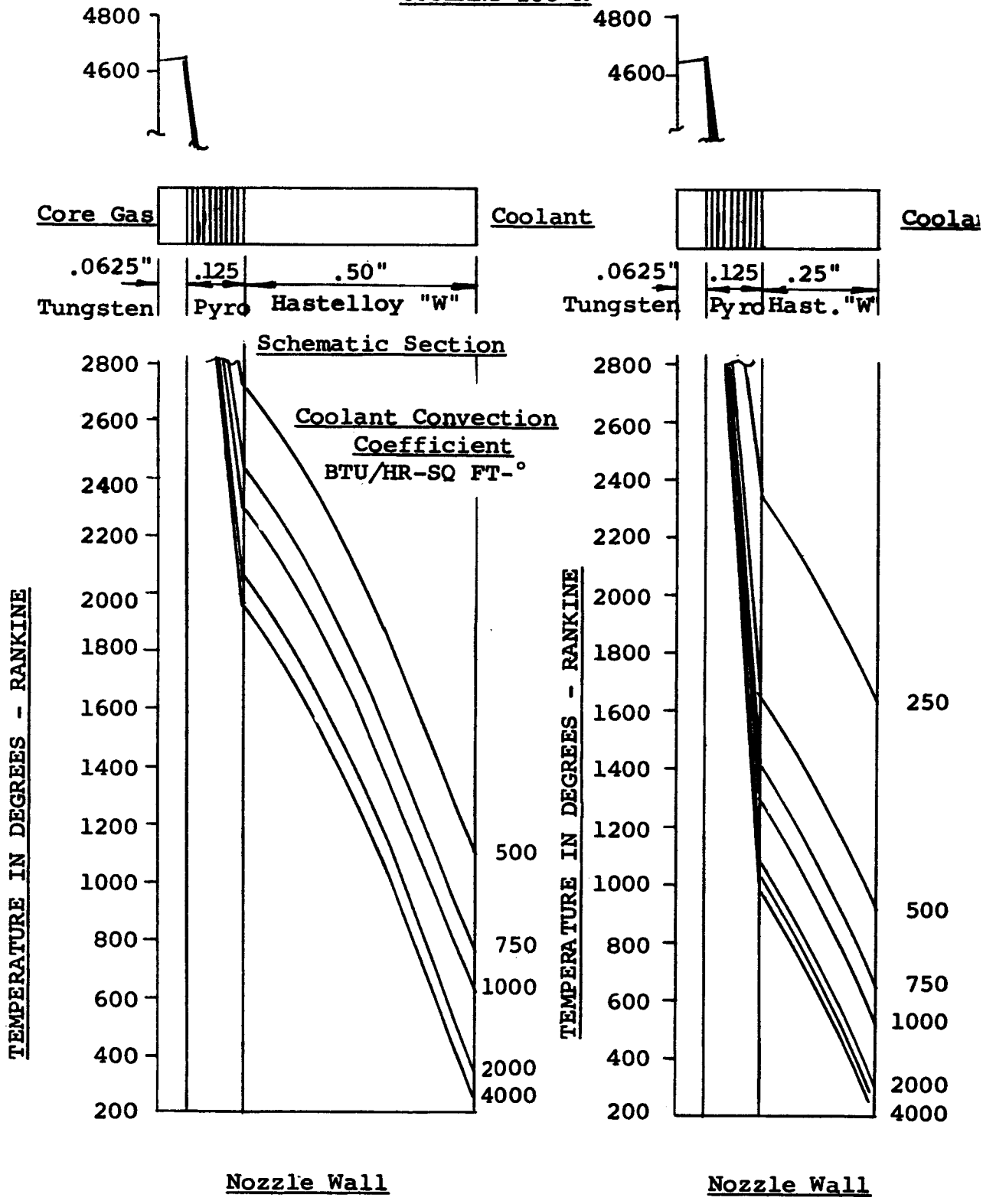

FIGURE 30

FIGURE 31

ARDE-PORTLAND NUCLEAR NOZZLE LIMITED COOLING STUDY

WALL TEMPERATURE DISTRIBUTION VS. COOLANT CONVECTION COEFFICIENT

COOLANT 800°R

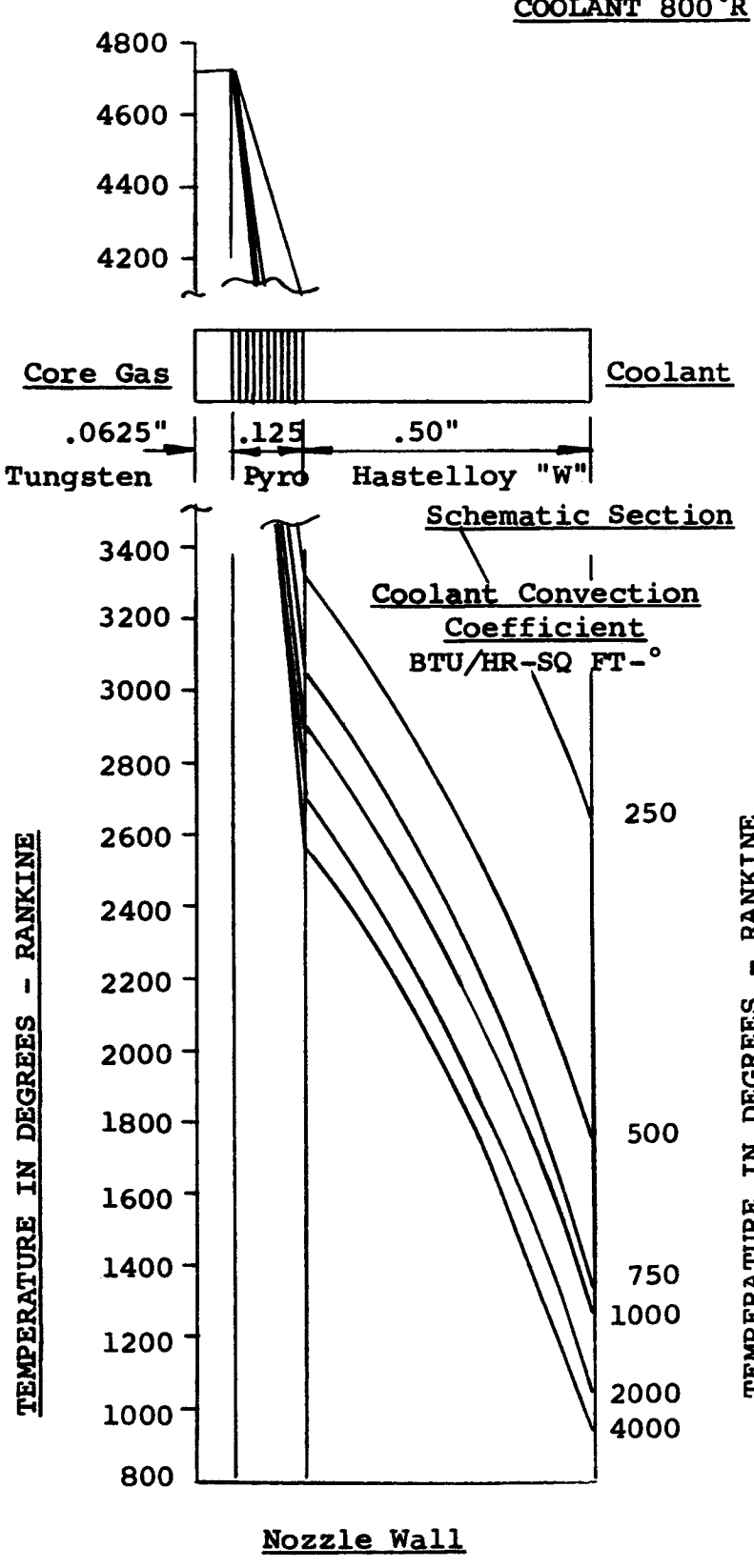

FIGURE 32

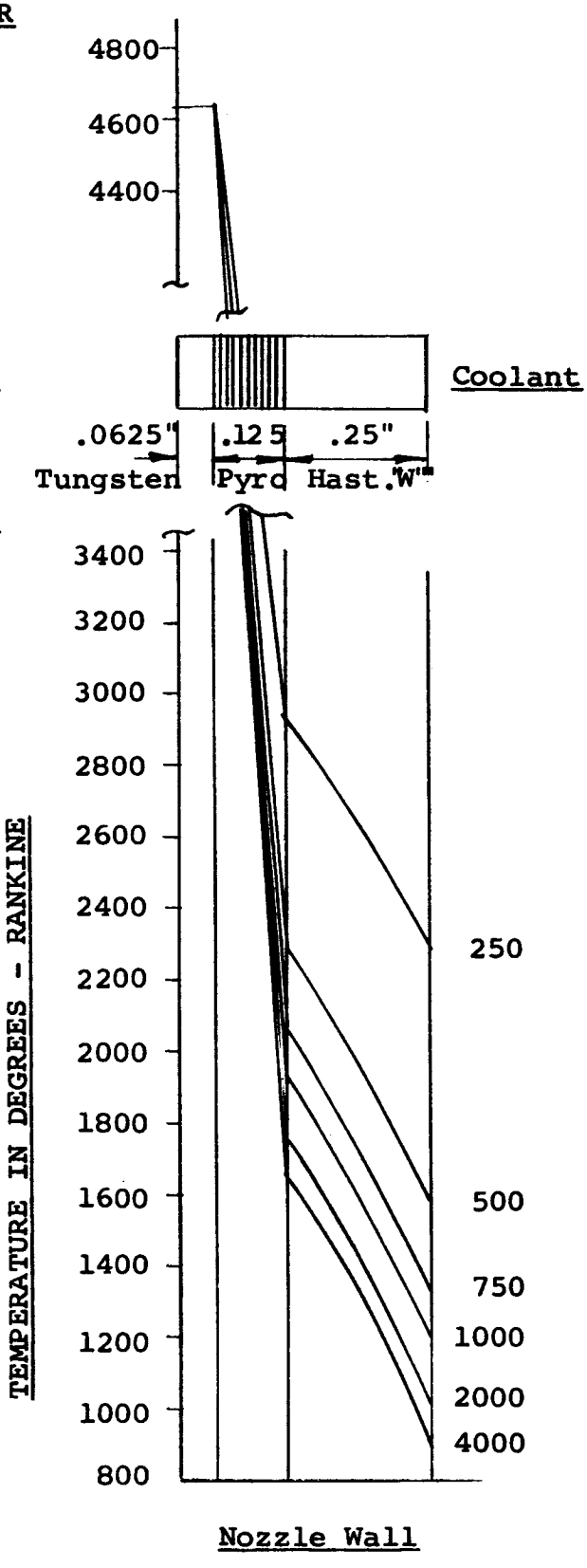

FIGURE 33

ARDE-PORTLAND NUCLEAR NOZZLE LIMITED COOLING STUDY

WALL SURFACE TEMPERATURE

AS A FUNCTION OF

HASTELLOY THICKNESS AND COOLANT TEMPERATURE

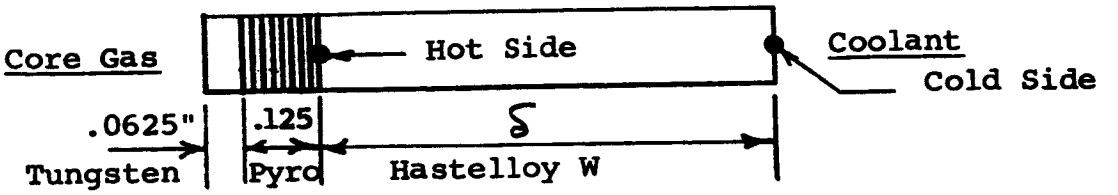

Schematic Section

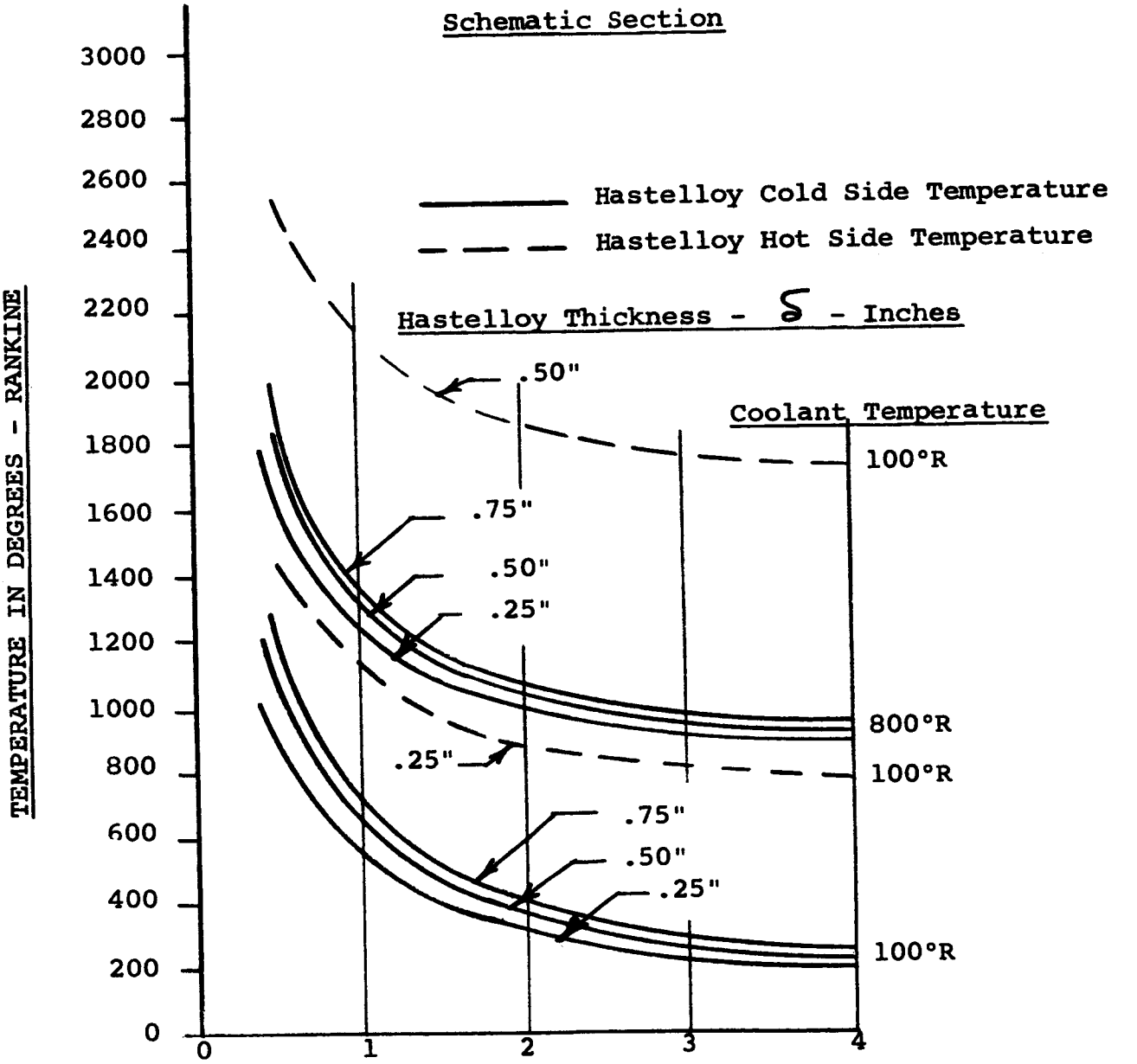

Coolant Convection Coefficient

1000 BTU/HR SQ FT °F

Figure 34

ARDE-PORTLAND NUCLEAR NOZZLE LIMITED COOLING STUDY

HEAT ABSORBED BY THE COOLANT

AS A FUNCTION OF

HASTELLOY THICKNESS AND COOLANT TEMPERATURE

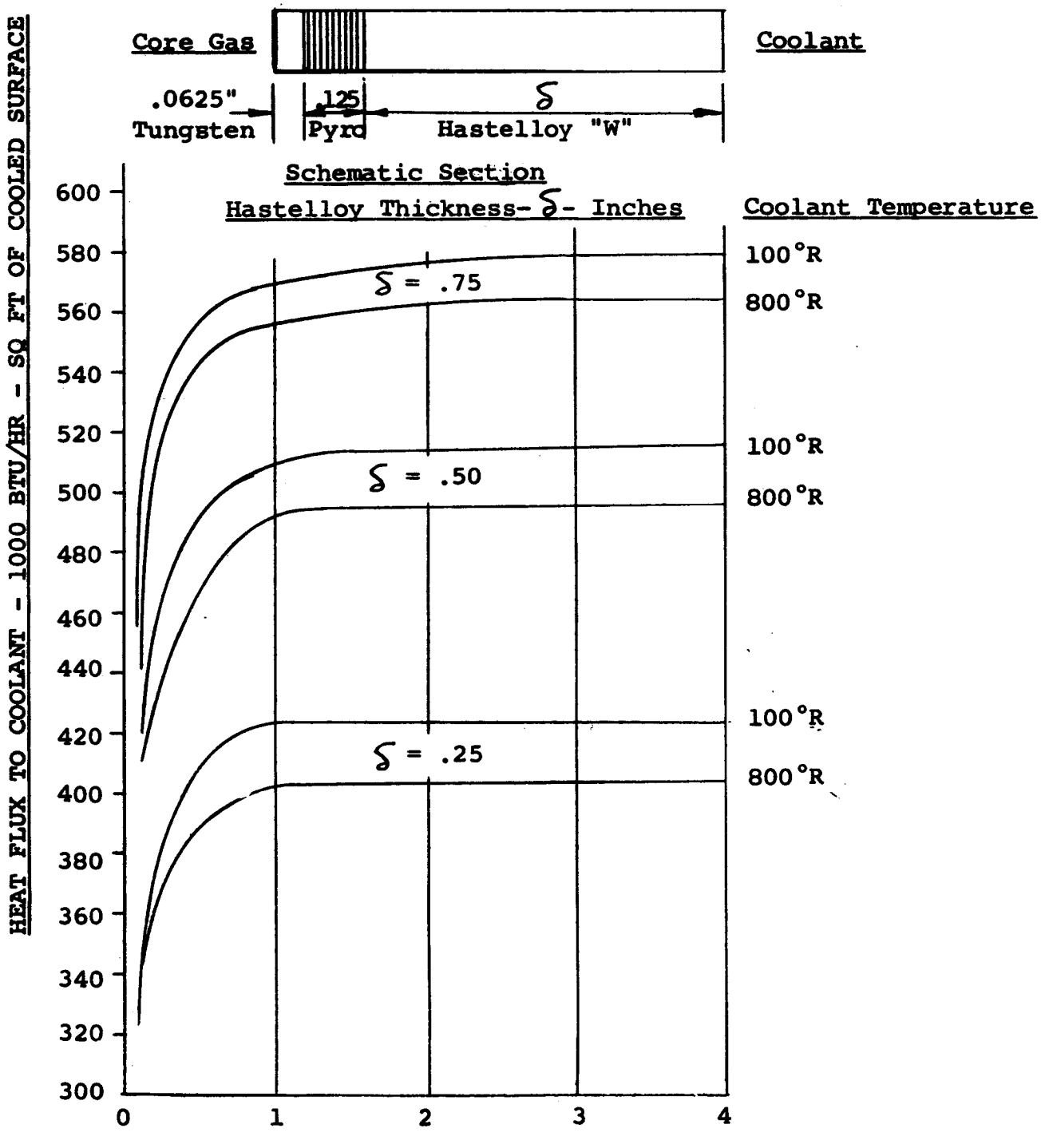

Coolant Convection Coefficient
1000 BTU/HR SQ FT°

FIGURE 35

ARDE-PORTLAND NUCLEAR NOZZLE LIMITED COOLING STUDY

DIVISION OF NOZZLE INTO STATIONS

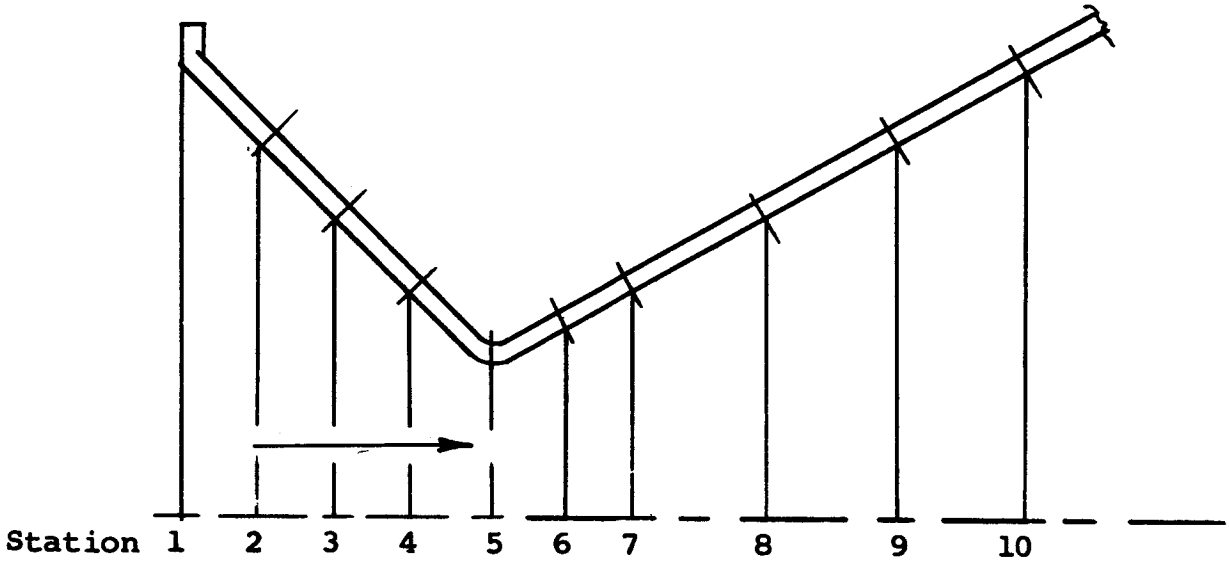

SCHEMATIC SECTION OF NOZZLE

STATION	DIAMETER INCHES	PRESSURE PSIA	VELOCITY
1	72	998	Subsonic
2	60	994	Subsonic
3	48	987	Subsonic
4	36	959	Subsonic
5	23	539	Sonic
6	30	133	Supersonic
7	36	72	Supersonic
8	48	29	Supersonic
9	60	15	Supersonic
10	72	8	Supersonic

FIGURE 36

ARDE-PORTLAND NUCLEAR NOZZLE LIMITED COOLING STUDY

VARIATION OF WALL THICKNESS WITH NOZZLE STATION

FOR SELECTED MATERIALS

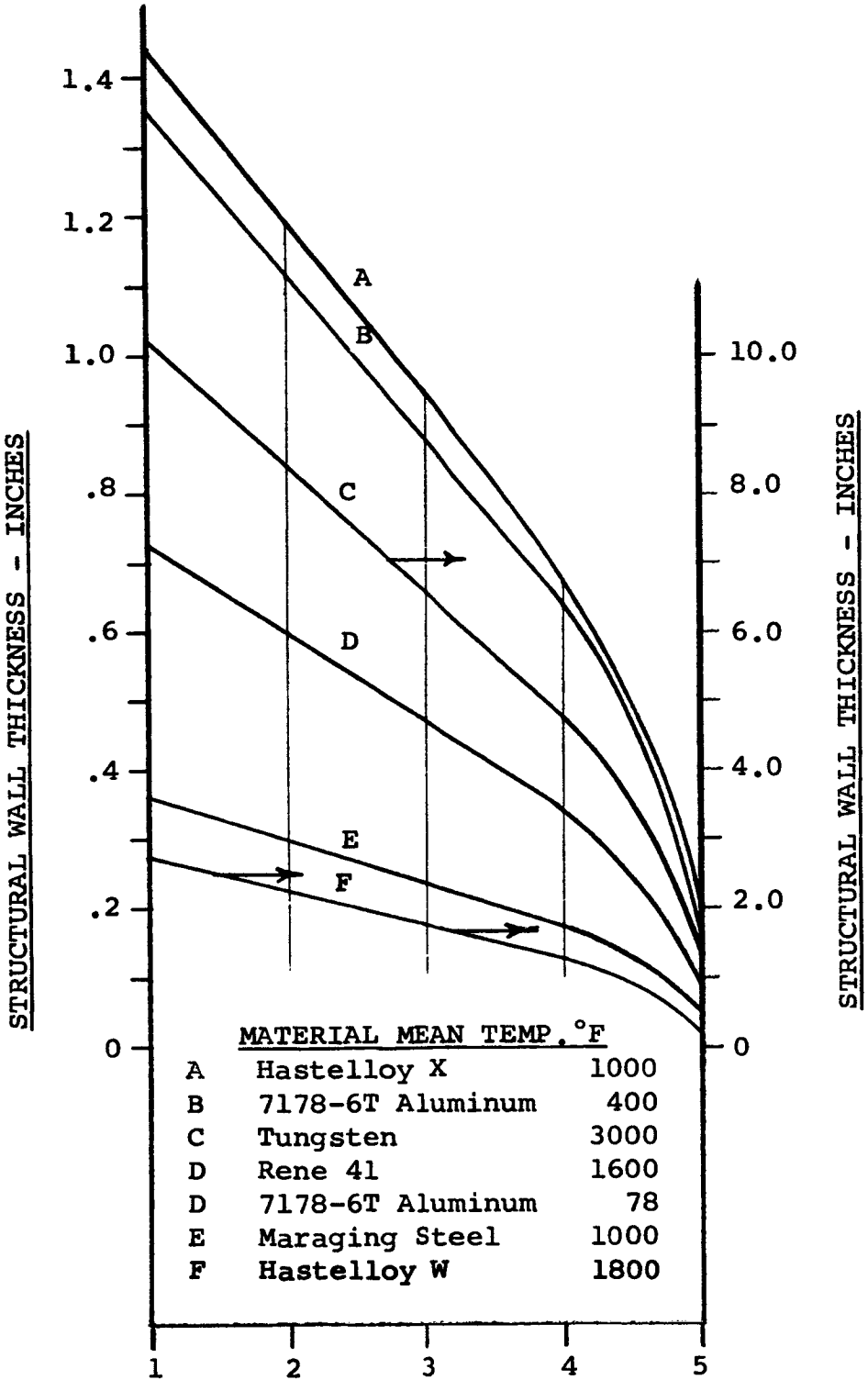

FIGURE 37

ARDE-PORTLAND NUCLEAR NOZZLE LIMITED COOLING STUDY

TYPICAL STEADY STATE TEMPERATURE DISTRIBUTIONS

100°R COOLANT AT OUTSIDE DIAMETER

CONVECTION COEFFICIENT - 2000 BTU/HR-SQ.FT.°

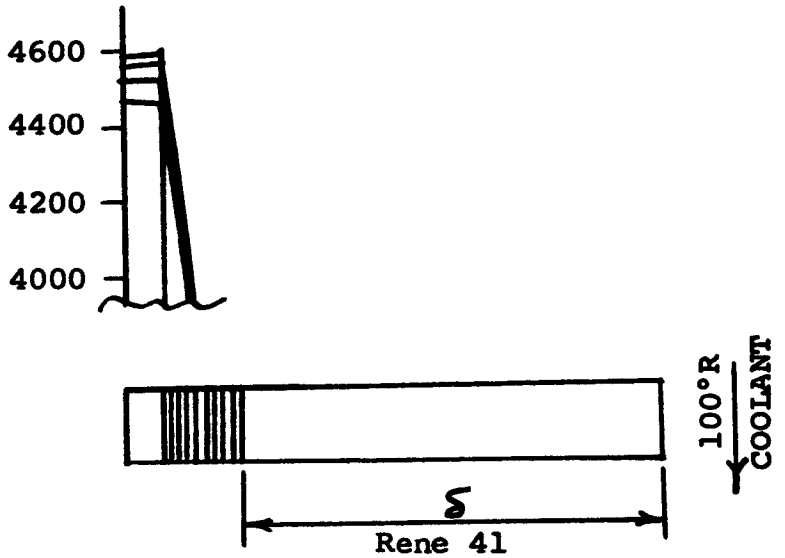

SCHEMATIC SECTION

RENE 41 THICKNESS	
Station	δ (inches)
1	.726
2	.602
3	.479
4	.348
5	.089

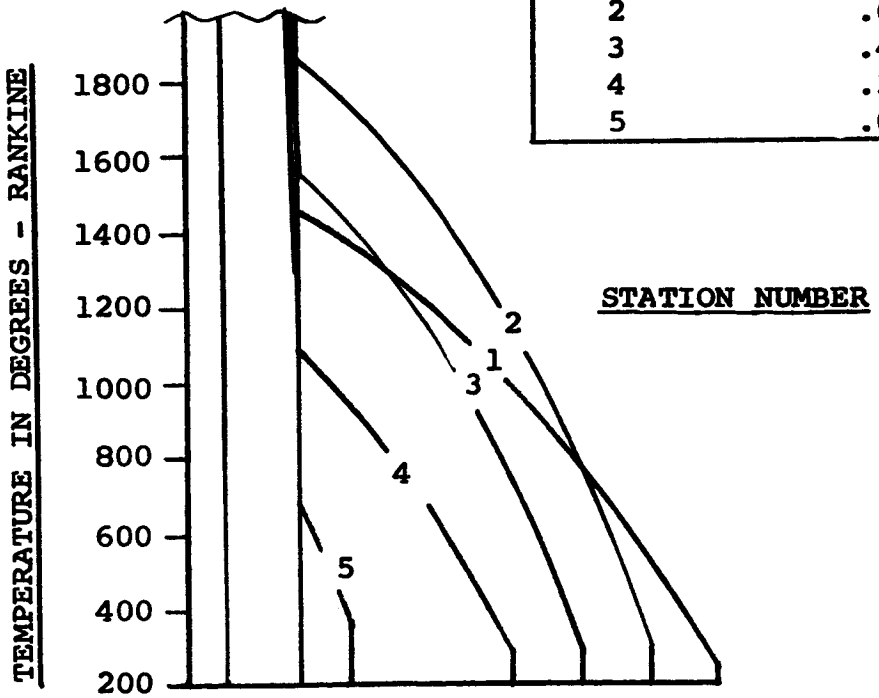

FIGURE 38

ARDE-PORTLAND NUCLEAR NOZZLE LIMITED COOLING STUDY

TYPICAL STEADY STATE TEMPERATURE DISTRIBUTIONS

800°R COOLANT AT OUTSIDE DIAMETER

CONVECTION COEFFICIENT - 2000 BTU/HR-SQ.FT.°

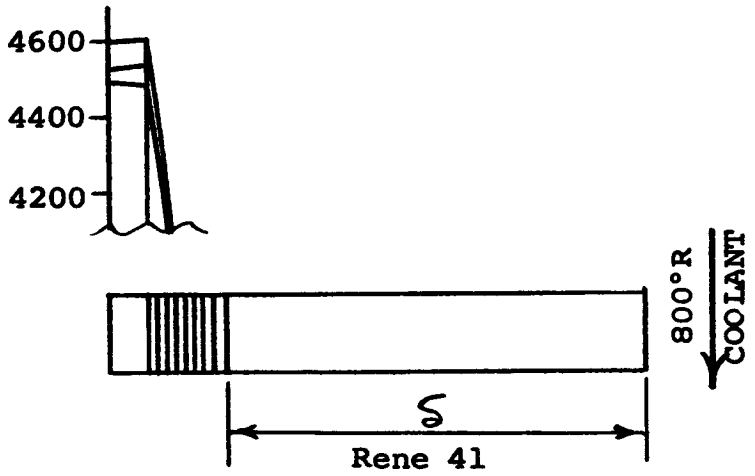

RENE 41 THICKNESS	
Station	δ (inches)
1	.726
2	.602
3	.479
4	.348
5	.089

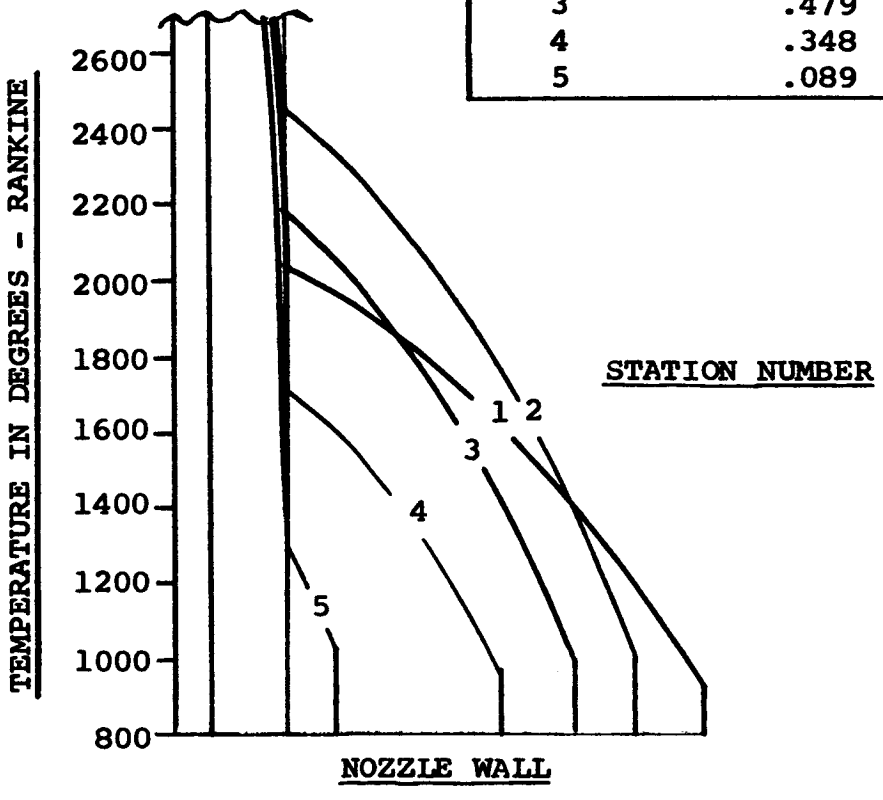

FIGURE 39

ARDE-PORTLAND NUCLEAR NOZZLE LIMITED COOLING STUDY

TYPICAL STEADY STATE TEMPERATURE DISTRIBUTIONS

100°R COOLANT AT OUTSIDE DIAMETER

CONVECTION COEFFICIENT - 2000 BTU/HR-SQ.FT.°

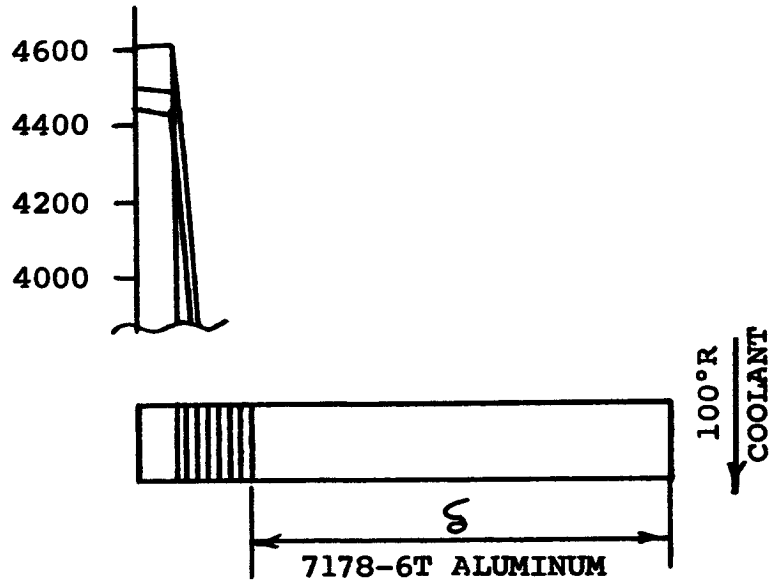

SCHEMATIC SECTION

ALUMINUM THICKNESS	
Station	δ (inches)
1	.726
2	.602
3	.479
4	.348
5	.089

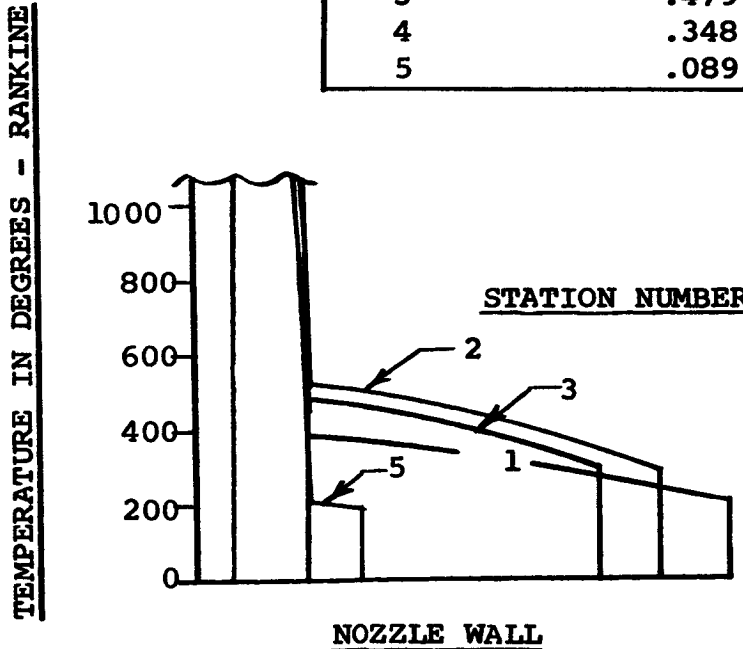

NOZZLE WALL

FIGURE 40

EFFECT OF STRUCTURAL WALL MATERIAL

ON

GAMMA HEAT GENERATION WITHIN WALL

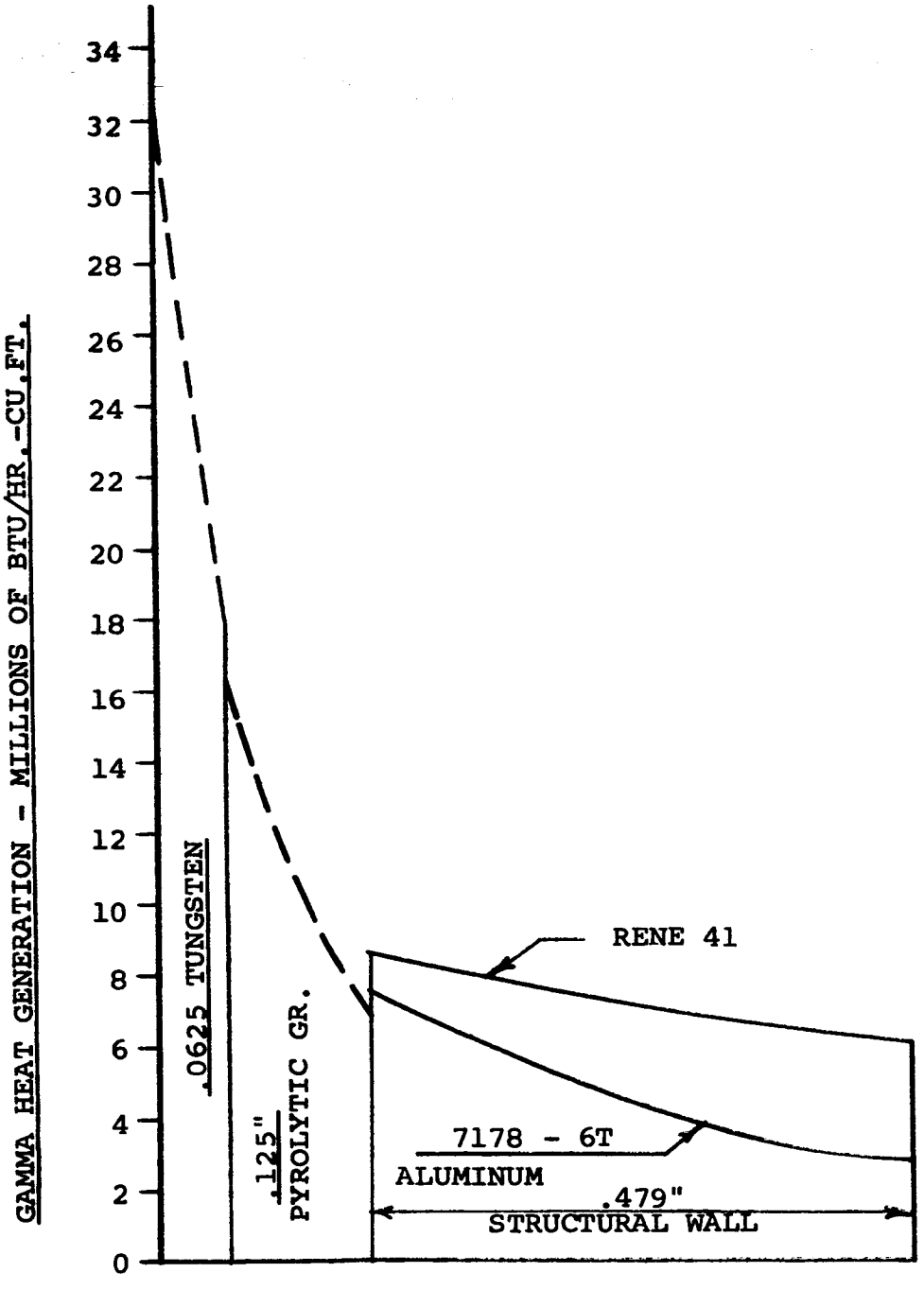

FIGURE 41

ARDE-PORTLAND NUCLEAR NOZZLE LIMITED COOLING STUDY

GAP HEIGHT REQUIRED FOR $h_{coolant} = 2000$

AS A FUNCTION OF NOZZLE STATION AND COOLANT TEMPERATURE

FOR AN ANNULAR COOLING PASSAGE

5% COOLANT FLOW

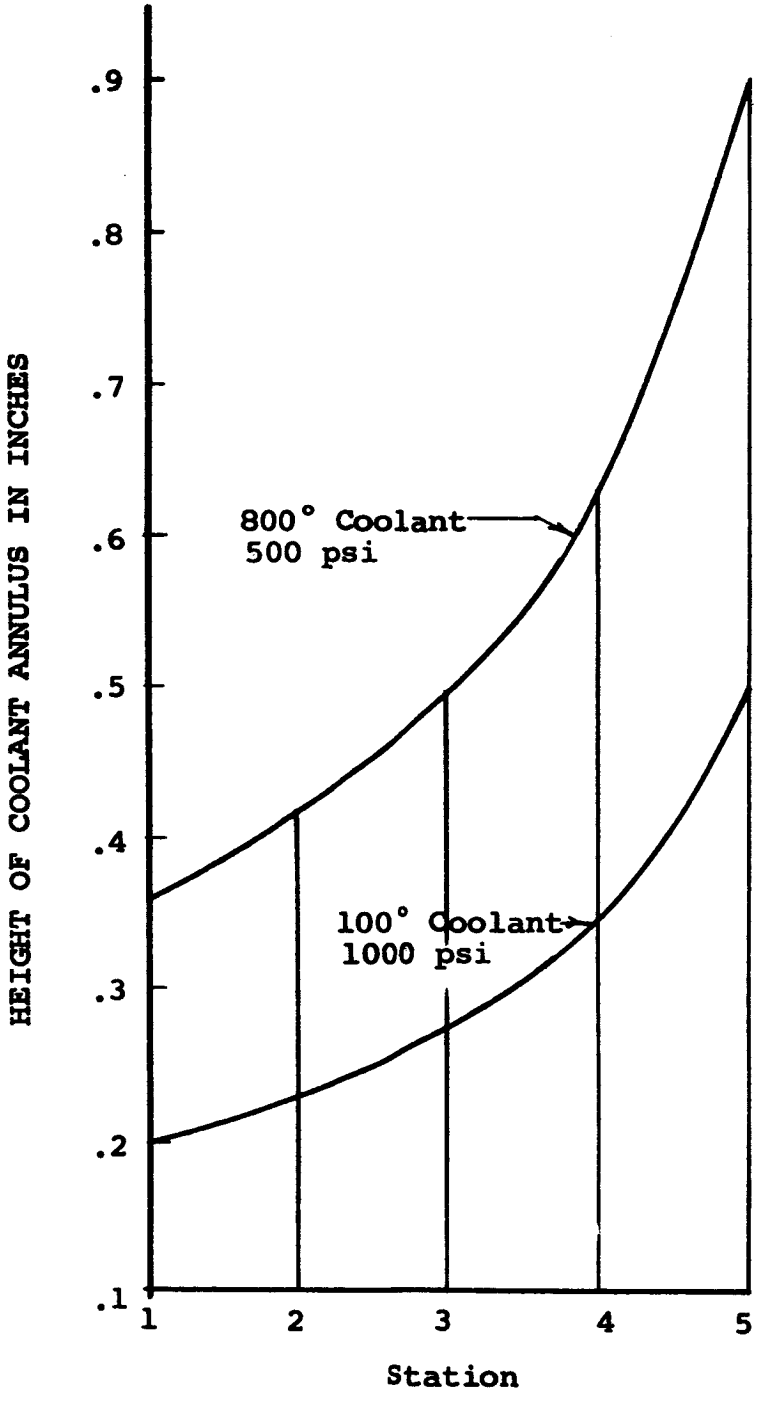

FIGURE 42

ARDE-PORTLAND NUCLEAR NOZZLE

TEMPERATURE HISTORY DURING START-UP

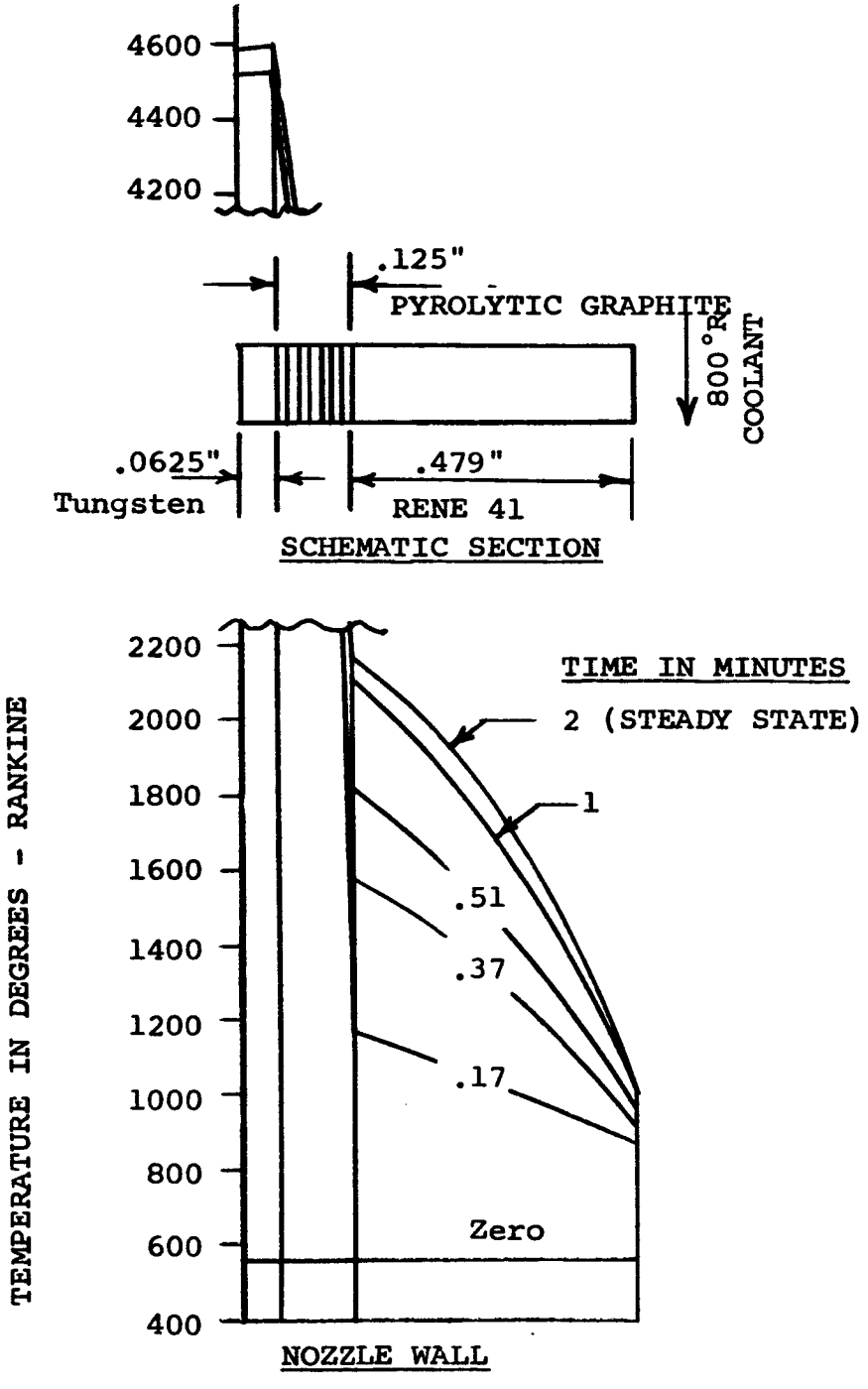

FIGURE 43

REACTOR POWER DECAY AFTER SHUTDOWN

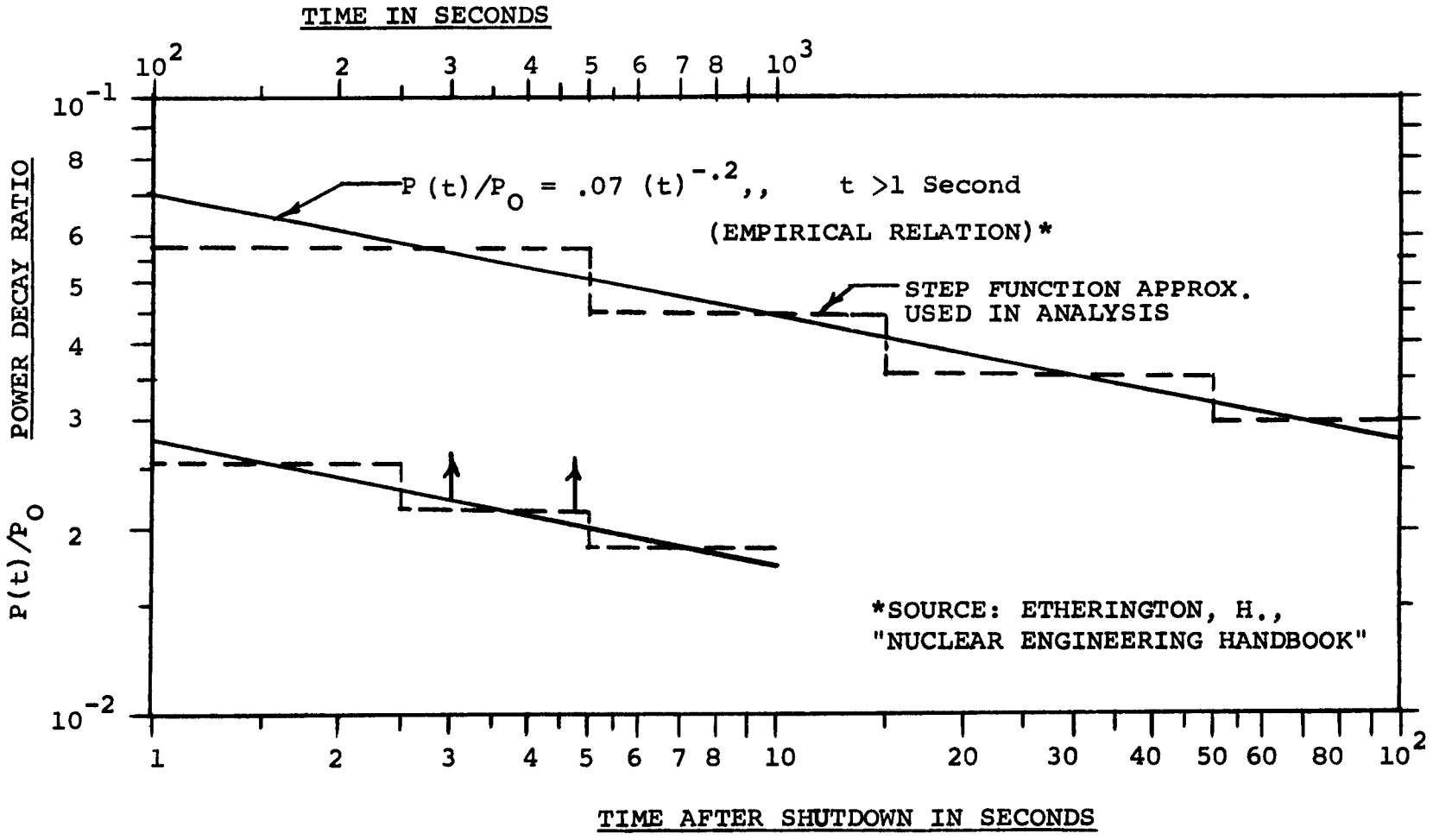

FIGURE 44

ARDE-PORTLAND NUCLEAR NOZZLE

WALL TEMPERATURE HISTORY AFTER REACTOR SHUTDOWN

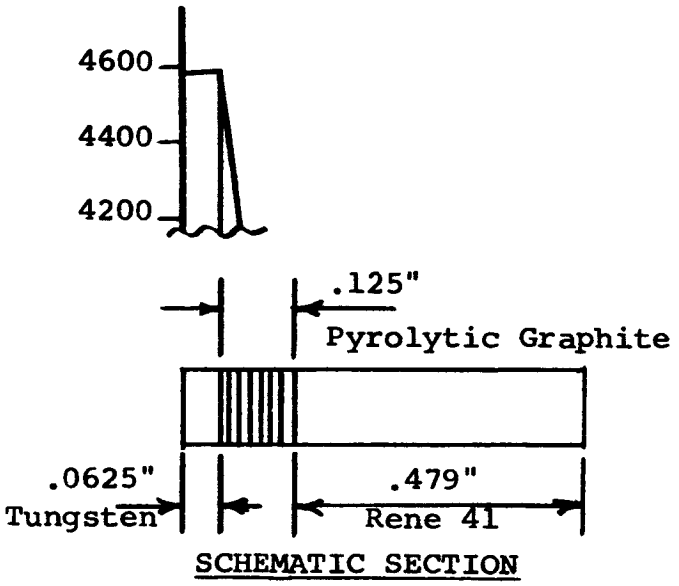

SCHEMATIC SECTION

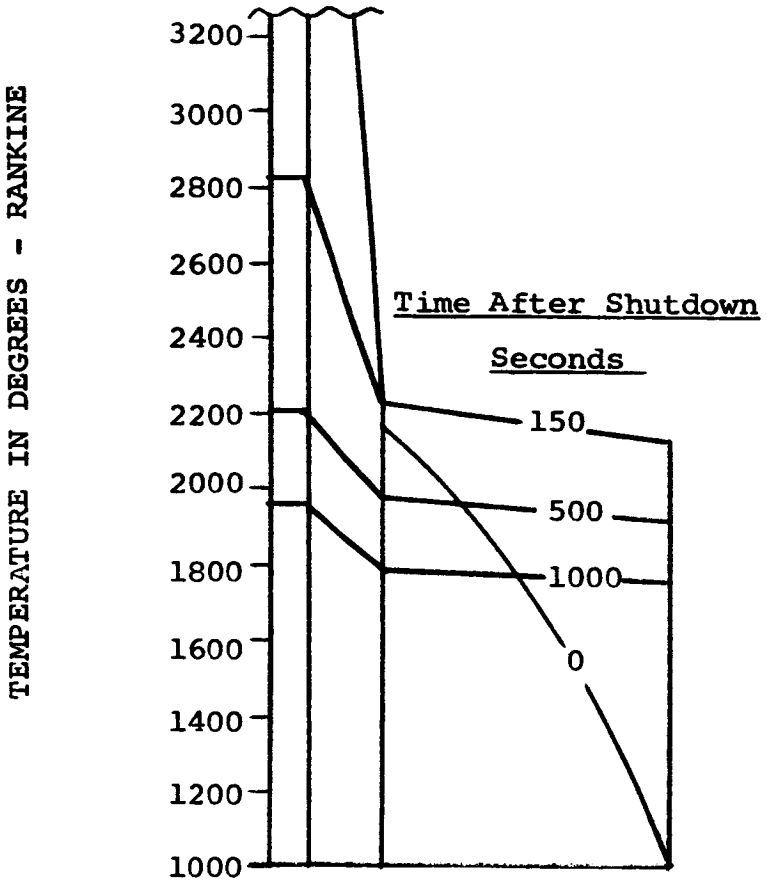

FIGURE 45

ARDE-PORTLAND NUCLEAR NOZZLE

WALL TEMPERATURE HISTORY AFTER REACTOR SHUTDOWN

.5% COOLANT FLOW

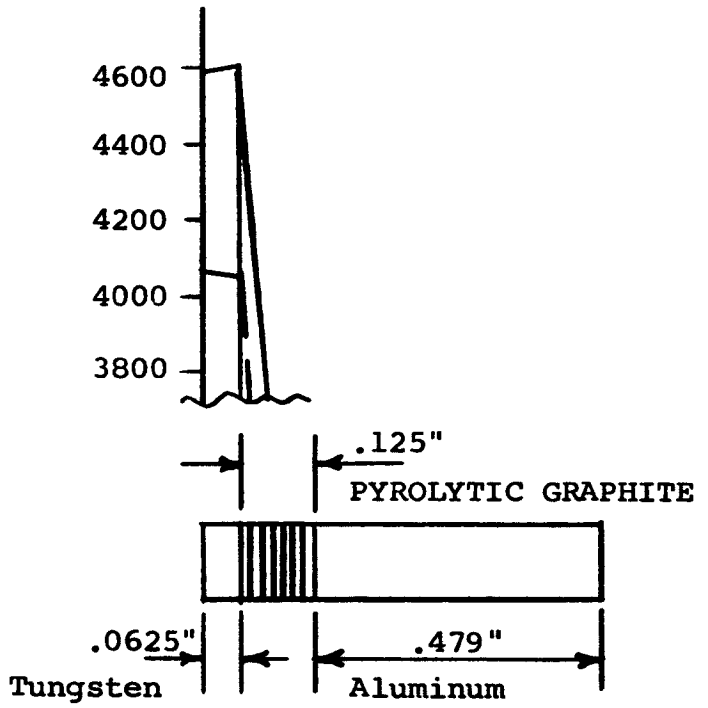

SCHEMATIC SECTION

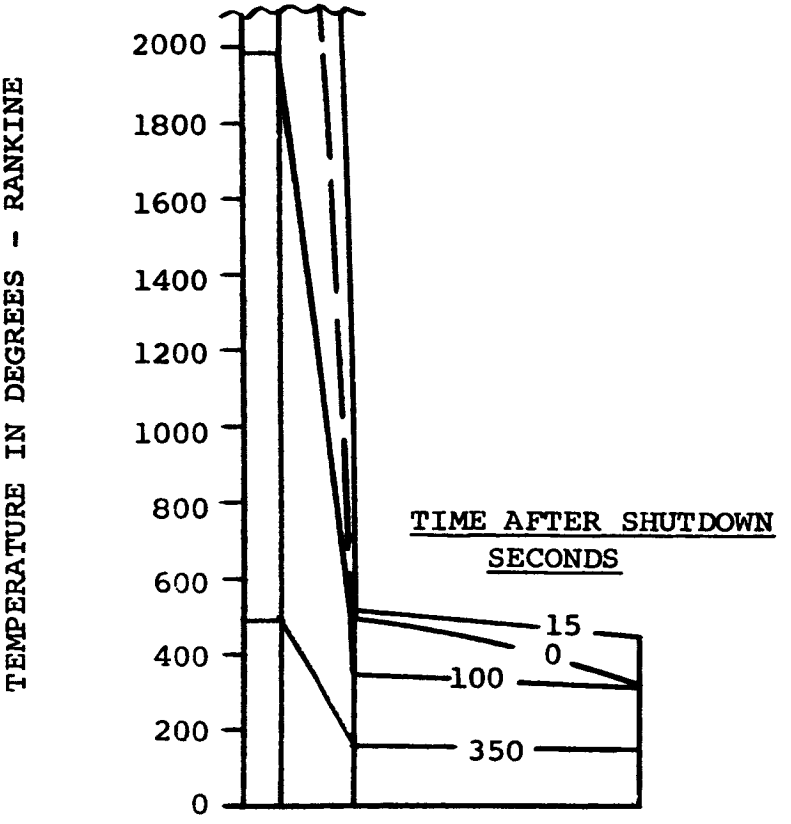

NOZZLE WALL

FIGURE 46

COMPARATIVE WEIGHTS

OF

COOLED AND UNCOOLED NOZZLES

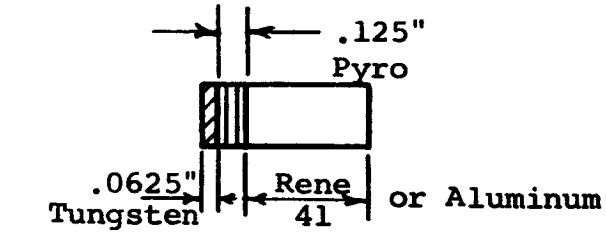

SECTION THROUGH COOLED WALL

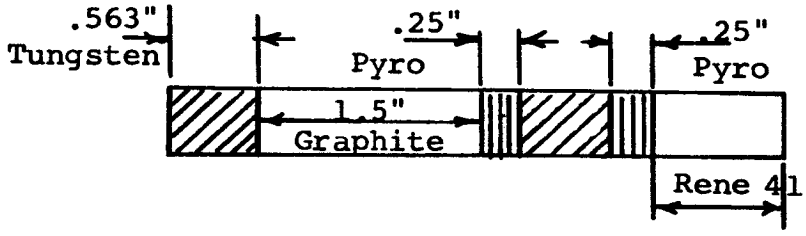

SECTION THROUGH UNCOOLED WALL

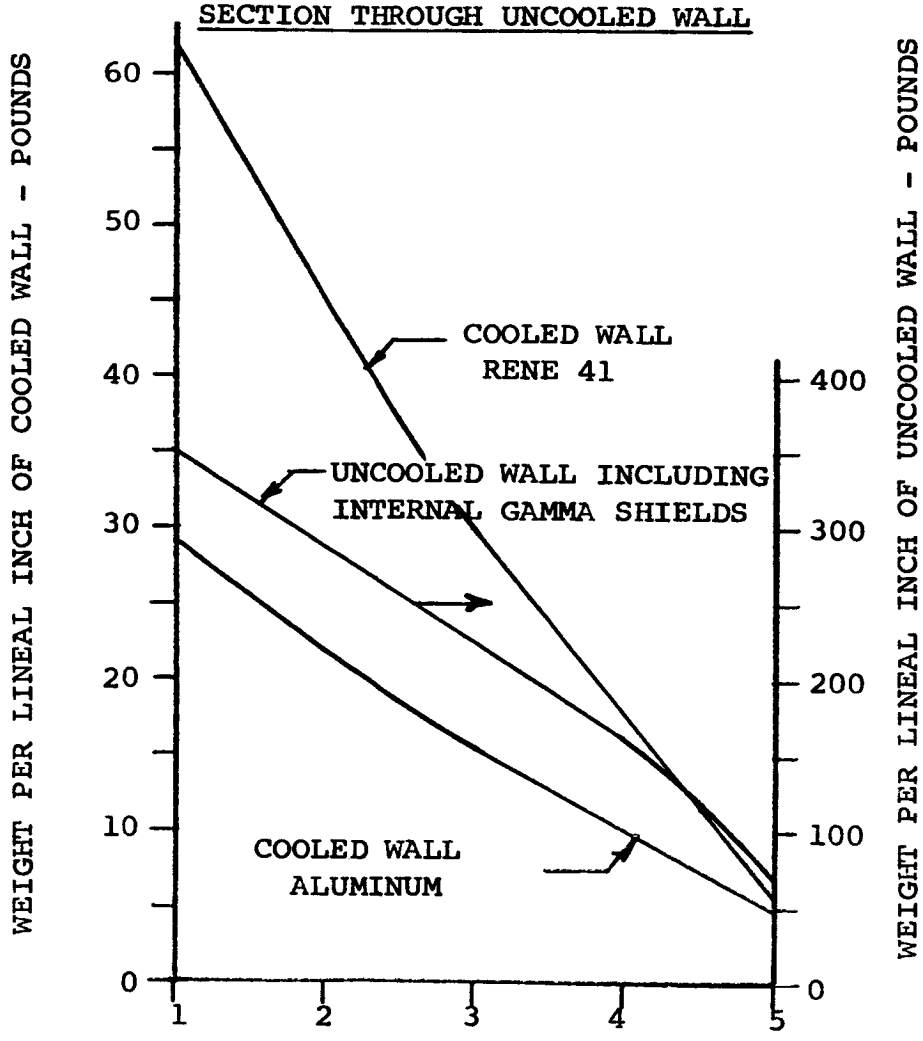

FIGURE 47

FINAL REPORT DISTRIBUTION

CONTRACT NAS 3-3670

National Aeronautics and Space Administration
Washington 25, D.C.
Attention: Harold B. Finger (NPO)

National Aeronautics and Space Administration
Washington 25, D.C.
Attention: Francis C. Schwenk (NPO)

National Aeronautics and Space Administration
Washington 25, D.C.
Attention: Paul G. Johnson (NPO)

National Aeronautics and Space Administration
Washington 25, D.C.
Attention: Norman Gerstein (NPO)

National Aeronautics and Space Administration
Ames Research Center
Moffet Field, California
Attention: Librarian

National Aeronautics and Space Administration
Goddard Space Flight Center
Greenbelt, Maryland
Attention: Librarian

National Aeronautics and Space Administration
Langley Research Center
Hampton, Virginia
Attention: Librarian

National Aeronautics and Space Administration
Lewis Research Center
21000 Brookpark Road
Cleveland, Ohio 44135
Attention: Librarian (2)
Attention: Solomon Weiss (MS 54-1)
Attention: A. D. & E. Procurement Section (MS 54-1)
Attention: Norman T. Musial, Patent Counsel (MS 77-1)
Attention: Report Control Office (MS 5-5)

National Aeronautics and Space Administration
Lewis Research Center
21000 Brookpark Road
Cleveland, Ohio 44135
Attention: Hugh M. Henneberry (MS 54-1)
Attention: John C. Sanders (MS 54-1)
Attention: Herman H. Ellerbrock (MS 54-1)
Attention: Rudolph A. Duscha (MS 54-1) (15)
Attention: Newell D. Sanders (MS 302-1)
Attention: William A. Benser (MS 6-1)
Attention: Irving A. Johnson (MS 0-5)
Attention: Howard W. Douglass (MS 0-5)

National Aeronautics and Space Administration
Manned Spacecraft Center
Houston 1, Texas
Attention: Librarian

National Aeronautics and Space Administration
George C. Marshall Space Flight Center
Huntsville, Alabama
Attention: Librarian

National Aeronautics and Space Administration
Jet Propulsion Laboratory
4800 Grove Drive
Pasadena 3, California

U. S. Atomic Energy Commission
Technical Information Service Extension
P. O. Box 62
Oak Ridge, Tennessee (3)

National Aeronautics and Space Administration
Scientific & Technical Information Facility
Box 5700
Bethesda 14, Maryland
Attention: NASA Representative (6 + 1 reproducible)

U. S. Atomic Energy Commission (3)
Technical Reports Library
Washington, D.C.